

NOG mice

Introduction and applications

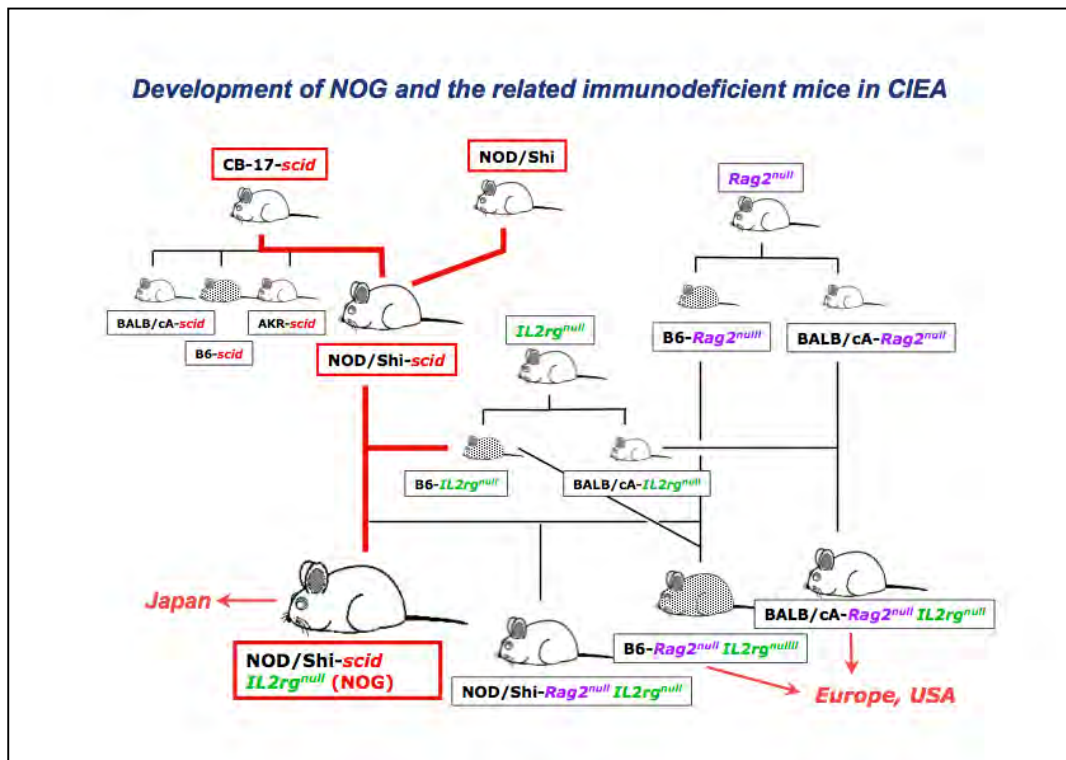
**August 3, 2009
Central Institute for Experimental Animals**



NOG mice

1. History
2. General characteristics
3. Basic characteristics
 - 3-1. Body weight
 - 3-2. Life span and tumors
 - 3-3. Organ weight and histology
 - 3-4. Irradiation sensitivity
 - 3-5. No B cell leakiness
 - 3-6. Clinical chemistry and hematology
 - 3-7. Immunological characteristics
 - 3-8. Microbiological agents affecting NOG mice
4. Humanized NOG after HSC transfer
5. Applications
 - 5-1. Infectious disease model
 - 5-1-1. HIV-1 infection
 - 5-1-2. ATL infection
 - 5-1-3. EBV infection
 - 5-2. Cancer model
 - 5-2-1. Liver metastasis
 - 5-2-2. Multiple myeloma
 - 5-2-3. Acute myeloid leukemia
 - 5-3. Human tissue or organ model
 - 5-3-1. Model with human ovary
 - 5-3-2. Model with human liver
 - 5-3-3. Model with human endometrium
 - 5-4. Other model
 - 5-4-1. GVHD model
 - 5-4-2. Efficacy test model for thrombopoietic drugs
 - 5-4-3. Tumorigenicity test model for human cell transplantation
6. Collaborative Studies at CIEA
7. Reference list

1. History



Strain nomenclature: CB-17-*scld*, C.BkaIgh^b-Prkdc^{scld}/IcrJic; NOD-*scld*, NOD.CB17- Prkdc^{scld}/ShiJic; BALB/cA-*Rag2*^{null}, C.129S1-*Rag2*^{tm1Fwa}/AJic; C57/B6J-*Rag2*^{null}, B6.129S1-*Rag2*^{tm1Fwa}/JJic; BALB/cA-*IL2r*^γ*null*, C.129S1-*IL2r*^γ*tm1Sug*/ShiJic; C57/B6J- *IL2r*^γ*null*, B6.129S1- *IL2r*^γ*tm1Sug*/Jic; NOG (NOD/Shi-*scld* *IL2r*^γ*null*); NOD.Cg-Prkdc^{scld} *IL2r*^γ*tm1Sug*/ShiJic, BALB/cA-*Rag2*^{null} *IL2r*^γ*null*, C.Cg-*Rag2*^{tm1Fwa} *IL2r*^γ*tm1Sug*/AJic; C57B6J-*Rag2*^{null} *IL2r*^γ*null*, B6.Cg-*Rag2*^{tm1Fwa} *IL2r*^γ*tm1Sug*/JJic; NOD/Shi-*Rag2*^{null} *IL2r*^γ*null*, NOD.Cg-*Rag2*^{tm1Fwa} *IL2r*^γ*tm1Sug*/ShiJic

(*Curr Top Microbiol Immunol* Vol. 324, (2008) p56 , “NOD/Shi-*scld* *IL2r*^γ*null* (NOG) mice more appropriate for humanized mouse models.”, Ito, M., Kobayashi, K. & Nakahata, T., Fig. 1. With kind permission of Springer Science+Business Media)

A schematic diagram of the development of NOG and the related immunodeficient mice is shown. NOG mice were established based on NOD/Shi-*scld* mice, one of the SCID congenic strains developed by the Central Institute for Experimental Animals (CIEA). NOD/Shi-*scld* *IL2r*^γ*null* (NOG) mice were established by introducing the *IL2r*^γ*null* gene of *IL2R*^γ*null* mice that were produced by Dr. Sugamura’s group in 1996 on NOD/Shi-*scld* mice by a 10th generation backcross mating in 2000. Our experimental studies with human hematopoietic stem cells transferred to NOG mice demonstrated that they were extremely efficient for humanized mice. The formal names for the NOD-*scld* *IL2r*^γ*null* mice are NOD.Cg-Prkdc^{scld}*IL2r*^γ*tm1Sug*.

In addition to the development of NOG mice, another type of immunodeficient mice with *Rag2*^{null} genes replacing the *scld* mutation has been developed because these inactive genes cause the same phenotypic T and B cell deficiency in the mice.

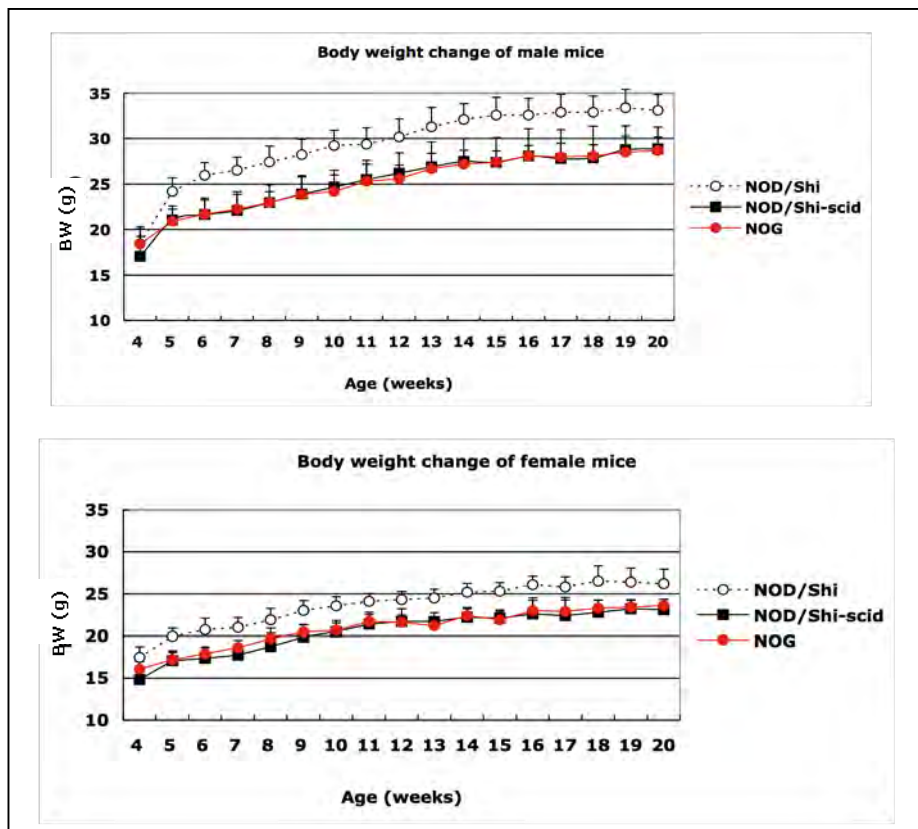
The NOG mice that we developed were mainly used in Japan for various research studies on xenotransplantation, including human hematopoiesis. BALB/cA and C57BL/6J- *Rag2*^{null} *IL2r*^γ*null* mice were sent to the United States and later on to Europe, with the successful development of humanized mice that used irradiated newborn BALB/c- *Rag2*^{null} *IL2r*^γ*null* mice, as reported by Dr. Traggiai et al. in 2003.

2. General characteristics of NOG mice

1. T and B cell deficient
2. NK cell deficient
3. Reduced macrophage and dendritic cell function
4. Complement activity deficient
5. No incidence of lymphoma
6. Sensitive to irradiation
7. Long life span
8. Sensitive to microbiological pathogens
9. High engraftment for xenotransplants

3. Basic characteristics

3-1. Body weight



The body weight of 10 males and females of three strains of mice was measured every week until the age of 20 weeks .

3-2. Life span and tumors

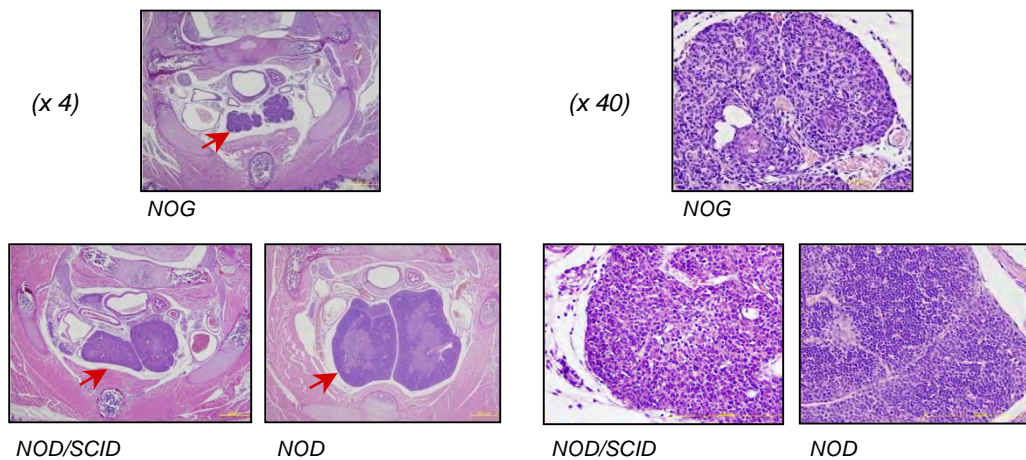
Thymic lymphoma that often occurred in NOD-*scid* mice was rarely observed in NOG mice. A recent publication by Kato C et al. (Lab. Animals, 2009) reported that lymphoma occurred in only 0.7 % (16 of 2406) of NOG mice. Therefore NOG mice have a long life span and survive at least one and a half years under strict SPF conditions.

3-3. Organ weight and histology

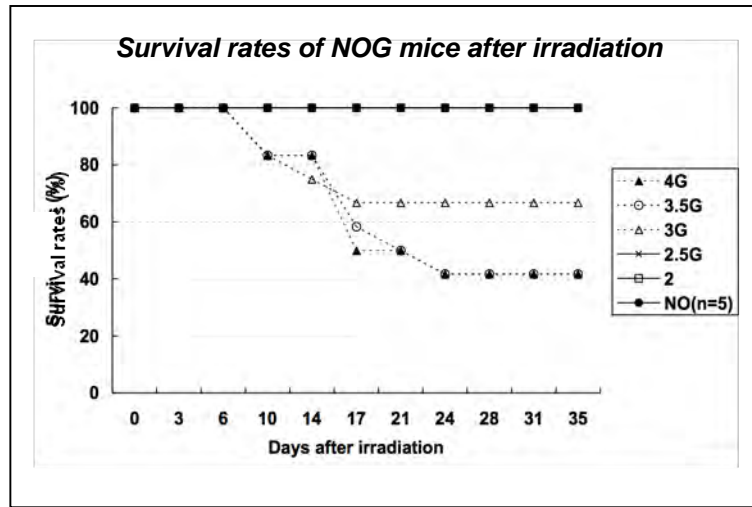
Age (weeks)	Sex	No. of mice	BW (g)	Brain (mg)	Thyroid gland (mg)	Mandibular gland (mg)	Lung (mg)	Thymus (mg)
12	Male	10	24.5 ± 1.53	450 ± 32	1.4 ± 0.9	182 ± 23	141 ± 7	4.7 ± 4.3
	Female	10	21.3 ± 0.53	479 ± 27	1.2 ± 0.8	107 ± 11	148 ± 10	2.3 ± 1.2
20	Male	10	28.1 ± 1.15	478 ± 25	1.7 ± 0.7	213 ± 20	180 ± 18	2.5 ± 1.9
	Female	10	23.2 ± 1.2	504 ± 32	2.0 ± 0.9	111 ± 11	165 ± 11	2.2 ± 0.9

Age (weeks)	Sex	Heart (mg)	Liver (g)	Spleen (mg)	Kidney (mg)	Adrenal gland (mg)	Testis (mg)	Ovary (mg)
12	Male	108 ± 12	1.25 ± 0.12	20.7 ± 2.3	384 ± 25	5.8 ± 1.2	175 ± 11	
	Female	95 ± 8	0.99 ± 0.07	23.7 ± 4.0	279 ± 13	7.1 ± 0.5		15.2 ± 2.1
20	Male	115.9 ± 38	1.44 ± 0.17	28.3 ± 8.9	449 ± 24	6.9 ± 1.3	192 ± 12	
	Female	111 ± 10	1.11 ± 0.12	28.4 ± 10	322 ± 29	8.4 ± 1.1		17.7 ± 2.7

Histology of thymus from newborn mice

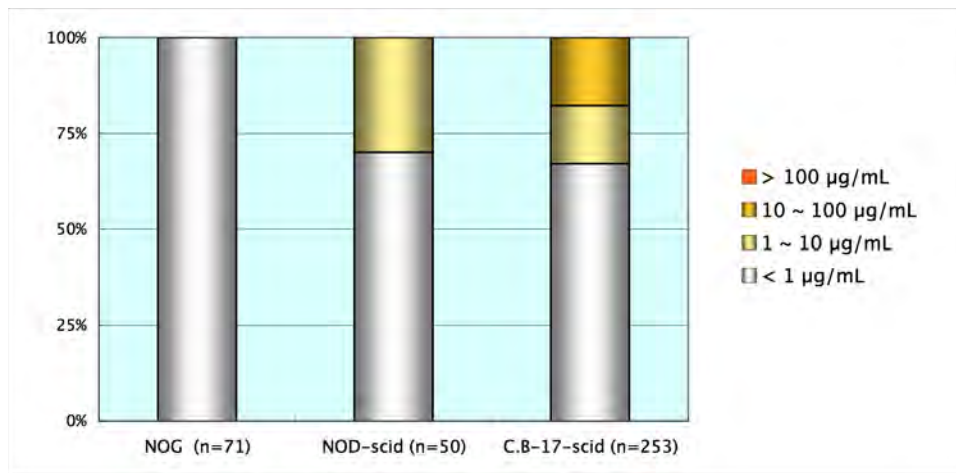


3-4. Irradiation sensitivity



Five mice in each group were irradiated with 2 to 4 Gy with using an X-ray device (MBR-1505R, Hitachi Medical Co., Tokyo) at age of 8 weeks.

3-5. No B cell leakiness



IgG+M antibody levels in the sera from aged NOG (7-10 months old) and NOD-scid (6-7 months old) mice were measured by ELISA. In C.B-17-scid (6-9 months old) mice, serum IgG+M+A antibody levels measured in 1989 were used in this figure.

3-6. Clinical chemistry and hematology

a. Clinical chemistry

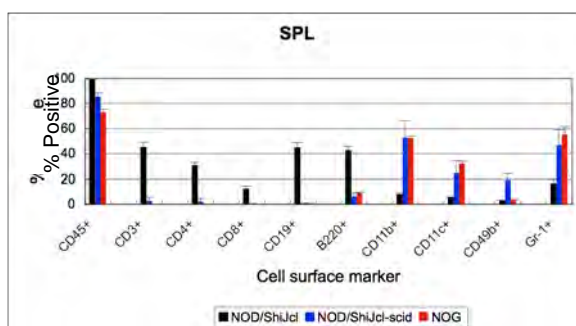
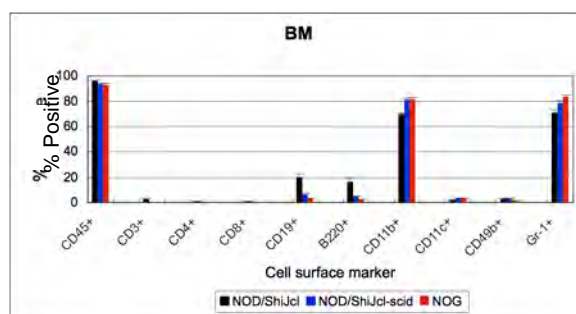
		AST	ALT	ALP	Ca	TG	UN	Crea	TP	T-Cho
		IU/L	IU/L	IU/L	mg/dL	mg/dL	mg/dL	mg/dL	g/dL	mg/dL
Male	N=8	49.38 ±12.24	25.00 ±13.79	133.25 ±15.6	7.49 ±0.44	37.13 ±11.90	25.24 ±1.53	0.32 ±0.02	3.98 ±0.16	61.13 ±6.13
Female	N= 10	67.30 ±12.37	23.90 ±5.4	212.30 ±18.14	7.28 ±0.29	30.40 ±17.04	22.21 ±2.52	0.30 ±0.04	3.65 ±0.14	45.50 ±5.19

b. Hematology

		WBC	RBC	HGB	HCT	MCV	MCH	MCHC	PLT
		x10 / μ L	x10 / μ L	g/dl	%	fl	pg	%	x10 / μ L
Male	N=8	6.50 ±1.93	766.25 ±28.62	12.31 ±0.45	39.34 ±1.73	51.34 ±0.58	16.04 ±0.16	31.31 ±0.36	106.73 ±5.92
Female	N= 10	11.80 ±3.79	773.00 ±45.12	12.72 ±0.59	39.12 ±2.26	50.73 ±0.39	16.47 ±0.26	32.47 ±0.50	83.85 ±8.89

Blood was collected from retro-orbital venous plexus of mice at 12 weeks of age under slight anesthesia with Isoflurane. Differential diagnosis of blood cells was performed with an automatic blood cell counter (XT-2000i, Sysmex, Osaka).

c. Mouse hematopoietic cells in spleen and bone marrow



Bone marrow (BM) and spleen (SPL) were removed from 12-week-old NOG mice. Single cell suspensions prepared in the usual manner were stained with FITC- or PE-labeled anti-mouse CD45+, CD3+, CD4+, CD8+, CD19+, B220+, CD11b+, CD11c+, Gr-1+ and analyzed with FACSCanto (BD Sciences, CA)

3-7. Immunological characteristics

a. Defect of NK cells and NK activity

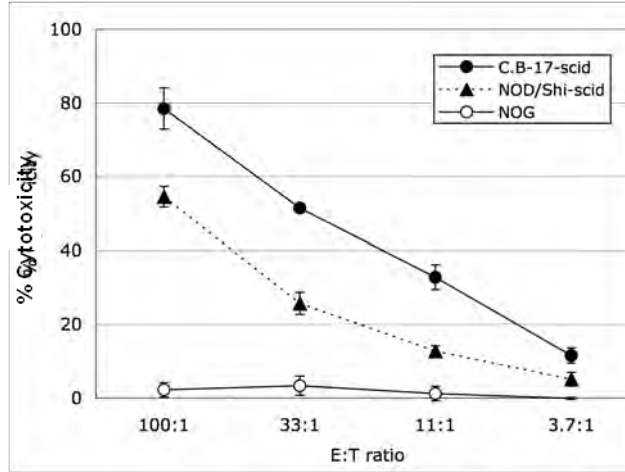


Figure 1. NK cell Activity of NOG mice

The NK cell activity was determined by a cytotoxicity test using NK sensitive YAC-1 cells as a target cell. Mice were intraperitoneally inoculated with 100 mg of polyinosinic-polycytidylic acid (poly I:C, SIGMA Chemical Co., St. Louis, MO) to stimulate NK cell activity for 48 hrs before assay. Spleen cells were separated from 4 mice of each strain of mice, pooled and co-cultured with ^{51}Cr -labeled YAC-1 cells as target cells for 4 hrs at 37C in 5% CO_2 . The supernatants harvested were assayed on a gamma counter. The present specific ^{51}Cr release was calculated using the following formula, where X is the mean experimental release from triplicate wells. Total release (T) was determined from wells with ^{51}Cr labeled YAC-1 cells and 1H HCl, and spontaneous release (S) was determined from wells with ^{51}Cr labeled YAC-1 cells and medium: % specific release = $[(X-S)/(T-S)] \times 100$.

(This research was originally published in Blood. Ito, M. *et al.* NOD/SCID/gamma(c)(null) mouse: an excellent recipient mouse model for engraftment of human cells. Blood. 2002;100: 3175-3182. © the American Society of Hematology.)

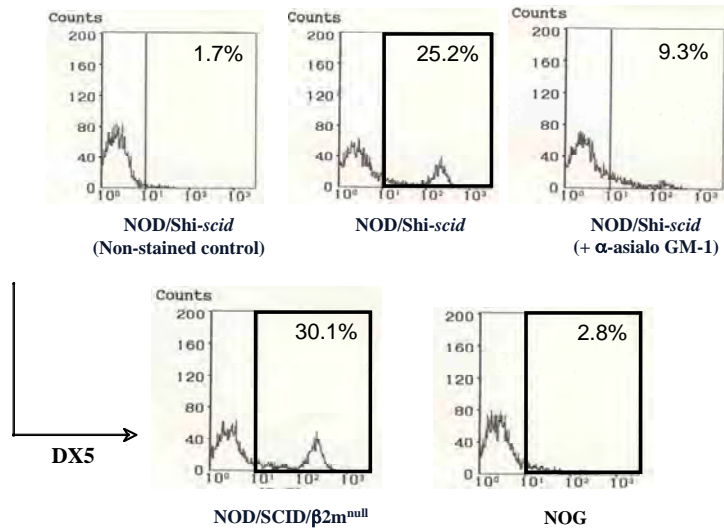


Figure 2. NK cells in NOG mice.

Spleen cells from mice were stained with streptavidin-FITC and biotin-labeled anti-pan NK cell antibody. No NK cells were observed in spleen cells from NOG mice and NOD/Shi-scid treated with asialo GM1 antibody to eliminate NK cells.

(This research was originally published in Blood. Ito, M. *et al.* NOD/SCID/gamma(c)(null) mouse: an excellent recipient mouse model for engraftment of human cells. Blood. 2002; 100: 3175-3182 © the American Society of Hematology.)

b. Reduced IL-1 production from macrophages

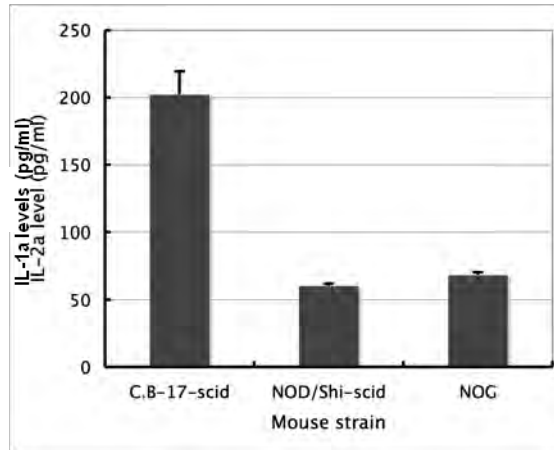


Figure 3. IL-1 production from bone marrow cells

IL-1 production from bone marrow cells stimulated with IFN- γ and LPS was determined. Bone marrow cells were cultured with 500 U/ml human rM-CSF, with and without 10 U/ml rat rIFN- γ and cultured for 4 days at 37 in 5% CO₂. After 4 days, the medium was replaced with fresh medium alone or with medium containing Escherichia coli LPS at 10 mg/ml. After an additional 24 hr incubation period, the culture supernatants were harvested and assayed for IL-1 α levels using ELISA kits. (This research was originally published in Blood. Ito, M. *et al.* NOD/SCID/gamma(c)(null) mouse: an excellent recipient mouse model for engraftment of human cells. Blood. 2002; 100: 3175-3182. © the American Society of Hematology.)

c. Defect of hemolytic complement activity in serum

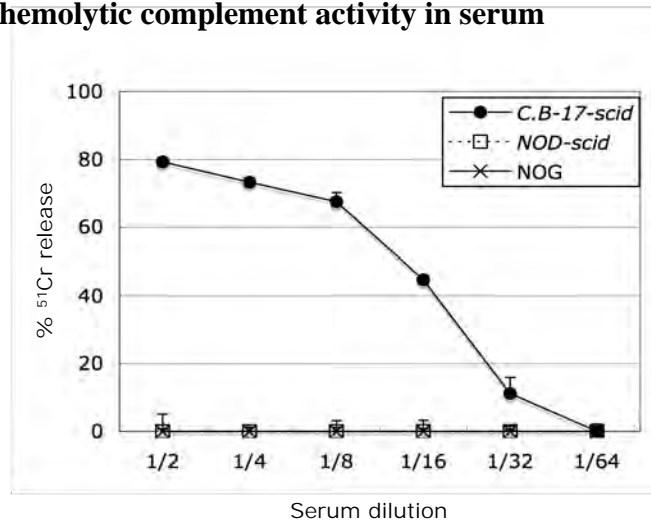


Figure 4. Complement-dependent hemolytic activity

Complement-dependent hemolytic activity in sera was determined by measurement of ⁵¹Cr released in the supernatants after 30 min incubation of mouse sera and ⁵¹Cr labeled SRBC/anti SRBC antibody conjugates. Spontaneous release (S) was determined from wells with ⁵¹Cr SRBC-Ab conjugate in media. Total release (T) was determined from wells with ⁵¹Cr SRBC-Ab conjugates and 100 ml 2% SDS. Percent specific release = [(X-S)/(T-S)] x 100. (This research was originally published in Blood. Ito, M. *et al.* NOD/SCID/gamma(c)(null) mouse: an excellent recipient mouse model for engraftment of human cells. Blood. 2002; 100: 3175-3182. © the American Society of Hematology.)

d. No production of IFN γ from spleen cells of NOG mice

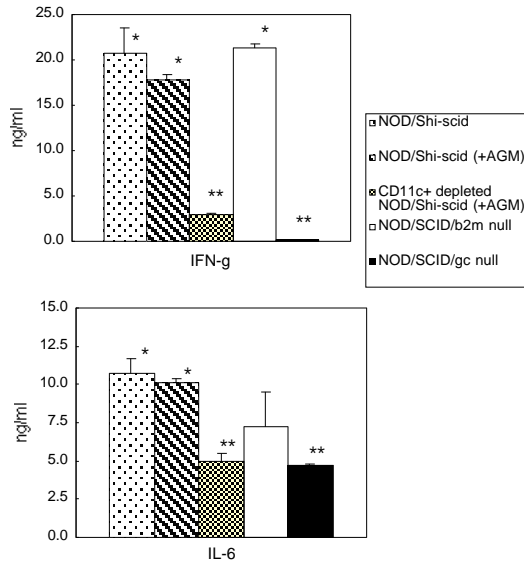


Figure 5. In vitro cytokine production of *L. monocytogenes*-stimulated spleen cells from 3 strains of mice

Spleen cells were separated after injection of 1 ml of 1 mg/ml collagenase D solution into the spleen. CD11c⁺ cells were depleted from spleen cells from NOD/Shi-scid mice treated with anti-asialo GM1 antiserum, using anti-CD11c antibody labeled magnetic beads, by a magnetic cell sorter (MACS). The cell suspension was co-cultured with 10⁷ of heat-killed *L. monocytogenes* for 8 hrs at 37°C. The IFN- γ and IL-6 levels in the supernatants were determined using ELISA kits. Asterisk indicates a significant difference (* vs **: P<0.01).

(This research was originally published in Blood. Ito, M. *et al.* NOD/SCID/gamma(c)(null) mouse: an excellent recipient mouse model for engraftment of human cells. Blood. 2002; 100: 3175-3182. © the American Society of Hematology.)

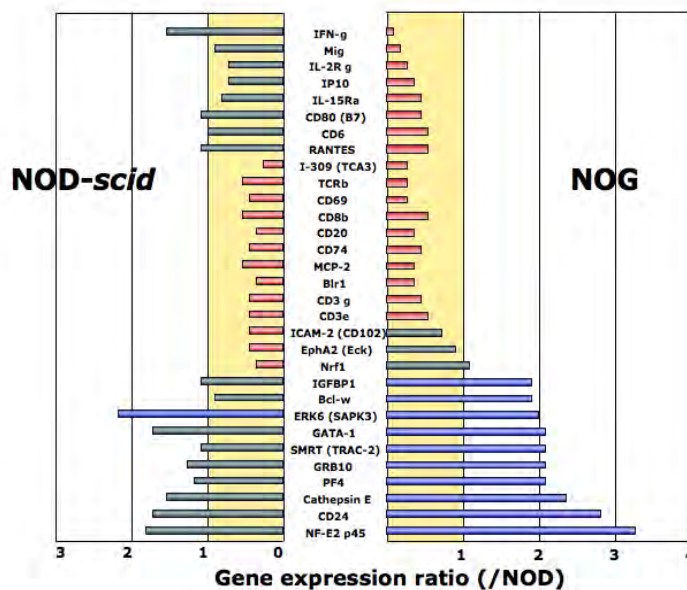


Figure 6. Expression of the genes associated with immunological responses in NOD, NOD/Shi-scid and NOG mice

At 48 hrs after intraperitoneal infection of 1 x 10⁷ *Listeria monocytogenes*, spleens were removed and the RNA was extracted. Gene expression was examined by microarray (Toyobo Inc.). The yellow areas express the intensity of gene expression in the NOD mice. The blue bars express higher intensity, and the grey bars express lower intensity when compared with those of the NOD/Shi mice.

(*Curr Top Microbiol Immunol* Vol. 324, (2008) p59, "NOD/Shi-scid IL2rgamma(null) (NOG) mice more appropriate for humanized mouse models.", Ito, M., Kobayashi, K. & Nakahata, T., Fig. 2. With kind permission of Springer Science+Business Media) e.

3-8. Microbiological agents affecting NOG mice

NOG mice may have higher sensitivity against opportunistic pathogens because they are more immunodeficient than conventional immunodeficient mice, i. e., nude and SCID mice. Therefore, NOG mice must be maintained in a facility under strict SPF conditions. NOG mice may also be easily affected by stress, therefore control of environmental factors in sites is required to assure reproducibility of the results of animal experiments. Therefore, we recommend to maintenance of NOG mice in a special room not together with other stains of mice. The room should be changed evert year.

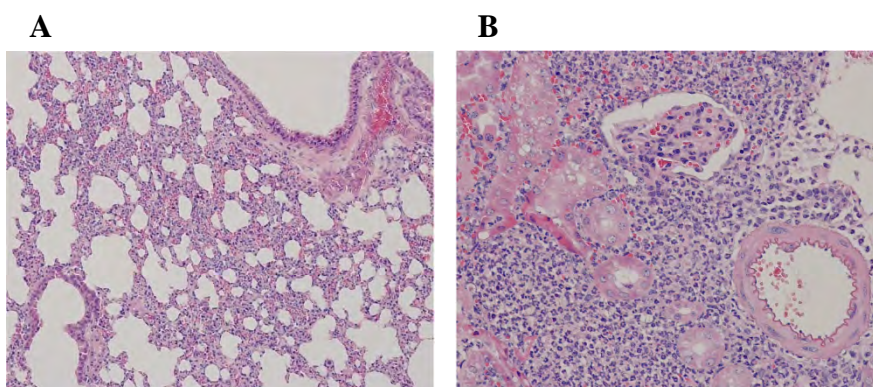


Figure 1. Histopathological diagnosis of bacteremia in NOG mice infected with *Pseudomonas aeruginosa*. Interstitial pneumonitis and suppurative nephritis were found in the lungs and kidneys of affected mice. A. Interstitial pneumonitis (H&E, x 200). B. Suppurative nephritis (H&E, x200). *P. aeruginosa* was isolated from blood and lesions in the mice.

(*Curr Top Microbiol Immunol* Vol. 324, (2008) p17, “Basic concept of development and practical application of animal models for human diseases. ”, Nomura, T., Tamaoki, N., Takakura, A. & Suemizu, H. , Fig. 7. With kind permission of Springer Science+Business Media)

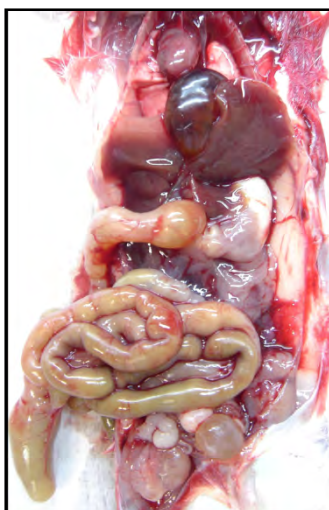


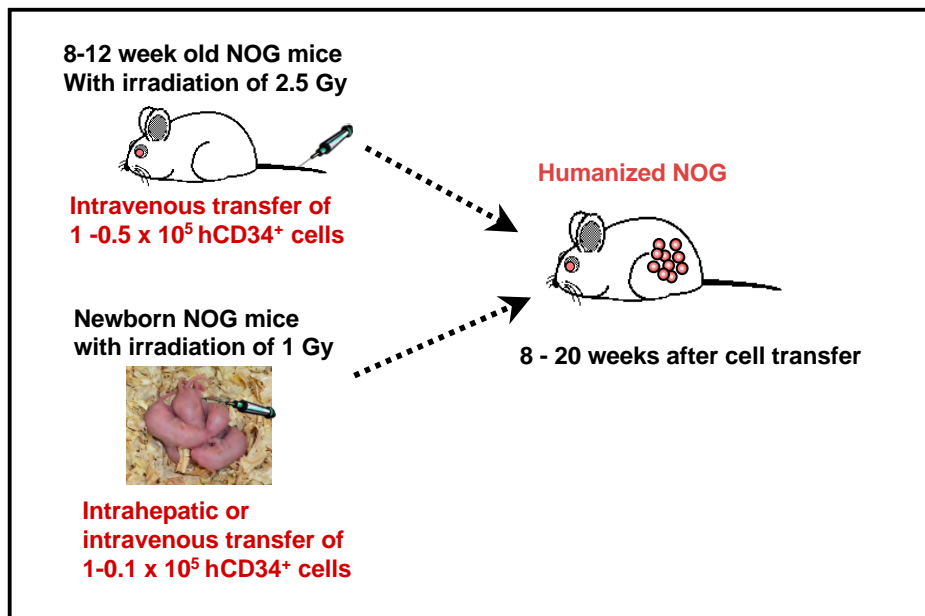
Figure 2. Results of necropsy of diarrheal NOG mouse that died with unknown causes. Severe diarrhea, bile congestion, duodenitis, and intestinal hypertrophy were observed in the mouse.

(*Curr Top Microbiol Immunol* Vol. 324, (2008) p19, “Basic concept of development and practical application of animal models for human diseases. ”, Nomura, T., Tamaoki, N., Takakura, A. & Suemizu, H. , Fig. 8. With kind permission of Springer Science+Business Media)

4. Humanized NOG after HSC transfer

4-1. Human cells developed in humanized NOG mice after transfer of human cord blood CD34+ hematopoietic stem cells (HSCs).

General protocol of human HSC transfer



Generally, human cord blood derived CD34⁺ cells were used as a source of hematopoietic stem cells. CD34⁺ cells from bone marrow and peripheral blood can be also used although their reconstitution capacity is relatively lower than those from cord blood.

Purification of CD34⁺ cells from human cord blood

Umbilical cord blood (CB) cells are collected during normal full-term deliveries after obtaining informed consent. Mononuclear cells (MNC) are separated by Ficoll-Hypaque density gradient centrifugation after depletion of phagocytes with Silica (Immuno Biological Laboratories, Fujioka, Japan). MNC separated from CB are suspended at 4×10^7 cells/ml in phosphate buffered saline (PBS) containing 2% bovine serum albumin (BSA), 0.6% citrate, and 100 IU/ml of penicillin and streptomycin. The MNC suspension is incubated at 4°C for 30 min with Dynabeads M-450 CD34 (DynaL AS, Oslo, Norway) with a bead-to-cell ratio of 1:1. The beads with attached cells are collected using a Magnetic Particle Concentrator (MPC, Dynal) and incubated with DETACHaBEAD CD34 (DynaL) at 37°C for 15 min to release the cells which are collected by MPC. The purity is evaluated by flow cytometric analysis. Approximately 95% of the cells were CD34 positive. Commercially available CB CD34⁺ cells can be also used for reconstitution of human cells.

Transplantation protocol of human HSC into NOG mice

Mice:

For adult mice, 10 -12 week-old NOG mice are usually used. For newborn mice, mice at 1-2 days after birth are used.

Irradiation:

Irradiation with 2 - 2.5 Gy of adult mice and with 1 Gy of newborns is performed under SPF conditions one day before cell transfer. Mice weighting less than 18 g will sometimes die at this dose of irradiation.

Cell preparation

1. When CD34+ cells (e.g. 1×10^6 /tube) are frozen, thaw the cells in a 37°C water bath.
2. Transfer cells into a 50 mL conical tube and add 1 mL of PBS containing 2% fetal bovine serum (2%FBS-PBS) drop by drop, shaking the tube slowly.
3. After further addition of 18 mL of 2% FBS-PBS, centrifuge at 1,200 rpm for 5 min at room temperature.
4. Resuspend the cells in 10 mL of 2% FBS-PBS and re-centrifuge.
5. Resuspend in 2 mL of PBS.
6. Using 15 μ L of the suspension, count the cells and determine viability after adding 15 μ L of 0.25% trypan-blue solution. Add 3 mL of PBS to adjust to a total of 5 mL.
7. Transfer 1mL of the cell suspension into each 1.5 mL cryotube.
8. Place the tubes in a 50 mL conical tube and take it to the animal facility.
9. After dipping the tube in an antiseptic solution, take it into the animal room.

Cell transfer

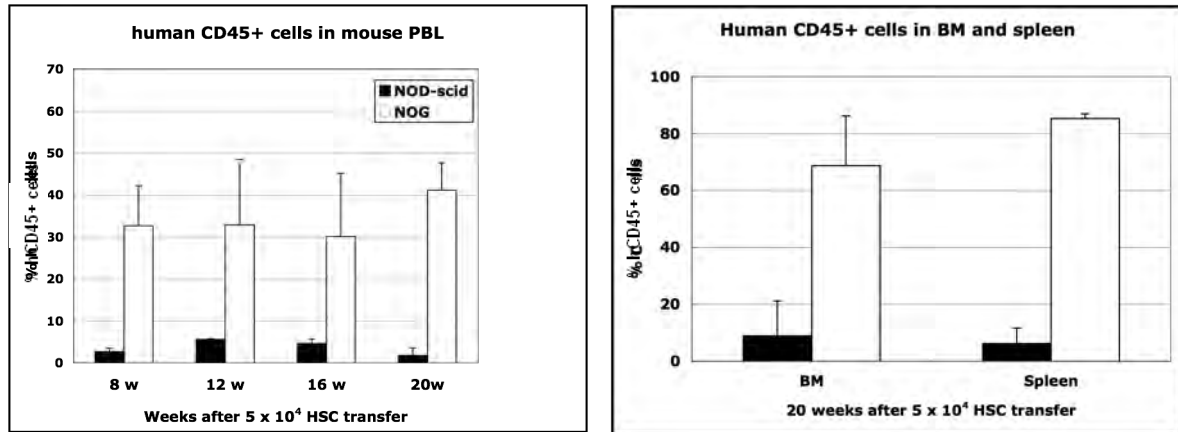
For adult mice

1. Inject 0.25 mL ($1 - 0.5 \times 10^4$) of the cell suspension into the mice via the tail vein with a 1 mL syringe with a 27 G needle or a microinjector syringe with a 29 G needle under slight anesthesia with isoflurane.

For newborn mice

1. Slightly anesthetize the newborn mice with isoflurane.
2. Hold the newborn mice by the left hand with the mouse head facing the right.
3. Inject 0.1 mL ($1-5 \times 10^4$) of the cell suspension via the face vein with a microinjector syringe with a 29 G needle.
4. Return the newborn mice to the mother gently, being careful not to apply any force.

4-2. High engraftment rate of human cells in NOG mice



At 8 - 20 weeks after intravenous transplantation of 5×10^4 human cord blood derived CD34⁺ cells into NOG and NOD-*scid* mice, human CD45⁺ hematopoietic cells were detected in peripheral blood of mice by flow cytometry. A high engraftment rate of human cells was observed in NOG mice.

Table 1. Limiting dilution assay in NOG mice.

CD34 ⁺ cell dose	No. of mice transplanted	No. of mice successfully engrafted*
1,000	5	5
200	3	2
100	6	3

* Successful engraftment was defined as the presence of at least 0.1% human CD45⁺ cells in bone marrow by flow cytometry.

(This research was originally published in Blood. Ito, M. *et al.* NOD/SCID/gamma(c)(null) mouse: an excellent recipient mouse model for engraftment of human cells. Blood. 2002; 100: 3175-3182. © the American Society of Hematology.)

In order to evaluate the frequency of CB CD34⁺ cells capable of engrafting in NOG mice, these mice were transplanted with CB CD34⁺ cells in a limiting dose. All recipient mice transplanted with 1×10^3 CB CD34⁺ cells showed successful engraftment (>0.1%). Further, as few as 100 cells could be engrafted in 2 of 6 mice and their multi-lineage differentiation.

4-3. Multi-lineage cell differentiation from HSCs in NOG mice

1. Ito, M., H. Hiramatsu, K. Kobayashi, K. Suzue, M. Kawahata, K. Hioki, Y. Ueyama, Y. Koyanagi, K. Sugamura, K. Tsuji, T. Heike, and T. Nakahata. 2002. NOD/SCID/gamma(c)(null) mouse: an excellent recipient mouse model for engraftment of human cells. *Blood* 100:3175-3182.
2. Yahata, T., K. Ando, Y. Nakamura, Y. Ueyama, K. Shimamura, N. Tamaoki, S. Kato, and T. Hotta. 2002. Functional human T lymphocyte development from cord blood CD34+ cells in nonobese diabetic/Shi-scid, IL-2 receptor gamma null mice. *J Immunol* 169:204-209.
3. Saito, Y., Y. Kametani, K. Hozumi, N. Mochida, K. Ando, M. Ito, T. Nomura, Y. Tokuda, H. Makuuchi, T. Tajima, and S. Habu. 2002. The in vivo development of human T cells from CD34(+) cells in the murine thymic environment. *Int Immunol* 14:1113-1124.
4. Hiramatsu, H., R. Nishikomori, T. Heike, M. Ito, K. Kobayashi, K. Katamura, and T. Nakahata. 2003. Complete reconstitution of human lymphocytes from cord blood CD34+ cells using the NOD/SCID/gammacnull mice model. *Blood* 102:873-880.
5. Watanabe, Y., T. Takahashi, A. Okajima, M. Shiokawa, N. Ishii, I. Katano, R. Ito, M. Ito, M. Minegishi, N. Minegishi, S. Tsuchiya, and K. Sugamura. 2009. The analysis of the functions of human B and T cells in humanized NOD/shi-scid/{gamma}cnull (NOG) mice (hu-HSC NOG mice). *Int Immunol*. 21:843-858

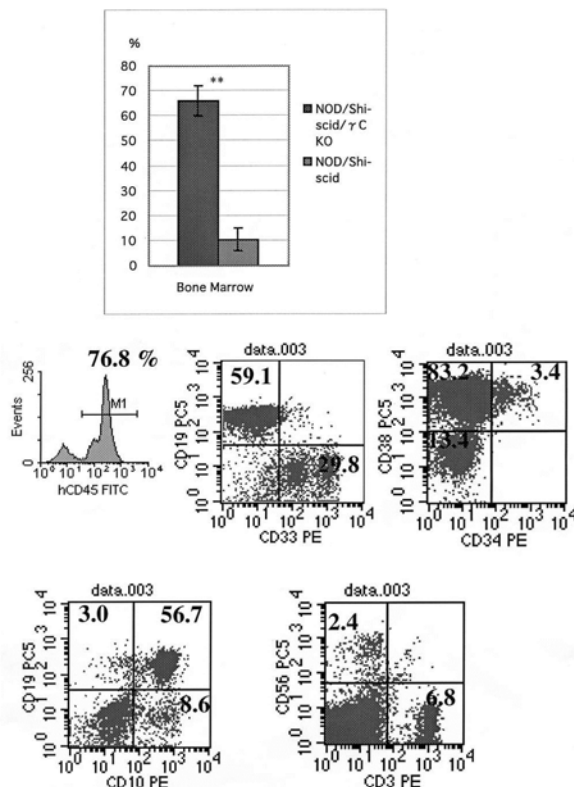


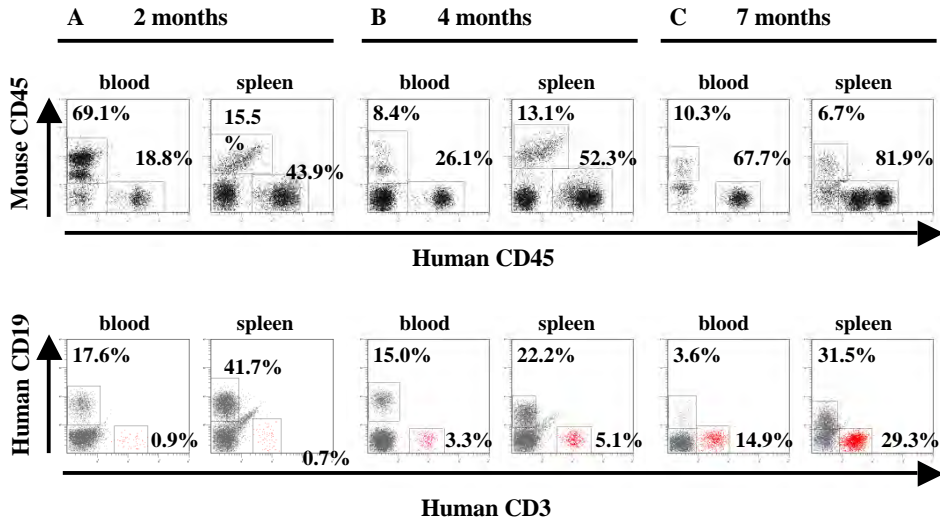
Figure 1. The rate of human CD45⁺ cells in bone marrow of transplanted mice and the high efficacy of multi-lineage cell differentiation

At 11 weeks after CD34⁺ cell transplantation, bone marrow was removed from NOD/SCID/g γ c^{null} and NOD/Shi-scid mice treated with anti-asialo GM1 antibody two days before transplantation, and subjected to flow cytometry. NOD/SCID/g γ c^{null} showed significantly higher percentage of CD45⁺ cells. Multi-lineage cells have been differentiated from CD34⁺ cells with high efficacy (* vs **: P<0.01).

(This research was originally published in *Blood*. Ito, M. *et al.* NOD/SCID/gamma(c)(null) mouse: an excellent recipient mouse model for engraftment of human cells. *Blood*. 2002; 100: 3175-3182. © the American Society of Hematology.)

4-3. Multi-lineage cell differentiation from HSCs in NOG mice

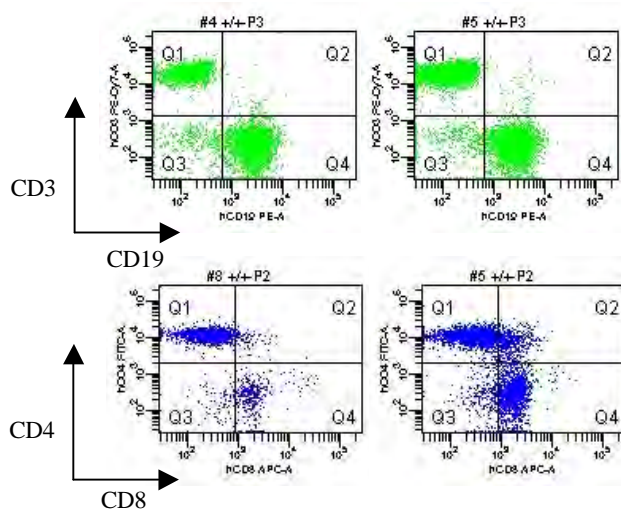
B cells develop prior to T cells.



(This research was originally published in Blood. Watanabe, S. *et al.* Hematopoietic stem cell-engrafted NOD/SCID/IL2Rgamma null mice develop human lymphoid systems and induce long-lasting HIV-1 infection with specific humoral immune responses. Blood. 2007; 109: 212-218. © the American Society of Hematology.)

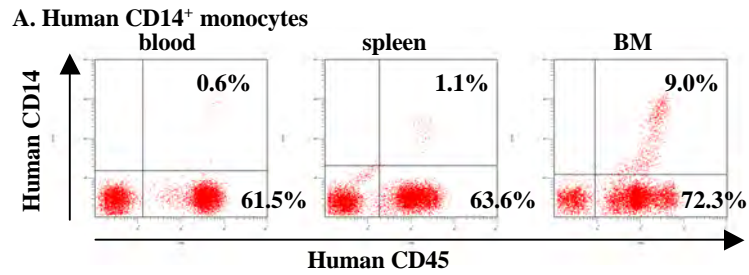
In development of human cells from HSCs in NOG mice, B cells develop of 4-8 weeks after transfer prior to T cells. T cells can be detected of 8-12 weeks after transfer and later become dominant in the periphery including peripheral blood and spleen.

Development of CD4+ and CD8+ T cells

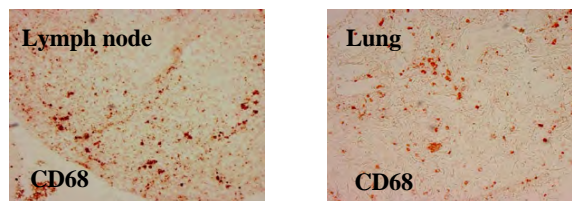


The above figure shows human cells in mouse peripheral blood of 20 weeks after intravenous human HSC cell transfer. Human T and B cells were developed in NOG mice. CD4+ and CD8+ T cells were also differentiated in NOG mice.

Development of human monocytes/macrophages and dendritic cells



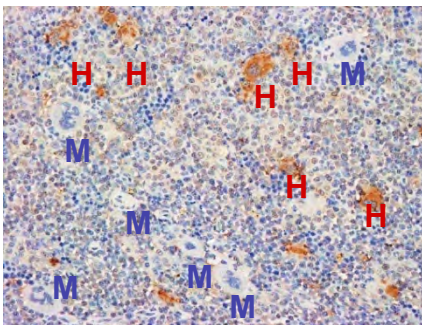
B. Human CD68⁺ macrophages in various organs



(This research was originally published in *Blood*. Watanabe, S. *et al.* Hematopoietic stem cell-engrafted NOD/SCID/IL2Rgamma null mice develop human lymphoid systems and induce long-lasting HIV-1 infection with specific humoral immune responses. *Blood*. 2007; 109: 212-218. © the American Society of Hematology.)

Development of human platelets in peripheral blood and megakaryocytes in bone marrow of NOG mice

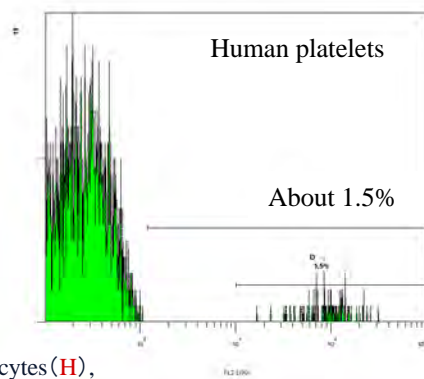
A. Bone marrow



A: Human (h) CD42b⁺ human megakaryocytes (H),
hCD42b⁻ mouse megakaryocytes (M)

B: hCD41⁺ human platelets

B. Peripheral blood



Courtesy of Dr. Y. Miyakawa, Keio Univ.

Development of human mast cells

The transplantation of primitive human cells into sublethally irradiated immunodeficient mice is the well-established *in vivo* system for the investigation of human hematopoietic stem cell function. Although mast cells are the progeny of hematopoietic stem cells, human mast cell development in mice that underwent human hematopoietic stem cell transplantation has not been reported. Here we report on human mast cell development after xenotransplantation of human hematopoietic stem cells into nonobese diabetic severe combined immunodeficiency (NOD/SCID)/ *c null* (NOG) mice with severe combined immunodeficiency and interleukin 2 (IL-2) receptor γ -chain allelic mutation. Supported by the murine environment, human mast cell clusters developed in mouse dermis, but they required more time than other forms of human cell reconstitution. In lung and gastric tract, mucosal-type mast cells containing tryptase but lacking chymase located on gastric mucosa and in alveoli, whereas connective tissue-type mast cells containing both tryptase and chymase located on gastric submucosa and around major airways, as seen in the human body. Mast cell development was also observed in lymph nodes, spleen, and peritoneal cavity but not in the peripheral blood. Xenotransplantation of human hematopoietic stem cells into NOG mice can be expected to result in a highly effective model for the investigation of human mast cell development and function *in vivo*. (Blood. 2004;103: 860-867)

(This research was originally published in Blood. Kambe N, Hiramatsu H, Shimonaka M, et al. Development of both human connective tissue-type and mucosal-type mast cells in mice from hematopoietic stem cells with identical distribution pattern to human body. Blood. 2004; 103: 860-867. ©the American Society of Hematology.)

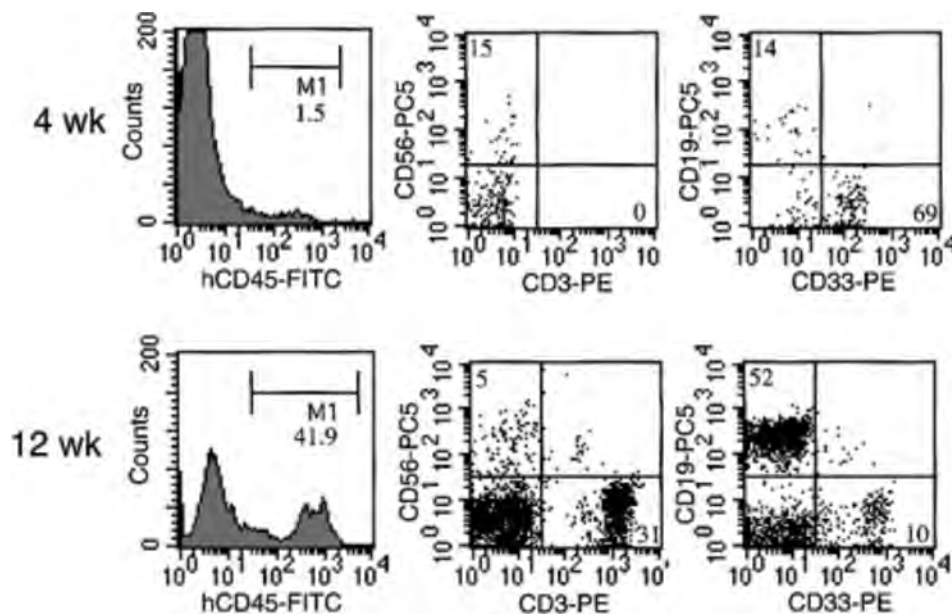


Figure 1. Representative flow cytometric analysis of peripheral blood from NOG mice after HSC transplantation. Four weeks after the transplantation, less than 2% of the cells were human CD45, in which CD33 myeloid cells were predominant, and CD19 B cells and CD56 NK cells were also present. Twelve weeks after the transplantation, more than 40% cells were replaced by human CD45 cells, among which abundant human CD3 T cells were identified. (This research was originally published in Blood. Kambe N, Hiramatsu H, Shimonaka M, et al. Development of both human connective tissue-type and mucosal-type mast cells in mice from hematopoietic stem cells with identical distribution pattern to human body. Blood. 2004; 103: 860-867. ©the American Society of Hematology.)

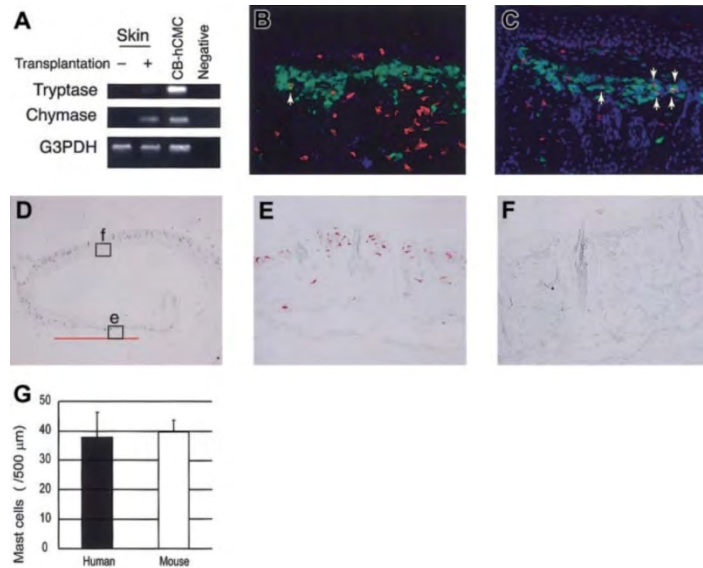


Figure 2. Human mast cell development in the mouse skin. (A) RT-PCR analysis for tryptase and chymase mRNA expression. The skin of NOG mice 12 weeks after the transplantation of human CD34 cells expressed human mast cell-specific tryptase and chymase mRNA. CB-hCMC indicates cord blood-derived human cultured mast cells. (B-C) Acetone-fixed frozen sections of NOG mouse skin 12 weeks (B) and 20 weeks (C) after the transplantation of human cord blood CD34 cells were stained for human CD45 (red fluorescent with Cy3), mast cells (yellowish green with FITC-avidin), and nuclei (blue with Hoechst 33342). Arrows indicate human CD45 mast cells, which are stained orange. Magnification, x 200. (D-F) Human MC specific chymase cells in the mouse skin. Acetone-fixed frozen sections of NOG mouse skin 24 weeks after the transplantation were stained with antihuman chymase mAb. Human chymase cells proliferated focally in the upper dermis (e), represented by the bar bellows, whereas in other lesions on the same samples nonstained granulated cells were located in the upper dermis (f). Magnification, x 12.5 (D) and x 200 (E-F). (G) The number of chymase human mast cells and nonstained granulated mouse mast cells in NOG mouse skin 24 weeks after the transplantation. The number of human and mouse mast cells supported by mouse dermis was almost identical. Bar graphs display mean \pm SD values from 5 different preparation. (This research was originally published in *Blood*. Kambe N, Hiramatsu H, Shimonaka M, et al. Development of both human connective tissue-type and mucosal-type mast cells in mice from hematopoietic stem cells with identical distribution pattern to human body. *Blood*. 2004; 103: 860-867. ©the American Society of Hematology.)

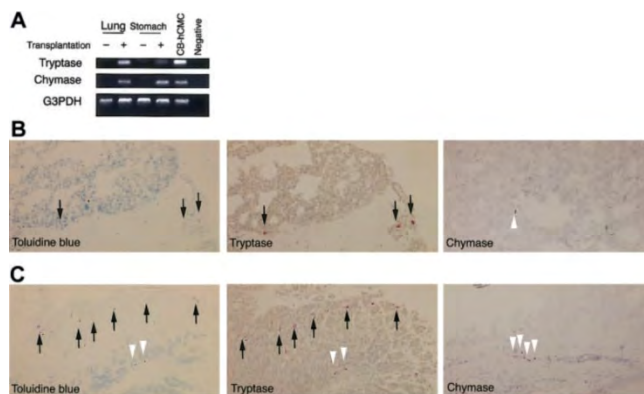
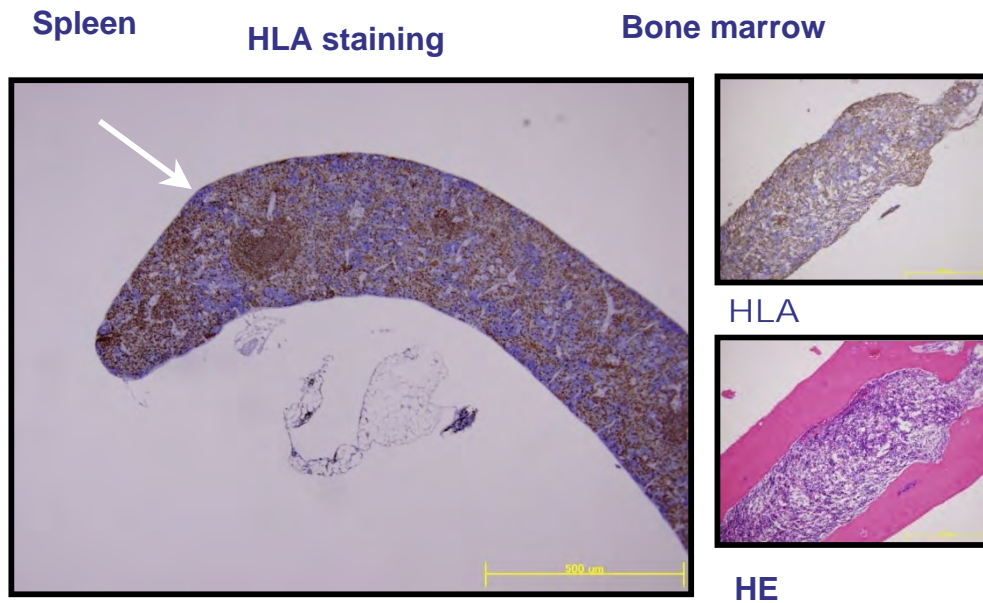
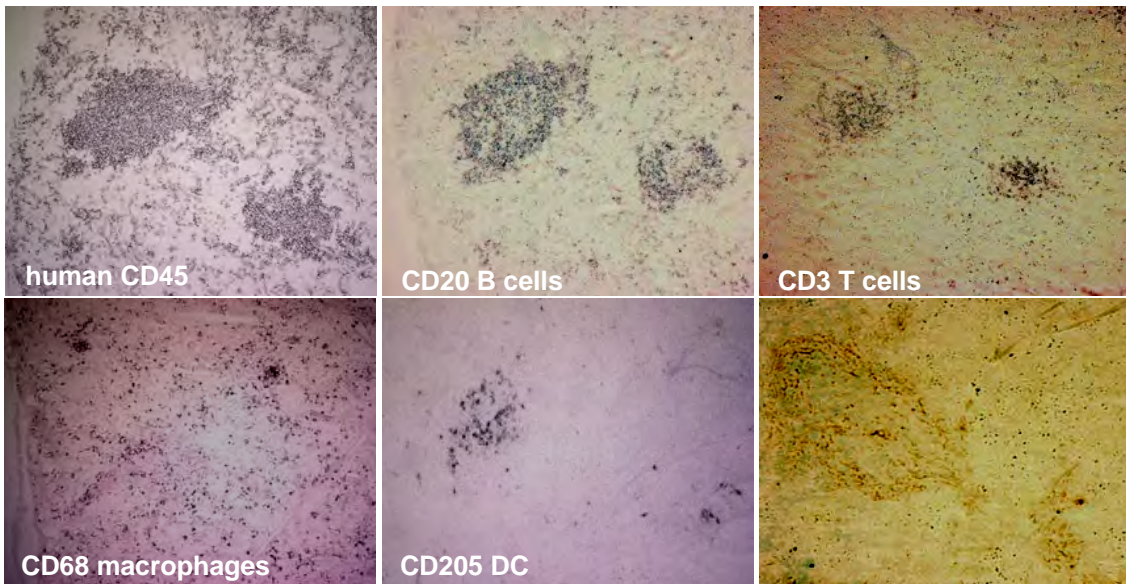


Figure 3. Human mast cell development in the mouse lung and gastric stomach. (A) RT-PCR analysis for tryptase and chymase mRNA expression. The lung and gastric stomach of NOG mice after the transplantation of human CD34 cells expressed human mast cell-specific tryptase and chymase mRNA. CB-hCMC indicates cord blood-derived human cultured mast cells. (B-C) Histologic findings for lung (B) and gastric stomach (C). Very small numbers of formalin resistant toluidine blue cells appeared in the lung 20 weeks after the transplantation and, in sequential sections, were almost identical to tryptase cells (arrows). In gastric stomach, formalin resistant toluidine blue cells were identified in both the mucosa and submucosa. In the acetone fixed frozen thin sections stained with antichymase mAb, chymase cells (white arrowheads) were located only in submucosal lesions. Magnification, x 200 (toluidine blue and tryptase) and x 100 (chymase). (This research was originally published in *Blood*. Kambe N, Hiramatsu H, Shimonaka M, et al. Development of both human connective tissue-type and mucosal-type mast cells in mice from hematopoietic stem cells with identical distribution pattern to human body. *Blood*. 2004; 103: 860-867. ©the American Society of Hematology.)

Reconstitution of human lymphoid-like structure in NOG spleen



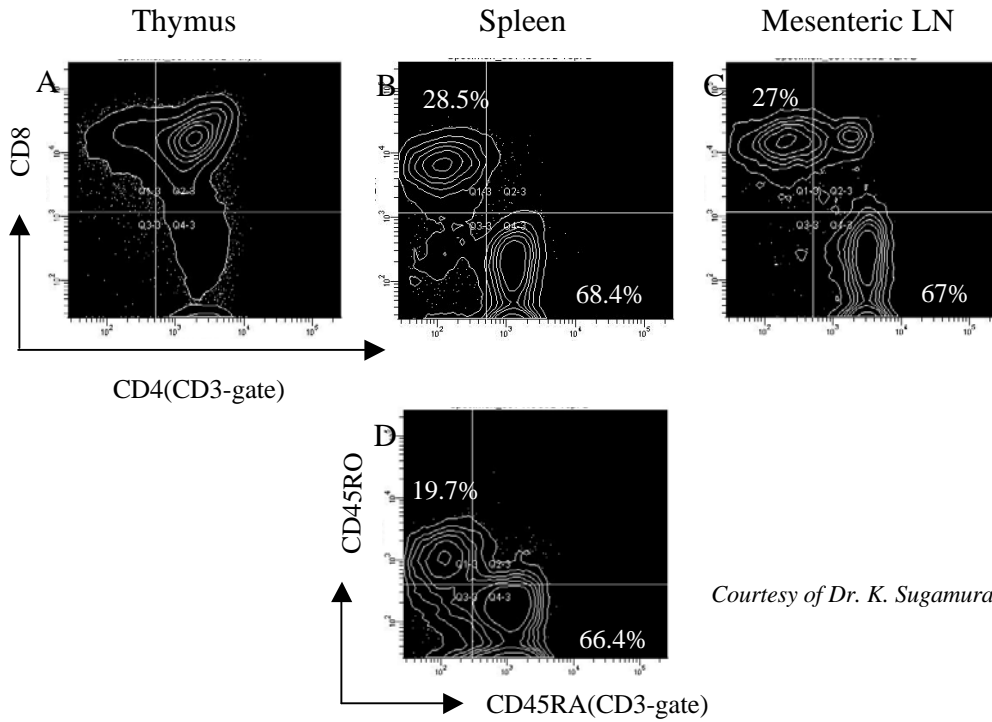
Human lymphoid follicle like structures (White arrow) were observed in spleen of NOG mice at 18 weeks after human HSC transfer



(This research was originally published in Blood. Watanabe, S. *et al.* Hematopoietic stem cell-engrafted NOD/SCID/IL2Rgamma null mice develop human lymphoid systems and induce long-lasting HIV-1 infection with specific humoral immune responses. Blood. 2007; 109: 212-218. © the American Society of Hematology.)

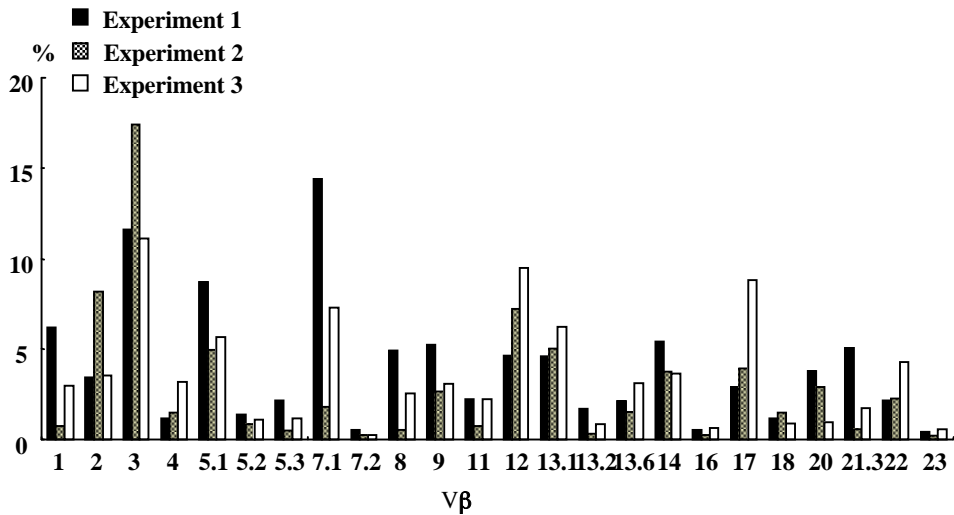
Human B, T cells and other monocytes/macrophages and DCs, but not FDCs were associated with the generation of lymphoid follicle-like structures observed in the spleen.

Human T cells in NOG mice of 4 months after transplantation



Courtesy of Dr. K. Sugamura Tohoku University.

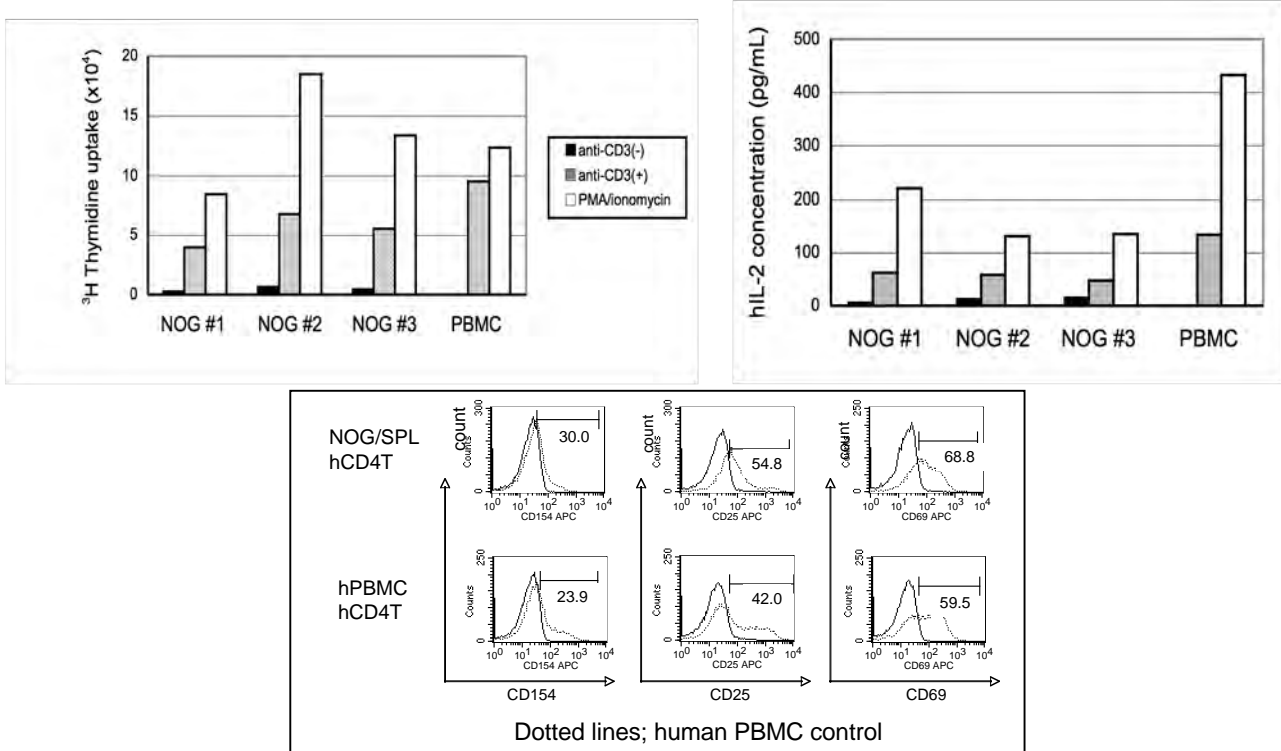
TCR V β repertoire analysis of human T cells in spleen.



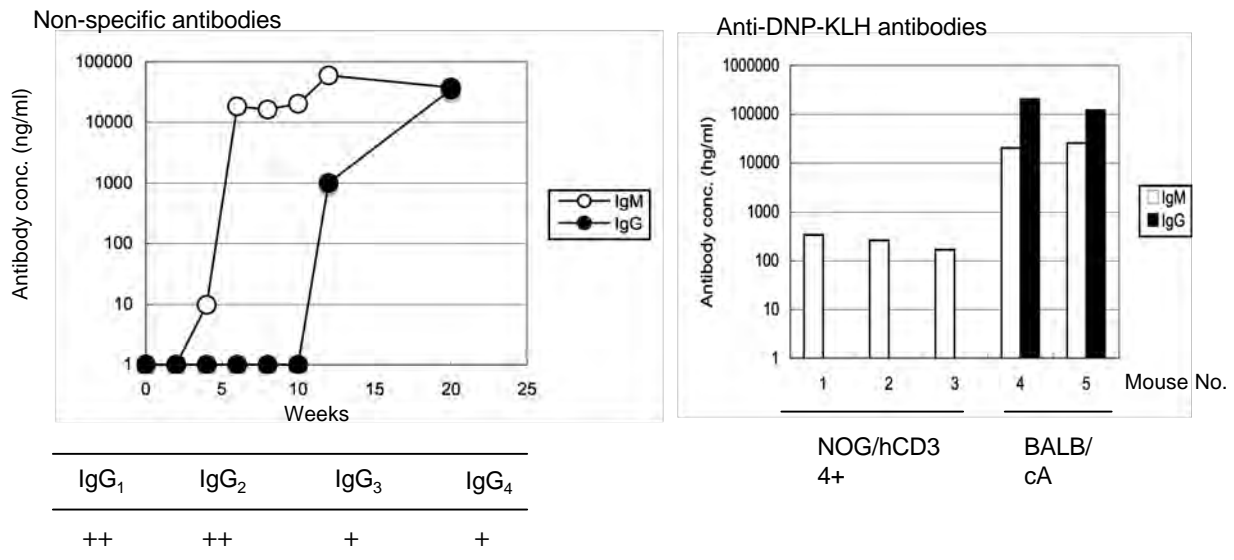
(This research was originally published in Blood. Hiramatsu, H., R. Nishikomori, T. Heike, M. Ito, K. Kobayashi, K. Katamura, and T. Nakahata. Complete reconstitution of human lymphocytes from cord blood CD34⁺ cells using the NOD/SCID/gammacnull mice model. Blood. 2003; 102: 873-880. © the American Society of Hematology.)

At 4 to 6 months after transplantation of 2×10^4 to 5×10^4 CB CD34⁺ cells, spleen cells were taken and the TCR V β repertoire was analyzed by flow cytometry using a panel of 24 different antibodies. The results of three independent experiments are shown.

Activation of human T cells in the spleen of humanized NOG mouse by CD3 stimulation



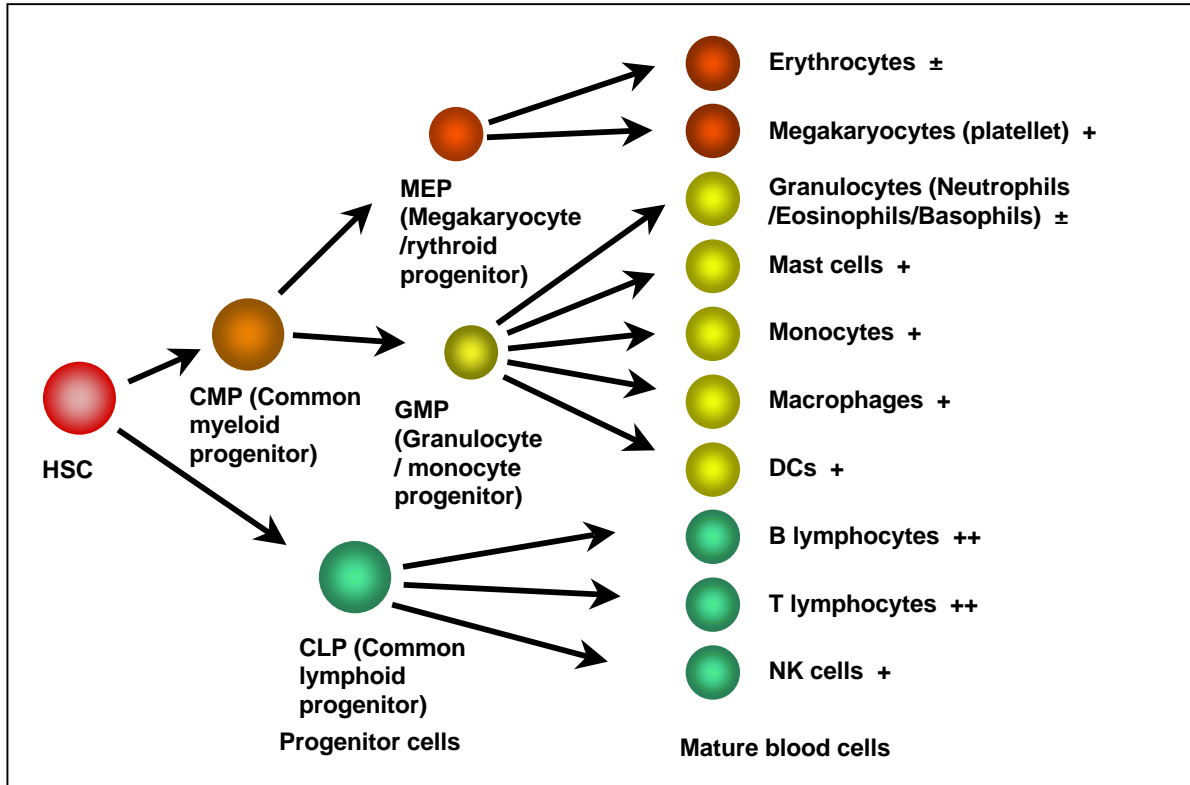
Antibody production in NOG mice transferred human HSCs



NOG mice transferred human HSCs can produce IgM and IgG antibodies. However, antigen-specific IgG but not IgM antibodies cannot be produced.

Courtesy of Dr. S. Habu, Tokai University

Summary of human hematopoietic cells differentiated from human cord blood derived CD34⁺ cells in NOG mice



Clonal analysis of short-term and long-term human HSCs

Hematopoiesis is a dynamic and strictly regulated process orchestrated by self-renewing hematopoietic stem cells (HSCs) and the supporting microenvironment. However, the exact mechanisms by which individual human HSCs sustain hematopoietic homeostasis remain to be clarified. To understand how the long-term repopulating cell (LTRC) activity of individual human HSCs and the hematopoietic hierarchy are maintained in the bone marrow (BM) microenvironment, we traced the repopulating dynamics of individual human HSC clones using viral integration site analysis. Our study presents several lines of evidence regarding the *in vivo* dynamics of human hematopoiesis. First, human LTRCs exist as a population of CD34⁺CD38^{neg} cells that localized to the stem cell niches and maintained their stem cell activities while being in a quiescent state. Second, clonally distinct LTRCs controlled hematopoietic homeostasis and created a stem cell pool hierarchy by a symmetric self-renewal division that produced lineage-restricted short-term repopulating cells and long-lasting LTRCs. Third, we demonstrated that quiescent LTRC clones expanded remarkably to reconstitute the hematopoiesis of the secondary recipient. Finally, we further demonstrated that human mesenchymal stem cells differentiated into key components of the niche and maintained LTRC activity by closely interacting with quiescent human LTRCs, resulting in more LTRCs. Taken together, this study provides a novel insight into repopulation dynamics, turnover, hierarchical structure, and the cell cycle status of human HSCs in the recipient BM microenvironment. *STEM CELLS* 2008;26:3228–3236

(Reprinted from *Stem Cells*, 26 (2008) p3232, Yahata T, et al. "Quiescent human hematopoietic stem cells in the bone marrow niches organize hierarchical structure of hematopoiesis." AlphaMed Press)

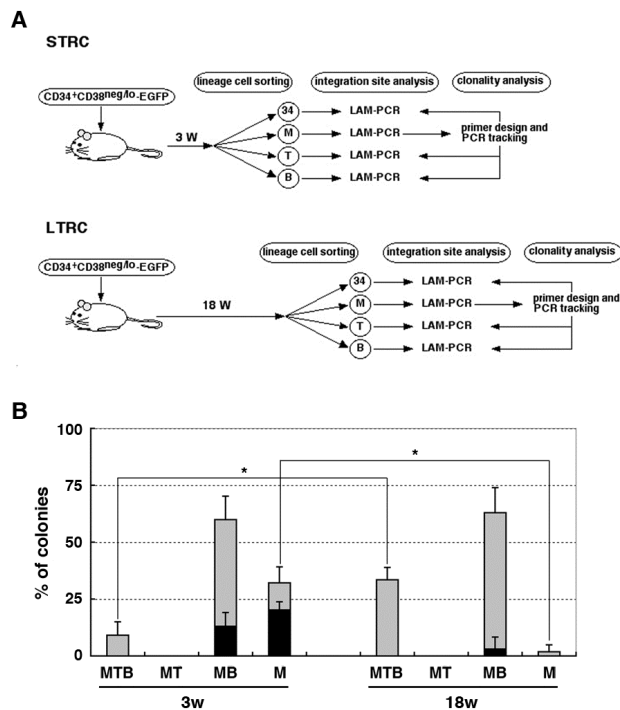


Figure 1. Differentiation ability and self-renewal capacity of individual SRC clones

(A) Study design for clonal analysis of STRC and LTRC activity. 34: CD34⁺ stem/progenitor cells. M: CD33⁺ myeloid lineage cells. B: CD19⁺ B-lymphoid lineage cells. T: CD3⁺ (spleen) or CD4/CD8 DP (thymus) T-lymphoid lineage cells. (B) Relative frequencies of each clone type. Gray areas in each bar represent the clones detected in CD34⁺ cells, and black areas represent the clones not detected in CD34⁺ cells. A total of 116 clones were analyzed (Table S1). Mean ± SD of 4 independent experiments are shown. *, *P* < 0.01. (Reprinted from *Stem Cells*, 26 (2008) p3232, Yahata T, et al. "Quiescent human hematopoietic stem cells in the bone marrow niches organize hierarchical structure of hematopoiesis." AlphaMed Press)

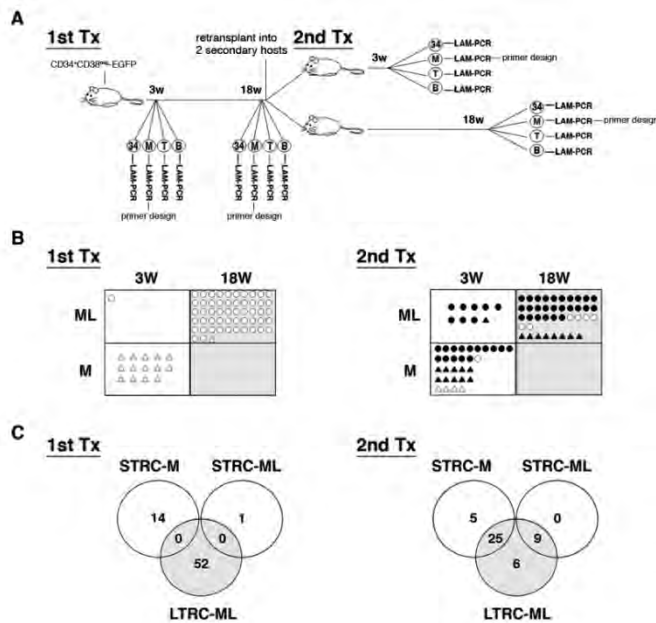


Figure 2. Differentiation ability and self-renewal capacity of individual SRC clones

(A) Study design for clonal analysis of STRC and LTRC activity. 34: CD34⁺ stem/progenitor cells. M: CD33⁺ myeloid lineage cells. B: CD19⁺ B-lymphoid lineage cells. T: CD3⁺ (spleen) or CD4/CD8 DP (thymus) T-lymphoid lineage cells. (B) Relative frequencies of each clone type. Gray areas in each bar represent the clones detected in CD34⁺ cells, and black areas represent the clones not detected in CD34⁺ cells. A total of 116 clones were analyzed (Table S1). Mean \pm SD of 4 independent experiments are shown. *, $P < 0.01$. (Reprinted from *Stem Cells*, 26 (2008) p3232, Yahata T, et al. "Quiescent human hematopoietic stem cells in the bone marrow niches organize hierarchical structure of hematopoiesis." AlphaMed Press)

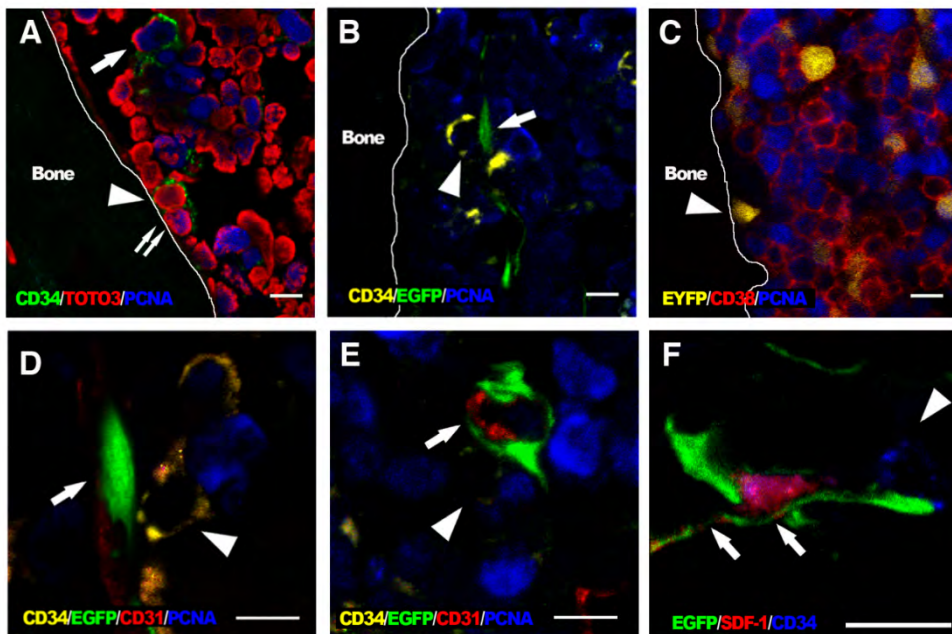


Figure 3. Quiescent human LTRCs interacted with niche components in the endosteal region

(A) Two human CD34⁺ cells, a PCNA-negative (arrowhead) and a PCNA-positive (double arrows), are adjacent to each other and are attached to the endosteum. A large CD34⁺PCNA-positive cell is found away from endosteum (arrow). (B) A PCNA-negative CD34⁺ cell (arrowhead) interacts with CD31-expressing murine endothelial cells (arrow) in the endosteal region. (C) Majority of human cells are positive for CD38. A CD38^{neg}PCNA-negative EYFP-transduced human cell is attached to the endosteum (arrowhead). (D and E) EGFP-marked HMRCs differentiate into fibroblastic reticular cells that associate with CD31⁺ vascular cells. PCNA-negative quiescent CD34⁺ cells (arrowheads) interact with human reticular cells (arrow). (F) HMRCs in the vascular niche express SDF-1 (arrows) and interact with a CD34⁺ cell (arrowhead). All bars in the figure represent 10 μ m.

(Reprinted from *Stem Cells*, 26 (2008) p3233, Yahata T, et al. "Quiescent human hematopoietic stem cells in the bone marrow niches organize hierarchical structure of hematopoiesis." AlphaMed Press)

5. Applications

5-1. Infectious disease model

5-1-1. HIV-1 infection

1. Watanabe, S., S. Ohta, M. Yajima, K. Terashima, M. Ito, H. Mugishima, S. Fujiwara, K. Shimizu, M. Honda, N. Shimizu, and N. Yamamoto. 2007. Humanized NOD/SCID/IL2R $\{\gamma\}$ null Mice Transplanted with Hematopoietic Stem Cells under non-Myeloablative Condition Show Prolonged Lifespans and Allow Detailed Analysis of HIV-1 Pathogenesis. *J Virol.*2.
2. Watanabe, S., K. Terashima, S. Ohta, S. Horibata, M. Yajima, Y. Shiozawa, M. Z. Dewan, Z. Yu, M. Ito, T. Morio, N. Shimizu, M. Honda, and N. Yamamoto. 2007. Hematopoietic stem cell-engrafted NOD/SCID/IL2R γ null mice develop human lymphoid systems and induce long-lasting HIV-1 infection with specific humoral immune responses. *Blood* 109:212-218.

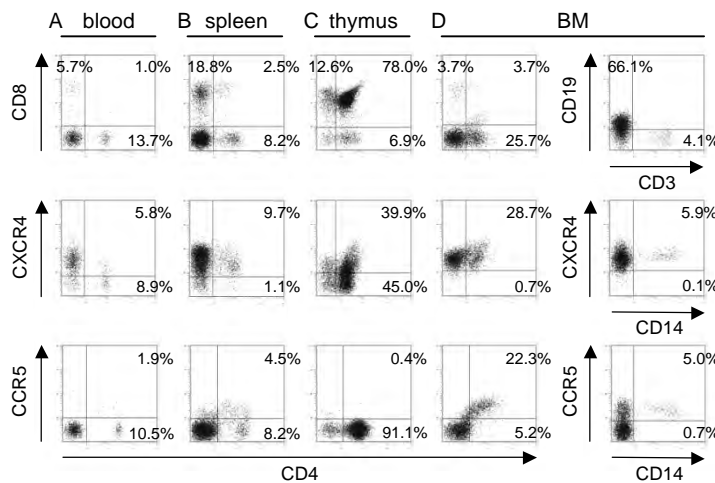


Figure 1. Surface expression of HIV-1 coreceptors on CD4 cells in various organs of mice 4 months after transplantation.

A representative FACS profile of human CXCR4 and CCR5 on CD4 cells shows the existence of CXCR4CD4 and CCR5CD4 cells in blood (A), spleen (B), and BM (D), but no CCR5CD4 cells in the thymus (C). BM results show that many CD4 cells are neither CD3 T cells nor CD14 monocytes. A gate was set on the human CD45 population. (This research was originally published in *Blood*. Watanabe S, Terashima K, Ohta S, et al. Hematopoietic stem cell-engrafted NOD/SCID/IL2R γ null mice develop human lymphoid systems and induce long-lasting HIV-1 infection with specific humoral immune responses. *Blood*. 2007;109:215. ©the American Society of Hematology.)

Table 1. Comparison of viral RNA copies in Plasma and HIV-DNA copies in the spleen, BM, and thymus from hNOG mice receiving low- and high-dose viral inoculations

Mouse ID no.	HIV strain	TCID ₅₀	Time after inoculation, d	RNA viral copies/mL	CD4/CD8 ratio	HIV-DNA copies/10 ⁶ human cells		
						Spleen	BM	Thymus
Low-dose viral inoculation group								
113-1	HIV-1 _{JRCSF}	200	18	6 240	1.8	34 177	11 785	3 495
112-2	HIV-1 _{JRCSF}	200	18	<500	1.2	< 100	< 100	< 100
113-2	HIV-1 _{JRCSF}	200	40	6 177	1.6	25 855	27 920	3 473
112-3	HIV-1 _{JRCSF}	200	40	<500	0.9	< 100	< 100	<100
112-4	HIV-1 _{Mdp}	180	18	72 477	1.3	18 873	100	ND
113-4	HIV-1 _{Mdp}	180	40	70 667	0.3	4 947	653	32 163
112-1	HIV-1 _{Mdp}	180	40	<500	0.9	< 100	< 100	< 100
High-dose viral inoculation group								
136-3	HIV-1 _{JRCSF}	65 000	25	252 381	0.8	958 871	1 797 600	232 155
136-2	HIV-1 _{JRCSF}	65 000	29	50 167	0.7	41 172	54 521	8 600
141-1	HIV-1 _{JRCSF}	65 000	30	67 667	2.2	27 735	52 430	429
161-3	HIV-1 _{JRCSF}	65 000	30	13 847	0.9	104 466	14 653	111 080
157-3	HIV-1 _{Mdp}	20 000	31	1 253 925	0.5	41 053	56 802	976 556
157-4	HIV-1 _{Mdp}	20 000	31	147 973	0.6	3 634	262	40 796
161-6	HIV-1 _{Mdp}	20 000	31	108 073	1.7	4 991	< 100	3 673

Seven mice inoculated with a low infection dose of HIV-1_{JRCSF} (200 TCID₅₀) or HIV-1_{JRCSF} (180 TCID₅₀), and 7 mice receiving a high dose of HIV-1_{JRCSF} (65000 TCID₅₀) or HIV-1_{JRCSF} (20000 TCID₅₀) were listed. ND indicates not done.

(This research was originally published in *Blood*. Watanabe S, Terashima K, Ohta S, et al. Hematopoietic stem cell-engrafted NOD/SCID/IL2R γ null mice develop human lymphoid systems and induce long-lasting HIV-1 infection with specific humoral immune responses. *Blood*. 2007;109:216. ©the American Society of Hematology.)

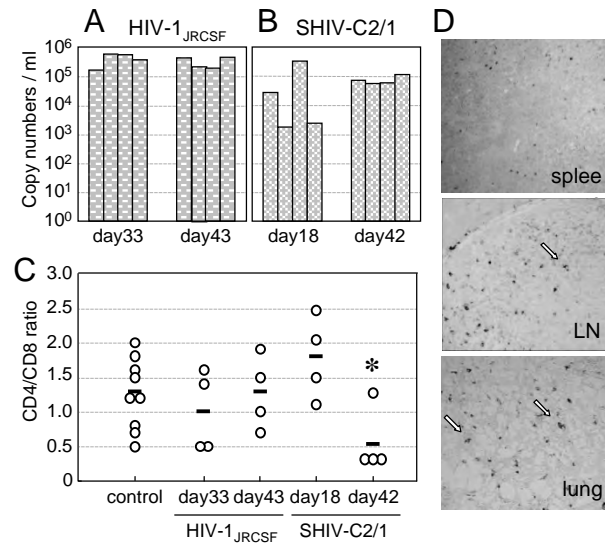


Figure 2. The numbers of RNA viral copies in plasma, CD4/CD8 T-cell ratios in the spleen, and p24 detection in the immunohistochemistry of HIV/SHIV-infected mice.

(A) Viral copy numbers of 8 mice inoculated with a high infectious dose of HIV-1_{JRCSF} (65 000 TCID₅₀) and killed on days 33 and 43 after inoculation. (B) Viral copy numbers of 8 mice inoculated with a high infectious dose of SHIV-C2/1 (50 000 TCID₅₀) and killed on days 18 and 42 after inoculation. Note that all the mice showed high levels of viremia that lasted more than 40 days after inoculation. (C) CD4/CD8 cell ratios in the spleens of 16 infected mice and 9 uninfected control mice. Control mice were not inoculated with HIV/SHIV and were killed on days 105 to 166 after stem cell transplantation. There was no significant rapid loss of CD4 cells in HIV-1_{JRCSF}-infected mice, while a decline of the CD4/CD8 ratio was detected in SHIV-C2/1-infected mice on day 42 after infection compared with uninfected control mice (*P < .05). The short bars indicate the means of each group. (D) P24 cells are clearly observed in the spleen, LNs, and lungs. Arrow indicates p24 positive for macrophage-like cells. Original magnification, x 100.

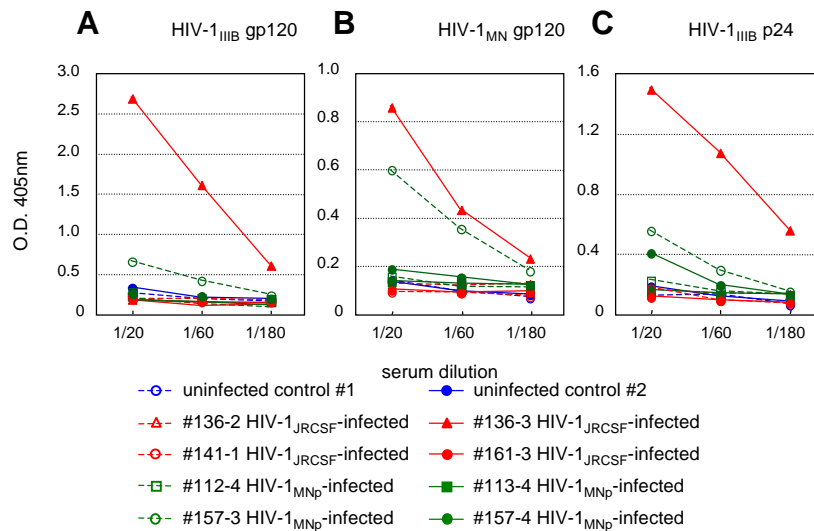


Figure 3. Detection of anti-HIV-1 antibodies from the plasma of HIV-1-infected mice.

An ELISA assay was conducted by using plasma from 14 mice inoculated with either HIV-1_{JRCSF} or HIV-1_{MNp}, and from 2 uninfected control mice. Representatives (n = 8) of the 14 HIV-1-inoculated mice, and the 2 uninfected mice, are shown in the panels. Measurements of specific human antibodies for HIV-1_{IIIB} gp120 (A), HIV-1_{MN} gp120 (B), and HIV-1_{IIIB} p24 antigens (C) were shown. Results are expressed as the means from triplicate assays in 3 different experiments.

(This research was originally published in Blood. Watanabe S, Terashima K, Ohta S, et al. Hematopoietic stem cell-engrafted NOD/SCID/IL2Rgamma null mice develop human lymphoid systems and induce long-lasting HIV-1 infection with specific humoral immune responses. Blood. 2007;109:216-217. ©the American Society of Hematology.)

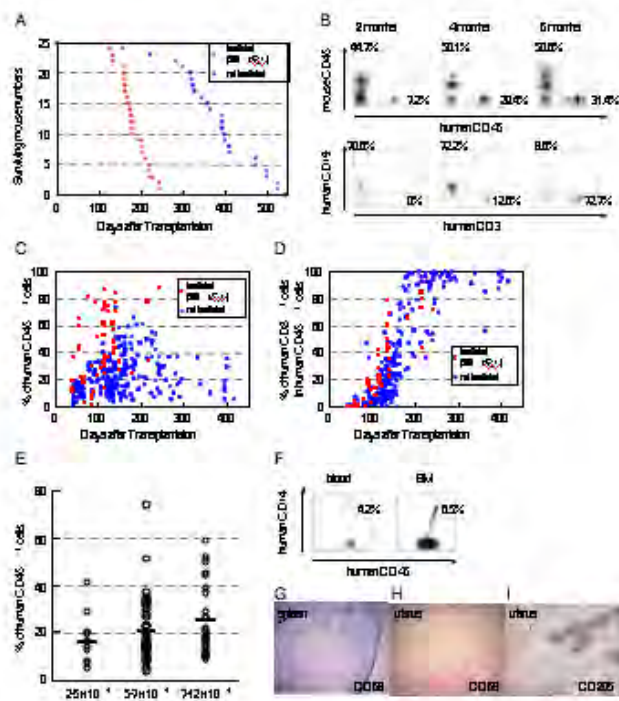


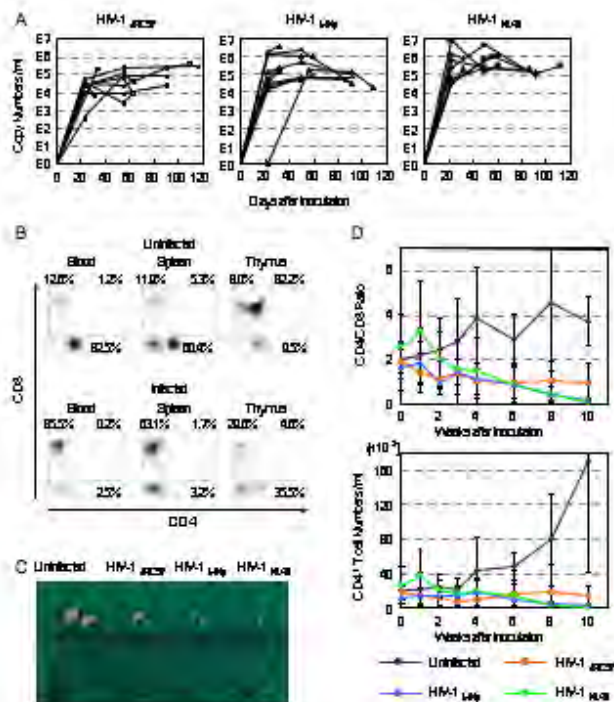
Figure 4. Human cell generation in hematopoietic stem cell-engrafted hNOG mice with or without myeloablation.

(A) Life spans of NOG mice transplanted with human stem cells after receiving 300 cGy irradiation (n = 25) or not receiving irradiation (n = 25). (B) Representative flow cytometric profiles of the mice from 2 to 6 months after transplantation without irradiation. The ratio of human to murine CD45+ cells and that of human CD3+ cells to CD19+ cells are shown. Note that the mice generated human CD45+ leukocytes that eventually developed human CD19+ B cells first and then CD3+ T cells. (C and D) Percentages of human CD45+ cells (C) and CD3+ T cells in human CD45+ cells (D) in peripheral blood from 65 mice that received 300 cGy irradiation and 222 nonirradiated mice 40 to 413 days after transplantation. (E) Summary of engraftment levels in nonirradiated mice transplanted with 2×10^4 to 5×10^4 cells (n = 11), 5×10^4 to 7×10^4 cells (n = 53), or 7×10^4 to 12×10^4 (n = 30) human stem cells. Percentages of human CD45+ leukocytes in peripheral blood during 4 to 5 months after transplantation were shown. The horizontal black bars indicate the averages of the groups. (F to I) Flow cytometric analysis and immunohistochemical analysis of the expression of myelomonocytic markers in nonirradiated mice 4 months after transplantation. Human CD14+ monocytes/macrophages were recognized in peripheral blood and BM (F). A gate was set on the human CD45+ population. Human CD68+ macrophages and CD205+ DCs were also detected in spleen (G) and uterus (H and I). Visualization was performed with 5-bromo-4-chloro-3-indolylphosphate (BCIP). The original magnifications were x100 (G and H) and x200 (I).

(J Virol. 2007;81:13260. Watanabe S, Ohta S, Yajima M, et al. Humanized NOD/SCID/IL2Rgamma(null) mice transplanted with hematopoietic stem cells under nonmyeloablative conditions show prolonged life spans and allow detailed analysis of human immunodeficiency virus

Figure 5. Long-lasting viremia and CD4+ T-cell depletion in R5- and X4-tropic HIV-1-infected hNOG mice.

(A) Viral copy numbers in plasma from 29 mice intravenously inoculated with R5-tropic HIV-1_{JRCSF} (65,000 TCID₅₀; n = 11), X4-tropic HIV-1_{MNP} (20,000 TCID₅₀; n = 10), and X4-tropic HIV-1_{NL4-3} (60,000 TCID₅₀; n = 8). RNA viral copy numbers were measured using a real-time PCR quantification assay as previously described (22). (B) The percentages of CD- CD8+ (top left), CD4+ CD8- (top right), and CD4+ CD8- (bottom right) cells in blood, spleen, and thymus from a uninfected control mouse and a V-INL4-3-infected mouse (32 days postinfection). These two mice were constructed with HSCs from the same cord blood donor, and sacrificed 181 and 169 days after transplantation, respectively. A gate was set on the human CD45+ population. (C) Comparison of the apparent size of mesenteric LN from uninfected mice or mice infected with HIV-1_{JRCSF} (109 days postinfection), HIV-1_{MNP} (109 days postinfection), or HIV-1_{NL4-3} (112 days postinfection). A uninfected control mouse was sacrificed 249 days after transplantation, and three HIV-1-infected mice were sacrificed 246, 246, and 249 days after transplantation. (D) Comparison of CD4/CD8 T-cell ratios and absolute CD4+ T-cell numbers in peripheral blood from uninfected control mice (n = 7), R5-tropic HIV-1_{JRCSF}-infected mice (n = 7), X4-tropic HIV-1_{MNP}-infected mice (n = 5), and X4-tropic HIV-1_{NL4-3}-infected mice (n = 6). Results are expressed as means / standard deviations (error bars). (J Virol. 2007;81:13261. Watanabe S, Ohta S, Yajima M, et al. Humanized NOD/SCID/IL2Rgamma(null) mice transplanted with hematopoietic stem cells under nonmyeloablative conditions show prolonged life spans and allow detailed analysis of human immunodeficiency virus type 1 pathogenesis., reproduced/amended with permission from American Society for Microbiology)



5-1-2. ATL infection

We established a novel experimental model for human T-cell leukemia virus type 1 (HTLV-1)-induced tumor using NOD-SCID/ cnull (NOG) mice. This model is very useful for investigating the mechanism of tumorigenesis and malignant cell growth of adult T-cell leukemia (ATL)/lymphoma, which still remains unclear. Nine HTLV-1-infected cell lines were inoculated subcutaneously in the postauricular region of NOG mice. As early as 2 to 3 weeks after inoculation, seven cell lines produced a visible tumor while two transformed cell lines failed to do so. Five of seven lines produced a progressively growing large tumor with leukemic infiltration of the cells in various organs that eventually killed the animals. Leukemic cell lines formed soft tumors, whereas some transformed cell lines developed into hemorrhagic hard tumors in NOG mice. One of the leukemic cell lines, ED-40515(), was unable to produce visible tumors in NOD-SCID mice with a common γ -chain after 2 weeks. In vivo NF- κ B DNA binding activity of the ED-40515() cell line was higher and the NF- κ B components were changed compared to cells in vitro. Bay 11-7082, a specific and effective NF- κ B inhibitor, prevented tumor growth at the sites of the primary region and leukemic infiltration in various organs of NOG mice. This in vivo model of ATL could provide a novel system for use in clarifying the mechanism of growth of HTLV-1-infected cells as well as for the development of new drugs against ATL.

(J Virol. 2003;77:5286. Dewan MZ, Terashima K, Taruishi M, et al. Rapid tumor formation of human T-cell leukemia virus type 1-infected cell lines in novel NOD-SCID/gammac(null) mice: suppression by an inhibitor against NF-kappaB., reproduced/amended with permission from American Society for Microbiology)

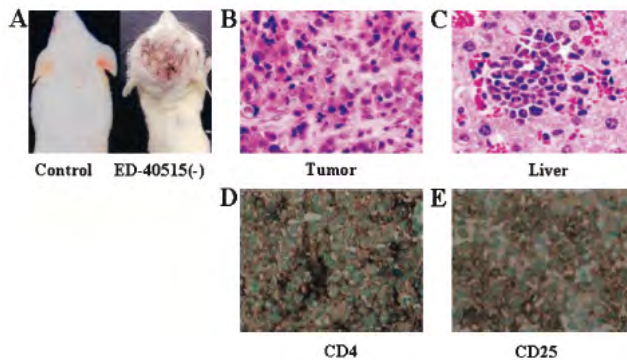


Figure 1. Tumor growth and infiltration in NOG mice.

(A) Photographs of normal NOG mice and those inoculated with ED-40515(-) cells subcutaneously in the postauricular region after 3 weeks. H&E staining of tumor tissue of an ED-40515(-) injected mouse (B) and a section of the tumor-bearing liver of an SLB-1-inoculated mouse (C). In vivo expression of CD4 and CD25 are revealed by immunohistochemistry. Immunohistochemical staining using anti-CD4 (D) and anti-CD25 (E) was conducted on tumor tissues from mice 2 weeks after inoculation of the ED-40515(-) cell line.

(J Virol. 2003;77:5289. Dewan MZ, Terashima K, Taruishi M, et al. Rapid tumor formation of human T-cell leukemia virus type 1-infected cell lines in novel NOD-SCID/gammac(null) mice: suppression by an inhibitor against NF-kappaB., reproduced/amended with permission from American Society for Microbiology)

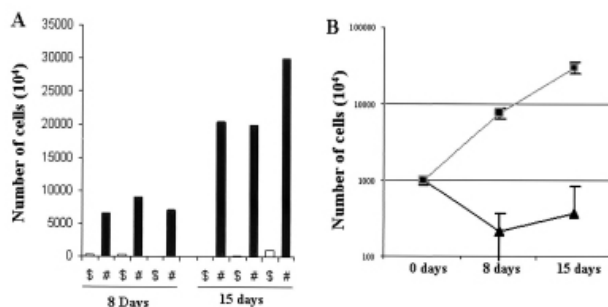


Figure 2. Comparison of ED-40515(-) cell growth

in NOG and NOD-SCID mice. To evaluate the in vivo growth pattern of tumor cells in SCID mice, we inoculated the ED-40515(-) cell line (10^7) in both NOD-SCID and NOG mice. (A) Tumor cells obtained from mice on day 8 and 15 were counted by the trypan blue method. Open and black bars represent the number of cells in individual NOD-SCID (\$) and NOG (#) mice, respectively. (B) Mean results standard error (error bars) from three mice of individual strains on day 8 and 15 (the squares and triangles represent NOG and NOD-SCID mice, respectively)

(J Virol. 2003;77:5290. Dewan MZ, Terashima K, Taruishi M, et al. Rapid tumor formation of human T-cell leukemia virus type 1-infected cell lines in novel NOD-SCID/gammac(null) mice: suppression by an inhibitor against NF-kappaB., reproduced/amended with permission from American Society for Microbiology).

5-1-3. EBV infection

The functional human immune system, including T, B, and natural killer lymphocytes, is reconstituted in NOD/Shi-scid/IL-2R null (NOG) mice that receive hematopoietic stem cell transplants. Here, we show that these humanized mice can recapitulate key aspects of Epstein-Barr virus (EBV) infection in humans. Inoculation with 1×10^3 TD₅₀ (50% transforming dose) of EBV caused B cell lymphoproliferative disorder, with histopathological findings and latent EBV gene expression remarkably similar to that in immunocompromised patients. Inoculation with a low dose of virus (1×10^1 TD₅₀), in contrast, resulted in apparently asymptomatic persistent infection. Levels of activated CD8⁺ T cells increased dramatically in the peripheral blood of infected mice, and enzyme-linked immunospot assay and flow cytometry demonstrated an EBV-specific T cell response. Immunoglobulin M antibody specific to the EBV-encoded protein BFRF3 was detected in serum from infected mice. The NOG mouse is the most comprehensive small-animal model of EBV infection described to date and should facilitate studies of the pathogenesis, prevention, and treatment of EBV infection.

Yajima M, Imadome K, Nakagawa A, et al. A new humanized mouse model of Epstein-Barr virus infection that reproduces persistent infection, lymphoproliferative disorder, and cell-mediated and humoral immune responses. *J Infect Dis.* 2008;198:673-682.

© 2008 by University of Chicago Press

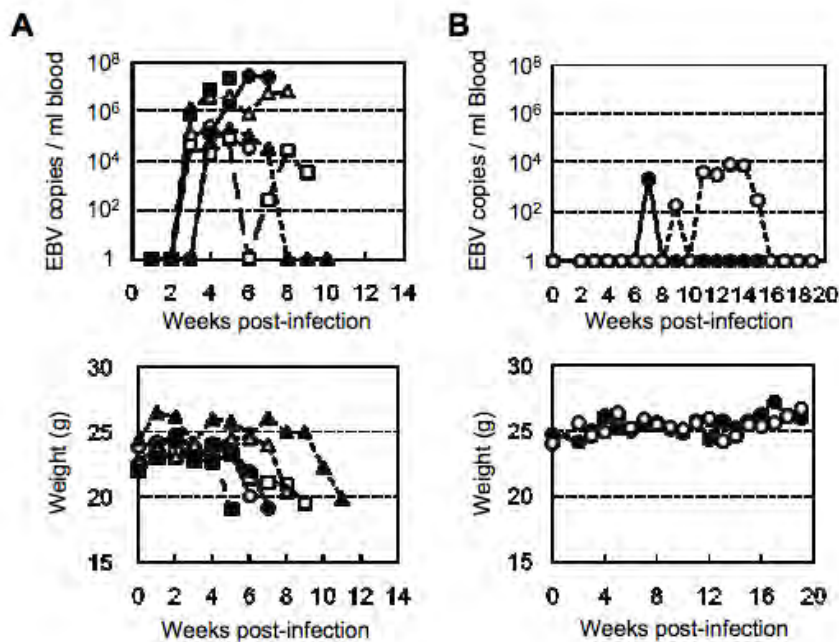


Figure 1. Peripheral blood Epstein Barr virus (EBV) DNA load and body weight in humanized NOG (hNOG) mice infected with EBV. A, Infection at a high dose of virus. Six mice were inoculated intravenously with 1×10^3 TD₅₀ of EBV. Peripheral blood EBV DNA load (upper panels) and body weight (lower panels) were then determined weekly. Each symbol in the graphs represents an individual mouse. Interruption of records indicates the death or killing of a mouse. B, Infection at lower doses. Peripheral blood EBV DNA load (upper panel) and body weight (lower panel) of 2 mice inoculated with low doses of EBV (black circle, 1×10^1 TD₅₀; white circle, 1×10^1 TD₅₀) are shown. © 2008 by University of Chicago Press

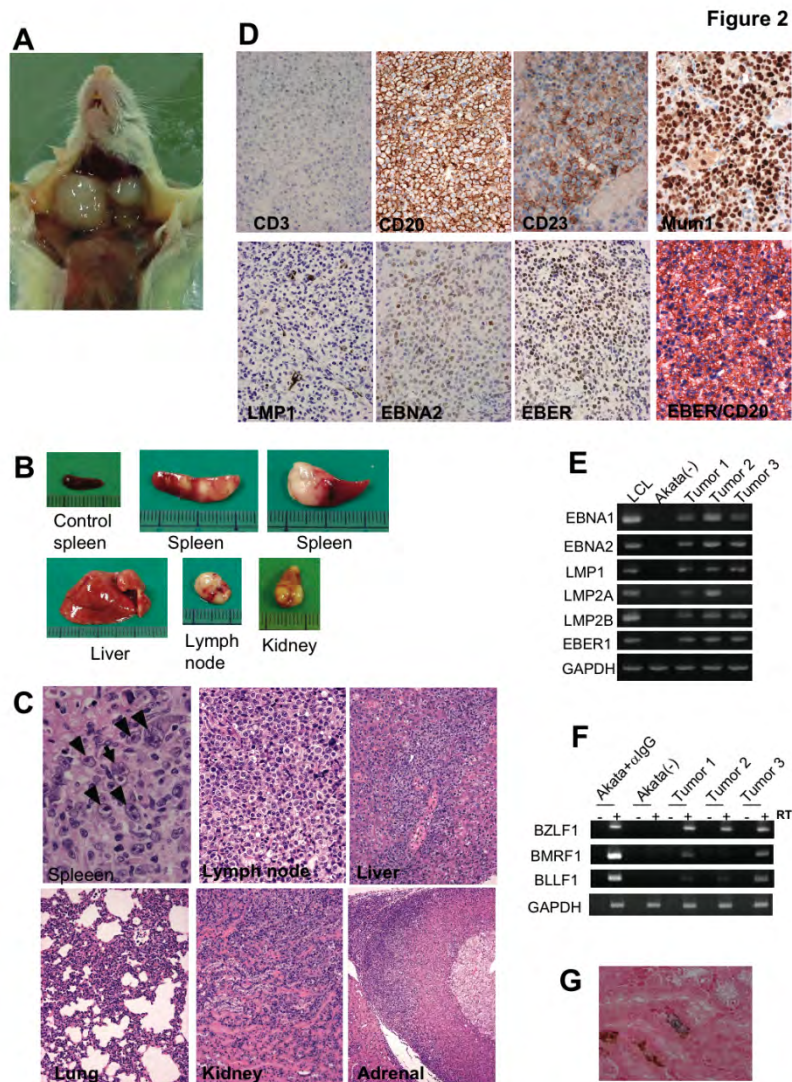


Figure 2. Pathological analyses of Epstein-Barr virus (EBV)-infected humanized NOG (hNOG) mice. *A*, Photograph of an EBV-infected mouse showing tumors in the cervical area. *B*, Photographs of spleens, liver, lymph node, and kidney from EBV-infected mice with lymphoproliferative disorder. The upper left panel shows the spleen from an uninfected mouse. *C*, Photomicrographs of hematoxylin-eosin-stained tissues from mice with lymphoproliferative disorder. The arrow indicates a Reed-Sternberg-like cell, and the arrowheads indicate Hodgkin-like cells. Original magnifications, 1000 for spleen, 400 for lymph node, and 200 for liver, lung, kidney, and adrenal gland. *D*, Immunohistochemical staining for lymphocyte surface markers (CD3, CD20, CD23, and Mum1) and EBV-encoded proteins (latent membrane protein [LMP] 1 and Epstein-Barr nuclear antigen [EBNA] 2), as well as in situ hybridization for EBV-encoded small RNA (EBER), in a lymph node from a mouse with lymphoproliferative disorder. The bottom right panel represents double staining for EBER and CD20. Original magnifications, x200 for all except EBER/CD20, which is x400. *E* and *F*, Reverse-transcription polymerase chain reaction detection of latent-cycle (*E*) and lytic-cycle (*F*) EBV gene expression in tumors from EBV-infected hNOG mice. Spleen tumors from 3 different mice were examined for the expression of EBNA1, EBNA2, LMP1, LMP2A, LMP2B, EBER1, BZLF1, BMRF1, and BLLF1. RNA samples from a lymphoblastoid cell line (LCL) (*E*) and anti-IgG treated Akata cells (*F*) were used as positive controls, and an RNA sample from EBV-negative Akata cells (*E* and *F*) was used as a negative control. Assays were done with (+) or without (-) reverse transcriptase (RT) in panel *F*. Expression of GAPDH was examined as a reference. *G*, Double staining of EBER and CD20 in the liver of an hNOG mouse that was persistently infected with EBV without developing lymphoproliferative disorder. EBER is stained navy in the nucleus, and CD20 is stained brown in the membrane. Original magnification, x1000.

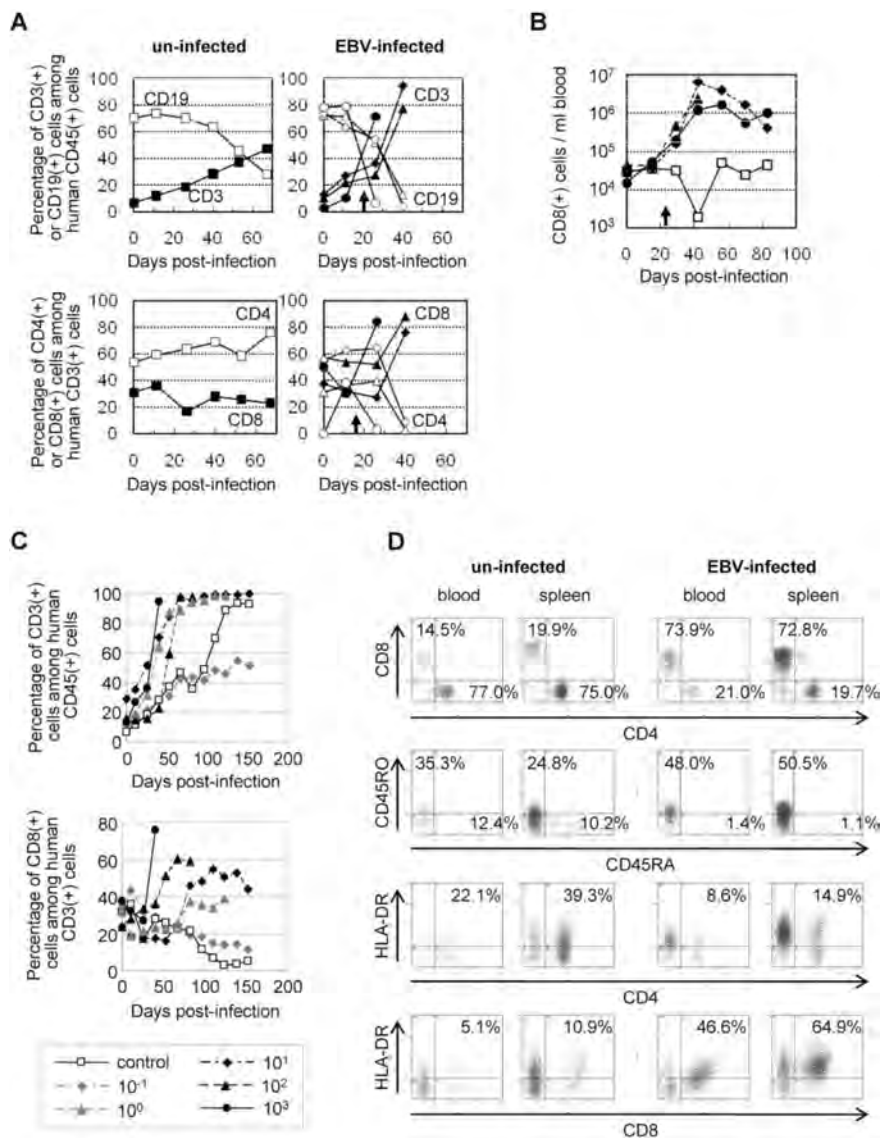


Figure 3. Surface marker expression by peripheral blood T cells in Epstein-Barr virus (EBV)-infected humanized NOG (hNOG) mice. *A*, Changes in the percentages of CD3⁺ T cells and CD19⁺ B cells among human CD45 leukocytes (*upper panels*) and in the percentages of CD8⁺ cells and CD4⁺ cells among CD3⁺ cells (*lower panels*) after infection with EBV. Results obtained from 3 EBV-infected mice and an uninfected mice are shown. White symbols indicate the percentage of CD19⁺ cells (*upper panels*) or CD4⁺ cells (*lower panels*); black symbols indicate the percentage of CD3⁺ cells (*upper panels*) or CD8⁺ cells (*lower panels*). A vertical arrow in the graph area shows the time point at which EBV DNA was first detected in peripheral blood. *B*, Changes in the no. of CD8⁺ T cells in the peripheral blood of EBV-infected hNOG mice. White symbols indicate uninfected mice, and black symbols indicate infected mice. Note that cell no. is plotted in a logarithmic scale. *C*, Viral dose-dependent T cell responses in hNOG mice inoculated with serially diluted EBV. Ten-fold serial dilutions of an EBV sample starting from 1 × 10³ TD50 per inoculate were injected intravenously into NOG mice that had undergone transplantation with the same lot of human hematopoietic stem cells (HSCs). Changes in the percentages of CD3⁺ T cells among human CD45⁺ leukocytes (*upper panel*) and in the percentages of CD8⁺ cells among CD3⁺ cells (*lower panel*) after inoculation with EBV are shown. The viral dose for each mouse is shown in the key. *D*, Comparison of surface marker expression between EBV-infected mice and control mice. Two mice that underwent transplantation with the same lot of human HSCs were either inoculated with EBV or left uninfected; 10 weeks after inoculation, mononuclear cells obtained from peripheral blood or spleen were gated for the expression of human CD3 and then examined for the expression of CD8 and CD4 (*top panels*), CD45RO and CD45RA (*second from top*), HLA-DR and CD4 (*second from bottom*), and HLA-DR and CD8 (*bottom*).

© 2008 by University of Chicago Press

5-2. Cancer model

5-2-1. Liver metastasis I

We developed a reliable new model system for assaying liver metastasis using NOD/SCID/ γ_c null (NOG) mice. Seven human pancreatic cancer cell lines were examined for their ability to form diverse metastatic foci in the livers of NOD/SCID and NOG mice. Capan-2 and PL45 showed no metastasis when seeded at up to 10^5 cells in both strains, and no BxPC-3 metastasis was observed in NOD/SCID mice. The NOD/SCID mice model could detect liver metastasis only in the AsPC-1 cell line when inoculated with more than 10^3 cells. In contrast, when inoculated with only 10^2 MIA PaCa-2, AsPC-1 and PANC-1 cells, liver metastasis was evident in 71.4% (5/7), 57.1% (4/7) and 37.5% (3/8) of the NOG mice, respectively. Capan-1 and BxPC-3 cells metastasized when seeded at 10^3 cells in 50% (5/10) and in 12.5% (1/8) of the mice, respectively. Using the NOG mice model system, we established a highly metastatic cell line, liver metastasized-BxPC-3 (LM-BxPC-3), from liver metastatic foci formed by the relatively poorly metastatic parental BxPC-3 cell line. These results demonstrated the feasibility of using the quantitative metastasis model to search for and develop new anti-cancer therapies, and novel drugs against this and other key molecules.

(Reprinted from *Int J Oncol*., Vol.31, H. Suemizu, M. Monnai, Y. Ohnishi, M. Ito, N. Tamaoki, and M. Nakamura. "Identification of a key molecular regulator of liver metastasis in human pancreatic carcinoma using a novel quantitative model of metastasis in NOD/SCID/gammacnull (NOG) mice." p741 (2007), with permission from Spandidos Publications.)

Table 1 Liver metastasis after intrasplenic injection of human pancreatic cancer cells.

Cell line	Cell dose (cells/head)	Number of animal with liver metastasis ^a (metastasis/total)		Metastatic score in NOG mice	
		NOD/SCID	NOG	%T/L ^b (mean \pm SD)	Liver surface area ^c (mm ² , mean \pm SD)
MIA PaCa-2	1×10^4	0/10 (0.0%)	10/10 (100.0%)	60.6 \pm 13.9	1056.0 \pm 338.0
	1×10^3	0/7 (0.0%)	5/6 (83.3%)	ND	ND
	1×10^2	0/6 (0.0%)	5/7 (71.4%)	ND	ND
AsPC-1	1×10^4	8/9 (88.9%)	9/9 (100.0%)	48.2 \pm 12.3	434.4 \pm 77.6
	1×10^3	2/8 (25.0%)	8/8 (100.0%)	ND	ND
	1×10^2	0/6 (0.0%)	4/7 (57.1%)	ND	ND
PANC-1	1×10^4	0/10 (0.0%)	8/8 (100.0%)	26.6 \pm 11.3	374.0 \pm 68.5
	1×10^3	0/6 (0.0%)	6/8 (75.0%)		ND
	1×10^2	0/7 (0.0%)	3/8 (37.5%)	ND	ND
Capan-1	1×10^4	0/10 (0.0%)	9/10 (90.0%)	15.6 \pm 5.3	425.6 \pm 38.5
	1×10^3	0/10 (0.0%)	5/10 (50.0%)	ND	ND
	1×10^2	0/8 (0.0%)	0/8 (0.0%)	ND	ND
BxPC-3	1×10^5	0/8 (0.0%)	8/8 (100.0%)	ND	ND
	1×10^4	0/8 (0.0%)	1/8 (12.5%)	0.0 \pm 0.0	409.4 \pm 37.3
Capan-2	1×10^5	0/8 (0.0%)	0/8 (0.0%)	ND	ND
	1×10^4	ND	0/10 (0.0%)	0.0 \pm 0.0	426.7 \pm 39.1
PL45	1×10^5	0/8 (0.0%)	0/8 (0.0%)	ND	ND
	1×10^4	ND	0/10 (0.0%)	0.0 \pm 0.0	395.0 \pm 36.1

^a Liver metastasis was evaluated 6 weeks after inoculation of 1×10^3 , 10^4 and 10^5 cancer cells, and 8 weeks after inoculation of 10^2 cancer cells. ^b All liver images showing liver metastases in response to injection of 1×10^4 cancer cells were used to calculate the percent tumor occupancy in the liver (T/L). ^c The surface area of the liver was calculated using all liver images obtained from mice that were injected with 1×10^4 cancer cells. ND, not done.
(Reprinted from *Int J Oncol*., Vol.31, H. Suemizu, M. Monnai, Y. Ohnishi, M. Ito, N. Tamaoki, and M. Nakamura. "Identification of a key molecular regulator of liver metastasis in human pancreatic carcinoma using a novel quantitative model of metastasis in NOD/SCID/gammacnull (NOG) mice." p743 (2007), with permission from Spandidos Publications.)

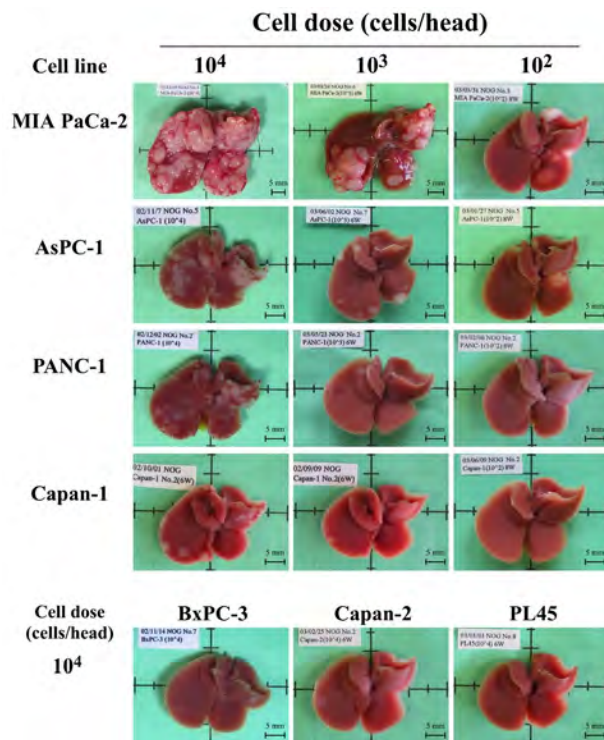


Figure 1. Representative gross findings of liver metastases of human pancreatic cancer cell lines. Seven human pancreatic cancer cell lines: MIA PaCa-2, AsPC-1, PANC-1, Capan-1, BxPC-3, Capan-2 and PL45 were intrasplenically implanted into NOG mice. The mice were sacrificed 6 weeks later, and liver metastases were enumerated immediately, without prior fixation.

(Reprinted from *Int J Oncol* ., Vol.31, H. Suemizu, M. Monnai, Y. Ohnishi, M. Ito, N. Tamaoki, and M. Nakamura. "Identification of a key molecular regulator of liver metastasis in human pancreatic carcinoma using a novel quantitative model of metastasis in NOD/SCID/gammacnull (NOG) mice. " p744 (2007), with permission from Spandidos Publications.)

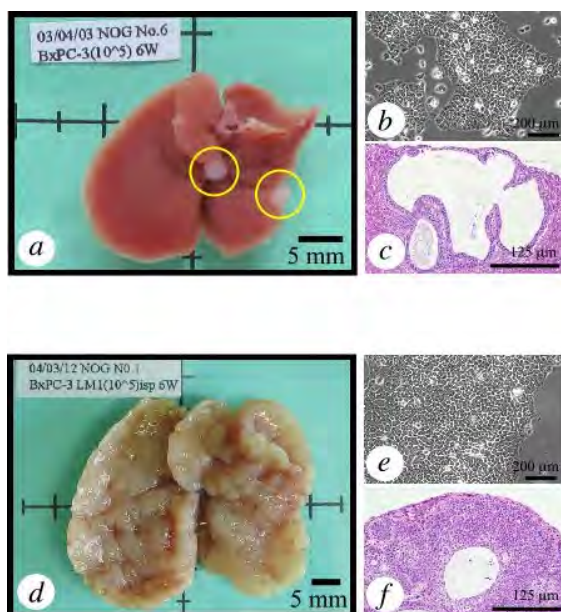


Figure 2. Establishment of a highly liver metastatic cell line. Primary tumors were generated by intrasplenic injection of 1×10^5 BxPC-3 cells into NOG mice (a-c). Cells from liver metastatic foci (open circles in Fig. 2 a) were isolated and designated as LM-BxPC-3. Metastatic ability of the LM-BxPC-3 cell line was evaluated by intrasplenic injection with 1×10^5 cells (d-f).

(Reprinted from *Int J Oncol* ., Vol.31, H. Suemizu, M. Monnai, Y. Ohnishi, M. Ito, N. Tamaoki, and M. Nakamura. "Identification of a key molecular regulator of liver metastasis in human pancreatic carcinoma using a novel quantitative model of metastasis in NOD/SCID/gammacnull (NOG) mice. " p744 (2007), with permission from Spandidos Publications.)

5-2-2. Liver metastasis II

To examine the drug efficacy of a novel farnesyltransferase inhibitor (FTI), CH4512600, *in vivo*, we developed a reliable liver metastasis model of human colon cancer using NOD/Shi-*scid IL2Rg^{null}* (NOG) mice. Eleven human colon cancer cell lines were examined for their ability to form diverse metastatic foci in the livers of NOG mice as phenotypic and biological characters. When inoculated with 10⁴ COLO320DM, HCT 116, HT-29, WiDr, LoVo and LS174T cells, liver metastasis was evident in 100% (6/6), 100% (6/6), 88.9% (8/9), 87.5% (7/8), 83.3% (5/6) and 50.0% (3/6) of the NOG mice, respectively. CaCo2, COLO201, LS123, SW48 and SW1417 showed no metastasis when seeded at 10⁴ cells even in NOG mice. The mRNA expression levels and genetic mutations of *N*, *H* and *K-RAS* genes, which directly affects the levels of cellular *RAS* protein that would be molecular target for FTI, was also examined in these six metastasizable human colon cancer cell lines as molecular biological and genotypic characters. Only three cell lines had a point mutation in the *RAS* oncogene. LS174T cell line had a point mutation of the *K-RAS* gene at codon 12 (gly12 to asp; G12D), and HCT 116 and LoVo cell lines had a point mutation of the *K-RAS* gene at codon 13 (gly13 to asp; G13D). Relative gene expression levels of *N*, *H* and *K-RAS* genes in the HCT 116 cell line were 2.6 to 5.0 folds lower than that of LS174T and LoVo cell lines. We selected HCT 116 cell line from our liver metastasis model for evaluation of FTI CH4512600 efficacy in *in vivo*. Using the NOG mouse liver metastasis model, we demonstrated the effectiveness of FTI CH4512600 to suppress tumor growth *in vivo* and to prolong mouse survival significantly from 36.9 ± 2.9 to 50.3 ± 9.4 days.

(Reprinted from *Int J Oncol* ., Vol.32, Hamada, K., M. Monnai, K. Kawai, C. Nishime, C. Kito, N. Miyazaki, Y. Ohnishi, M. Nakamura, and H. Suemizu. "Liver metastasis models of colon cancer for evaluation of drug efficacy using NOD/Shi-*scid IL2Rg^{manull}* (NOG) mice." p153 (2008), with permission from Spandidos Publications.)

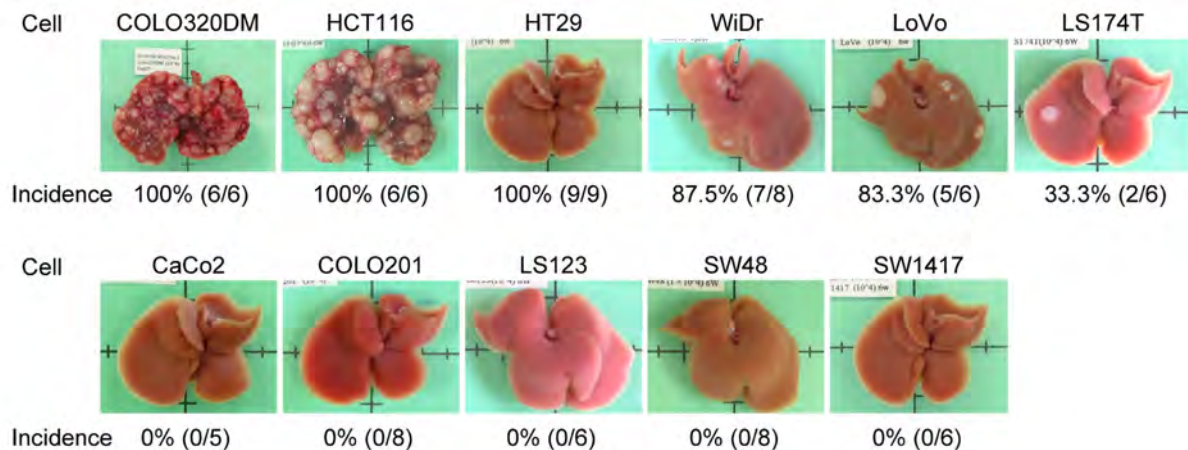


Figure 1. Representative gross findings of liver metastases of human colon cancer cell lines. Eleven human colon cancer cell lines: CaCo2, COLO201, COLO320DM, HCT 116, HT-29, LoVo, LS123, LS174T, SW48, SW1417 and WiDr, were intrasplenically implanted into NOG mice. The mice were sacrificed 6 weeks later, and liver metastases were enumerated immediately, without prior fixation.

(Reprinted from *Int J Oncol* ., Vol.32, Hamada, K., M. Monnai, K. Kawai, C. Nishime, C. Kito, N. Miyazaki, Y. Ohnishi, M. Nakamura, and H. Suemizu. "Liver metastasis models of colon cancer for evaluation of drug efficacy using NOD/Shi-*scid IL2Rg^{manull}* (NOG) mice." p155 (2008), with permission from Spandidos Publications.)

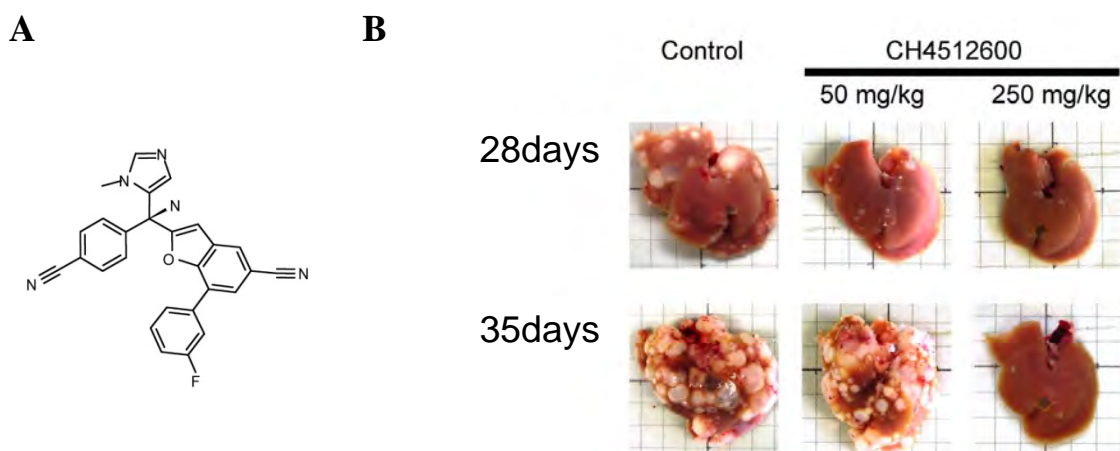
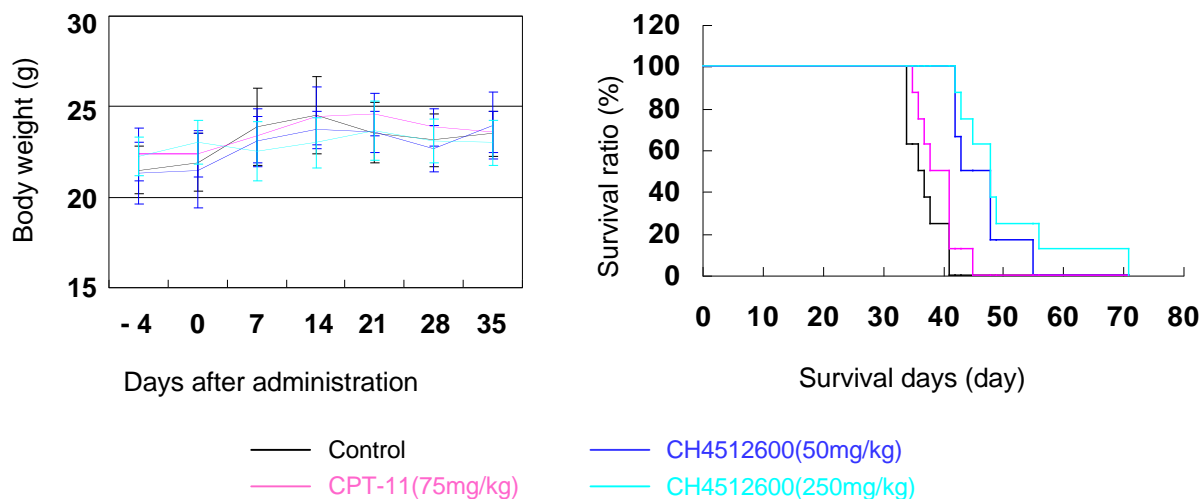


Figure 2. Effects of FTI CH4512600 on the liver metastasis model. A) Chemical structure of FTI CH4512600. B) HCT 116 cells (10^4 cells) transplanted into mouse liver was dissected at day 28 and day 35. FTI CH4512600 (50 mg/kg and 250 mg/kg, daily) was administered for 3 weeks. Representative photos are shown here (n=3). (Reprinted from *Int J Oncol.*, Vol.32, Hamada, K., M. Monnai, K. Kawai, C. Nishime, C. Kito, N. Miyazaki, Y. Ohnishi, M. Nakamura, and H. Suemizu. "Liver metastasis models of colon cancer for evaluation of drug efficacy using NOD/Shi-scid IL2R γ null (NOG) mice." p154(Fig.1), p157(Fig3), (2008), with permission from Spandidos Publications.)



5-2-3. Multiple myeloma

We developed a new experimental animal model of human multiple myeloma using immunodeficient NOD/SCID/cnullc (NOG) mice. A human myeloma cell line, U266, was intravenously inoculated into 20 NOG mice, all of which developed hind leg paralysis and distress around 6 weeks after transplantation. Pathological studies showed that only the bone marrow was infiltrated with U266 cells, and no cells were present in other organs. Osteolytic lesions in cortical bones and loss of trabecular bones were prominent in U266-transplanted NOG mice. In contrast, U266 cells were not detected in CB17scid or NOD/SCID mice 6 weeks after intravenous inoculation. Human IgE, produced by U266 cells, was detected in the serum of U266-transplanted NOG mice by ELISA. The results indicated that this hu-myeloma NOG model might be useful for studying the pathogenesis of myeloma and related osteolytic lesions, and are suggestive of its applicability to the future development of new drugs.

(Reprinted from *Biochem Biophys Res Commun* Vol. 313, Y. Miyakawa, Y. Ohnishi, M. Tomisawa, M. Monnai, K. Kohmura, Y. Ueyama, M. Ito, Y. Ikeda, M. Kizaki, and M. Nakamura. "Establishment of a new model of human multiple myeloma using NOD/SCID/gammac(null) (NOG) mice." , p258, Copyright(2004), with permission from Elsevier.)

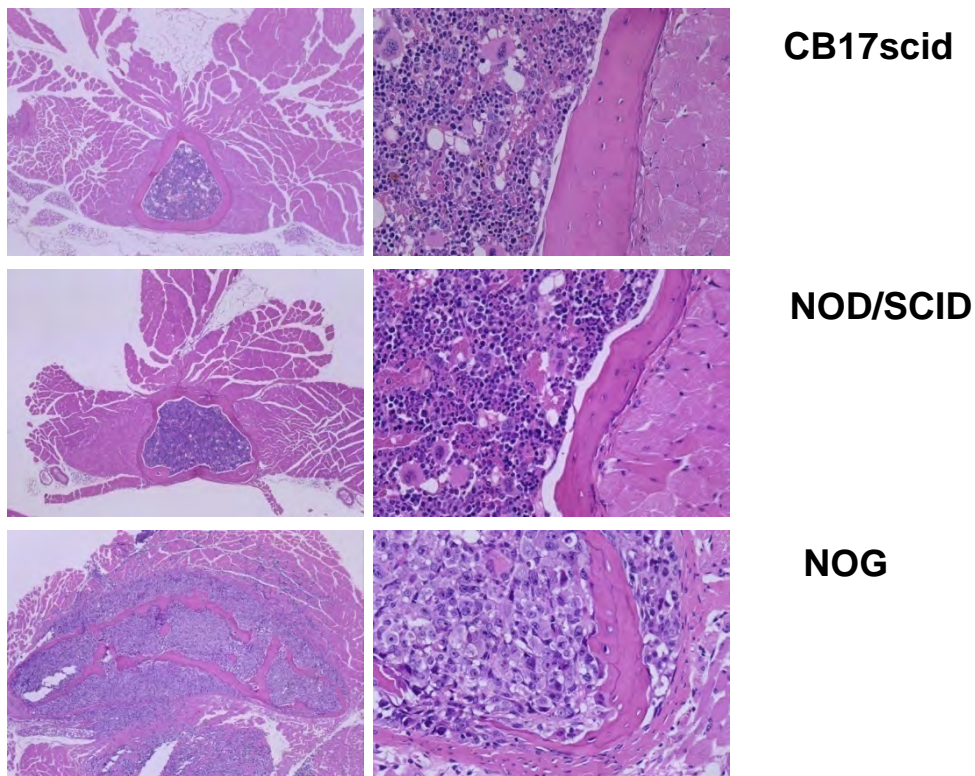


Figure 1. Histological analyses of bone marrow in CB17scid, NOD/SCID, and NOG mice after U266 myeloma cell transplantation. Five CB17scid, 5 NOD/SCID, and 20 NOG mice were intravenously injected with U266 cells after 2.4Gy irradiation. Six weeks after transplantation, all mice were sacrificed and their bone marrow from the sternum was analyzed histologically. There is no infiltration of U266 cells into the bone marrow of CB17scid (A, B) and NOD/SCID (C, D), but massive infiltration of U266 cells is observed in NOG (E, F), accompanied by osteolytic lesions (arrows in E,F). HE staining, magnification 100 x (A, C, and E), 200 x (B, D, and F).

(Reprinted from *Biochem Biophys Res Commun* Vol. 313, Y. Miyakawa, Y. Ohnishi, M. Tomisawa, M. Monnai, K. Kohmura, Y. Ueyama, M. Ito, Y. Ikeda, M. Kizaki, and M. Nakamura. "Establishment of a new model of human multiple myeloma using NOD/SCID/gammac(null) (NOG) mice." , p260, Copyright(2004), with permission from Elsevier)

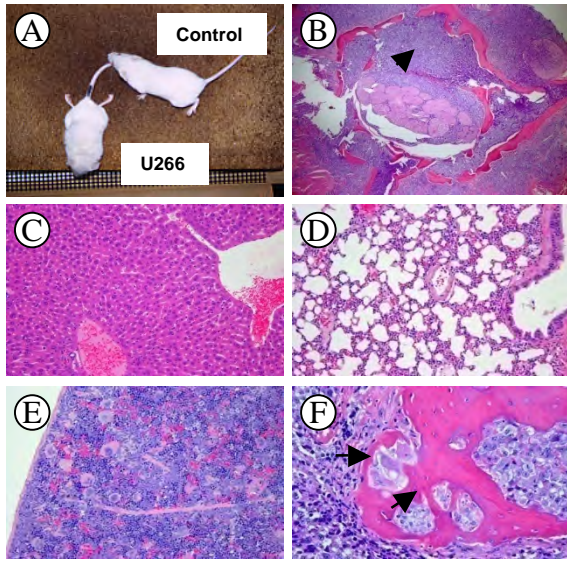


Figure 2. Clinical manifestation and histological analyses of U266-transplanted NOG mice. (A) U266-transplanted NOG mice but not control mice revealed hind leg paralyse around 6 weeks after transplantation. (B) Massive infiltration of U266 cells is observed in the lumbar bone lesions. U266 cells invade into the spinal cavity and muscles, accompanied by the osteolytic lesions. However, U266 cells are not histologically observed in other organs of NOG mice; (C) liver, (D) lungs, (E) spleen, and (F) eosinophilic osteoclasts are observed near the cortical bones of lumbar spines. HE staining. (Reprinted from *Biochem Biophys Res Commun* Vol. 313, Y. Miyakawa, Y. Ohnishi, M. Tomisawa, M. Monnai, K. Kohmura, Y. Ueyama, M. Ito, Y. Ikeda, M. Kizaki, and M. Nakamura. "Establishment of a new model of human multiple myeloma using NOD/SCID/gammac(null) (NOG) mice." , p260, Copyright(2004), with permission from Elsevier)

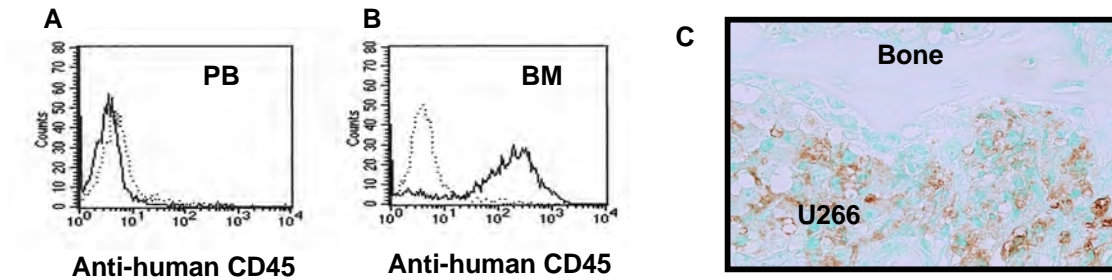


Figure 3. FACS and histological analyses of U266-transplanted NOG mice. (A) Peripheral blood of NOG mice was analyzed 6 weeks after U266 cell transplantation using a PE-conjugated anti-human CD45 antibody by FACS. Dotted lines, isotype-matched negative control. (B) Bone marrow of NOG mice was analyzed 6 weeks after U266 cell transplantation and approximately 84% was positive for human CD45. (C) Bone marrow of U266-transplanted NOG mice are stained with an anti-human IgE antibody.

(Reprinted from *Biochem Biophys Res Commun* Vol. 313, Y. Miyakawa, Y. Ohnishi, M. Tomisawa, M. Monnai, K. Kohmura, Y. Ueyama, M. Ito, Y. Ikeda, M. Kizaki, and M. Nakamura. "Establishment of a new model of human multiple myeloma using NOD/SCID/gammac(null) (NOG) mice." , p261, Copyright(2004), with permission from Elsevier)

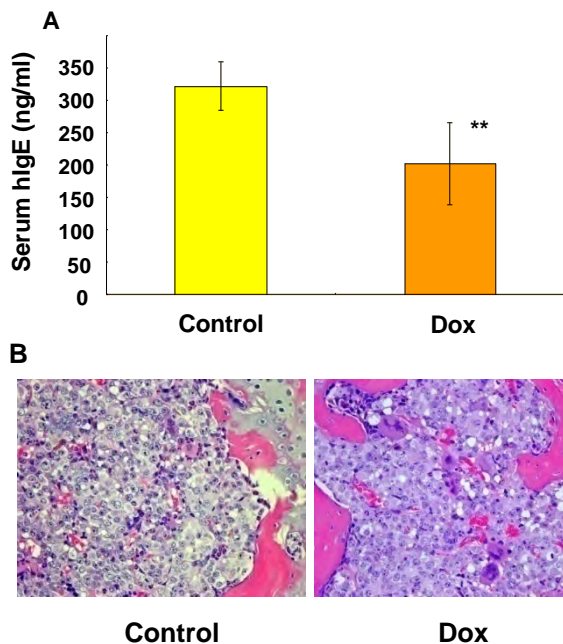


Figure 4. Serum levels of human IgE and histological studies in U266-transplanted NOG mice after treatment with doxorubicin. (A) Human IgE concentrations in serum of NOG mice 4 weeks after transplantation with U266 cells were analyzed by ELISA. Eight NOG mice were injected with 1 mg/kg doxorubicin (DOX) per day for 3 days, 1 week after transplantation (n= 8). Control mice were injected with PBS in the same schedule (n = 8). Values are given as means \pm SD of eight mice. Student's t test was performed to evaluate the statistical significances. **p < 0:01. (B) Histological studies of sternum of U266-transplanted NOG mice after treatment with or without doxorubicin in the same schedule as in (A).

(Reprinted from *Biochem Biophys Res Commun* Vol. 313, Y. Miyakawa, Y. Ohnishi, M. Tomisawa, M. Monnai, K. Kohmura, Y. Ueyama, M. Ito, Y. Ikeda, M. Kizaki, and M. Nakamura. "Establishment of a new model of human multiple myeloma using NOD/SCID/gammac(null) (NOG) mice." , p261, Copyright(2004), with permission from Elsevier)

5-3. Human tissue or organ model

5-3-1. Model with human ovary

Transplantation of human ovarian cortex into host mice may permit various kinds of challenges in reproductive medicine. A novel immunodeficient mouse strain (NOD/SCID/gammacnull: NOG) has been developed as a host of transplantation of human tissue. Human ovarian cortex was transplanted into various sites of NOG mice and human follicular development was examined by immunohistochemistry. Transplantation of human ovarian tissue into NOG mice resulted in approximately similar tissue survival and follicle growth as did transplantation into non-obese diabetic-severe combined immunodeficient mice. The human Graafian follicle from NOG mouse expressed the same steroidogenic enzymes as observed in human Graafian follicles, which developed in the human body. The NOG mice's ovarian bursa was better placed for transplantation than the back skin or kidney capsule. These results represent the successful generation and biological confirmation of the human Graafian follicles from the human ovarian cortex in the NOG mice.

Terada, Y., Y. Terunuma-Sato, T. Kakoi-Yoshimoto, H. Hasegawa, T. Ugajin, Y. Koyanagi, M. Ito, T. Murakami, H. Sasano, N. Yaegashi, and K. Okamura. 2008. Development of human Graafian follicles following transplantation of human ovarian tissue into NOD/SCID/gammacnull mice. *Am J Reprod Immunol* 60:534-540.

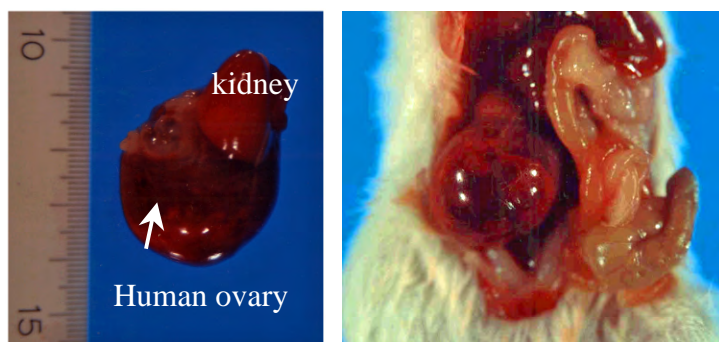


Figure 1. Macroscopic view of a human Graafian follicle (arrow) after transplantation of human ovarian cortex into the ovarian bursa of a NOG mouse.

Host mice were stimulated by daily intraperitoneal injection of human menogonadotropin for 14 days, 10 weeks after transplantation. Scale bar = 1 cm.

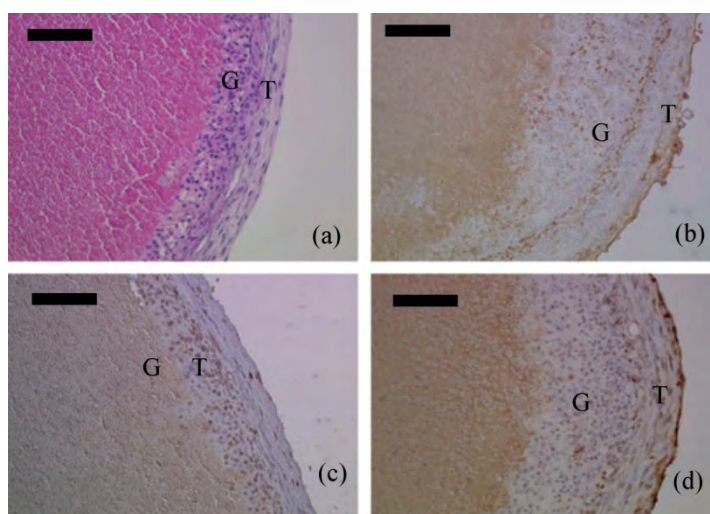


Figure 2. Characterization of a human Graafian follicle that developed in the ovarian bursa of a NOG mouse (same follicle as shown in Fig. 1).

(a) Hematoxylin and eosin staining showing the theca and granulosa cell layers. (b) Antibody staining for the steroidogenic enzyme P450 scc is localized to the cytoplasm of theca cells. (c) Immunohistochemistry for AD4-BP showing expression in the nuclei of both theca and granulosa cell layers. (d) ER antibody staining was detected in the theca cell layer. T, theca cells; G, granulosa cells. Scale bar = 100 μ m.

5-3-2. Model with human endometrium

Cultures of human endometrial tissue are useful for analysing the mechanisms underlying the menstrual cycle. However, long-term culture of endometrial tissue is difficult *in vitro*. Xenotransplantation of normal human endometrial tissue into immunodeficient mice could allow prolonged survival of the transplanted tissues. Proliferative-phase endometrial tissue samples from three women were transplanted into the subcutaneous space of ovariectomized, immunodeficient, non-obese diabetic (NOD)/severe combined immunodeficiency (SCID)/gCnull (NOG) mice. The mice were treated with 17 β -estradiol (E2) for the first 14 days after transplantation, followed by E2 plus progesterone for the next 14 days. The transplants were investigated morphologically and immunohistochemically at various times after implantation. **RESULTS:** The transplanted tissues contained large numbers of small glands, pseudostratification of the nuclei and dense stroma after treatment with E2 alone. After treatment with E2 plus progesterone, subnuclear vacuolation, luminal secretion and decidualization of the stroma were observed. When the hormone treatment ceased, tissue destruction occurred and the transplants returned to the proliferative phase. Lymphocytes were identified immunohistochemically: the numbers of CD56-positive and CD16-negative cells increased significantly in the stroma during the late secretory phase (day 28). Human endometrial tissue transplanted into NOG mice showed similar histological changes to eutopic endometrial tissue during treatment with sex steroid hormones for 1 month. Moreover, lymphocytes were produced in the transplanted human endometrial tissue. This system represents a new experimental model of the human endometrium *in vivo*.

(Reprinted from *Human Reproduction*, Vol 20, p1477, (2005) Matsuura-Sawada, R., T. Murakami, Y. Ozawa, H. Nabeshima, J. Akahira, Y. Sato, Y. Koyanagi, M. Ito, Y. Terada, and K. Okamura. "Reproduction of menstrual changes in transplanted human endometrial tissue in immunodeficient mice." Oxford Journals)

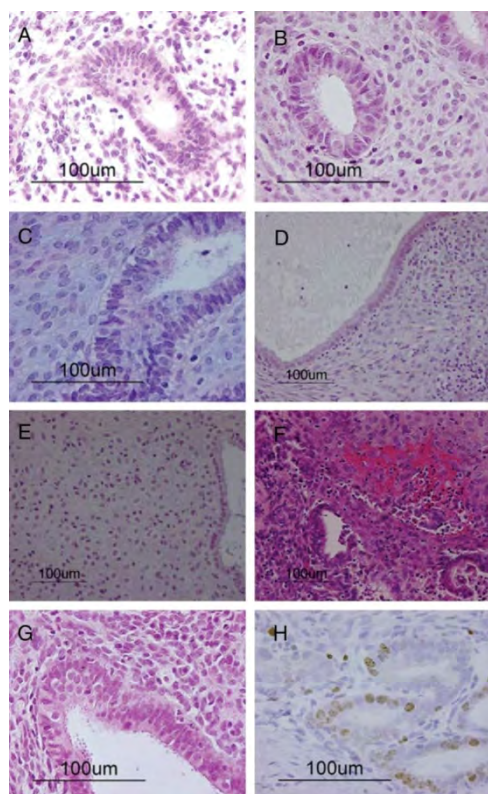


Figure 1. Histological sections stained with haematoxylin and eosin (A–G) and the immunohistochemical stain Ki-67 (H).

(A) Pretransplantation endometrial tissue: the proliferative phase. The glands are small straight and narrow, with columnar glandular cells and prominent pseudostratification of the nuclei. The stromal cells are dense (magnification $\times 400$). (B) Endometrial tissue 14 days after transplantation: E2 has been administered for 14 days. The glands are small and narrow, with tall columnar cells. Evidence of pseudostratification of the nuclei is present. The stromal cells are dense (magnification $\times 400$). (C) Endometrial tissue 16 days after transplantation: E2 has been administered for 14 days, followed by E2 plus progesterone for 2 days. The glands still show pseudostratified structures but they have begun to enlarge, and subnuclear vacuolation of the glandular cells is visible. The stromal cells remain dense (magnification $\times 400$). (D) Endometrial tissue 21 days after transplantation: E2 has been administered for 14 days, followed by E2 plus progesterone for 7 days. The glands are significantly dilated, the glandular cells are cuboidal and the pseudostratification of the nuclei has disappeared. Stromal decidualization is beginning. Many lymphocytes are present throughout the stroma and are aggregating around the glands (magnification $\times 200$). (E) Endometrial tissue 28 days after transplantation: E2 has been administered for 14 days, followed by E2 plus progesterone for 14 days. The glandular cells are cuboidal. Evidence of stromal decidualization is clearly seen and lymphocytes are present in the stroma (magnification $\times 200$). (F) Endometrial tissue 31 days after transplantation: E2 had been administered for 14 days, followed by E2 plus progesterone for 14 days, and then no hormones for the remaining 3 days. The glands and endometrial stroma have collapsed during the evolution of the transplant. There is prominent bleeding in the stroma (magnification $\times 200$). (G) Endometrial tissue 35 days after transplantation: E2 had been administered for 14 days, followed by E2.

(Reprinted from *Human Reproduction*, Vol 20, p1480, (2005) Matsuura-Sawada, R., T. Murakami, Y. Ozawa, H. Nabeshima, J. Akahira, Y. Sato, Y. Koyanagi, M. Ito, Y. Terada, and K. Okamura. "Reproduction of menstrual changes in transplanted human endometrial tissue in immunodeficient mice." Oxford Journals)

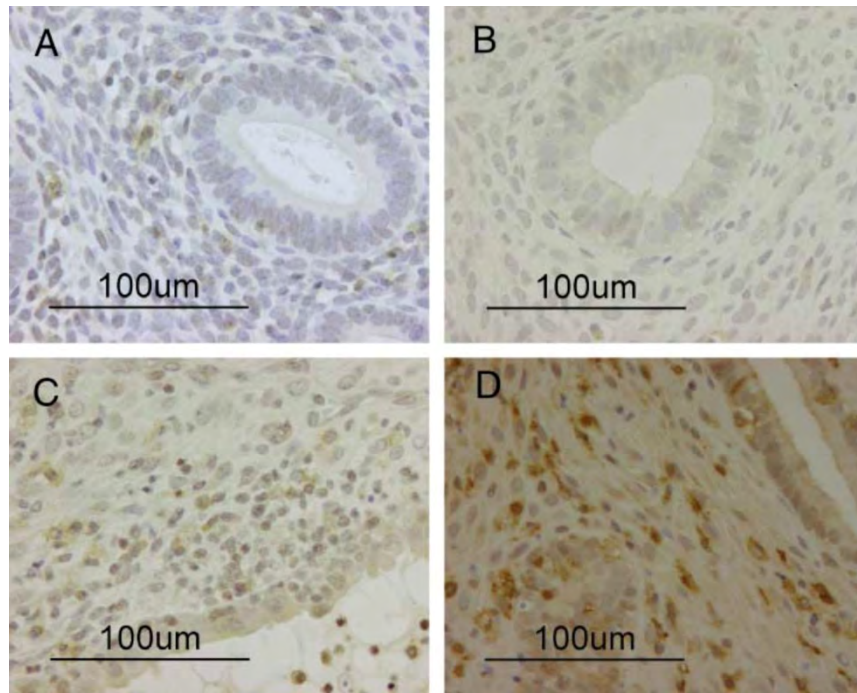


Figure 2. Immunohistochemical staining of human CD56.

(A) Pretransplantation endometrial tissue: human CD56-positive cells are present in small numbers (magnification $\times 400$). (B) Day 14 after transplantation: human CD56-positive cells have completely disappeared from the stroma (magnification $\times 400$). (C) Day 21 after transplantation: human CD56-positive cells are present in small numbers (magnification $\times 400$). (D) Day 28 after transplantation: human CD56-positive cells have significantly increased in number in the stroma (magnification $\times 400$).

(Reprinted from *Human Reproduction*, Vol 20, p1481, (2005) Matsuura-Sawada, R., T. Murakami, Y. Ozawa, H. Nabeshima, J. Akahira, Y. Sato, Y. Koyanagi, M. Ito, Y. Terada, and K. Okamura. "Reproduction of menstrual changes in transplanted human endometrial tissue in immunodeficient mice." Oxford Journals)

5-3-3. Model with human liver

Severely immunodeficient NOD/Shi-*scid* IL2Rg^{null} (NOG) mice are used as recipients for human tissue transplantation, which produces chimeric mice with various types of human tissue. NOG mice expressing transgenic urokinase-type plasminogen activator in the liver (uPA-NOG) were produced. Human hepatocytes injected into uPA-NOG mice re-populated the recipient livers with human cells. The uPA-NOG model has several advantages over previously produced chimeric mouse models of human liver: (1) the severely immunodeficient NOG background enables higher xenogeneic cell engraftment; (2) the absence of neonatal lethality enables mating of homozygotes, which increased the efficacy of homozygote production; and (3) donor xenogeneic human hepatocytes could be readily transplanted into young uPA-NOG mice, which provide easier surgical manipulation and improved recipient survival.

(Reprinted from *Biochem Biophys Res Commun* Vol. 377, H. Suemizu, M. Hasegawa, K. Kawai, K. Taniguchi, M. Monnai, M. Wakui, M. Suematsu, M. Ito, G. Peltz, and M. Nakamura. "Establishment of a humanized model of liver using NOD/Shi-*scid* IL2Rg(null) mice." , p248, Copyright(2008), with permission from Elsevier)

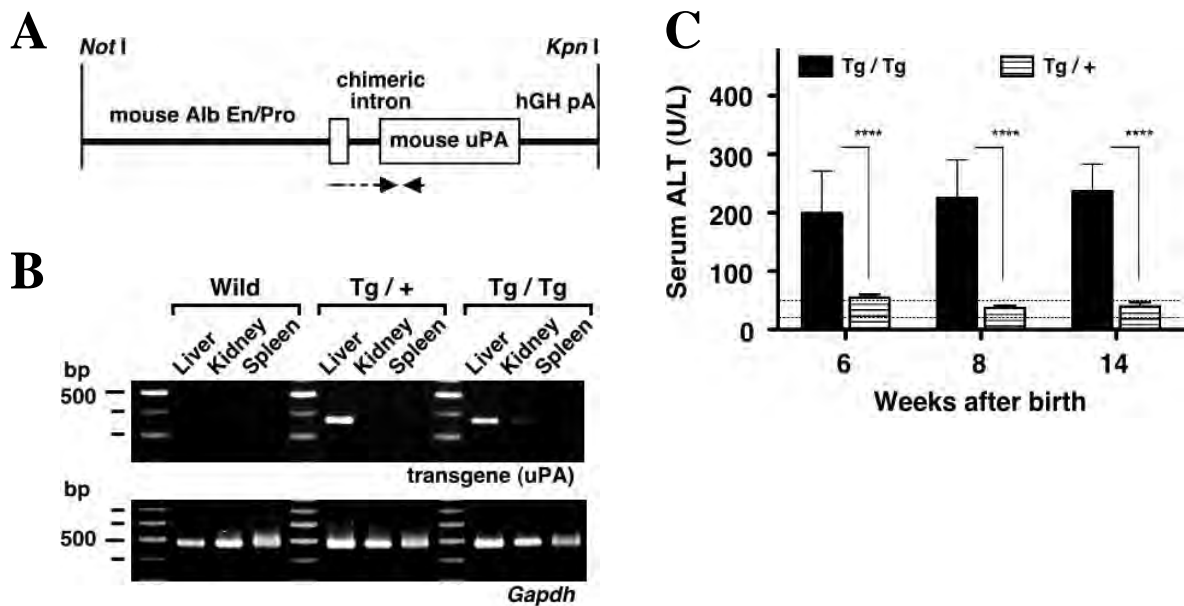


Figure 1. Establishment of the uPA-NOG mouse as a model of spontaneous hepatic injury.

(A) The uPA expression unit contains the mouse albumin enhancer/promoter (Alb En/Pro), the chimeric intron, mouse uPA cDNA, and the 3'-UTR of the human growth hormone gene with polyadenylation (pA) signal. Arrowheads depict the positions and directions of the RT-PCR primers. (B) RT-PCR analyses of uPA transgene expression. Wild, nontransgenic NOG; Tg/+, hemizygous; and Tg/Tg, homozygous uPA-NOG mice. *Gapdh* was used as an internal control. (C) ALT activities in uPA-NOG mice. All the values for the homozygous uPA-NOG (Tg/Tg) are significantly higher than those for the hemizygote (Tg/+) ($P < 0.0001$, unpaired *t*-test). Dashed lines indicate the two standard deviation ranges for the values for the nontransgenic NOG mice ($n = 7$). Each of the points for the hemizygous and homozygous uPA-NOG mice represent the mean \pm SD of four to seven samples.

(Reprinted from *Biochem Biophys Res Commun* Vol. 377, H. Suemizu, M. Hasegawa, K. Kawai, K. Taniguchi, M. Monnai, M. Wakui, M. Suematsu, M. Ito, G. Peltz, and M. Nakamura. "Establishment of a humanized model of liver using NOD/Shi-*scid* IL2Rg(null) mice." , p250, Copyright(2008), with permission from Elsevier)

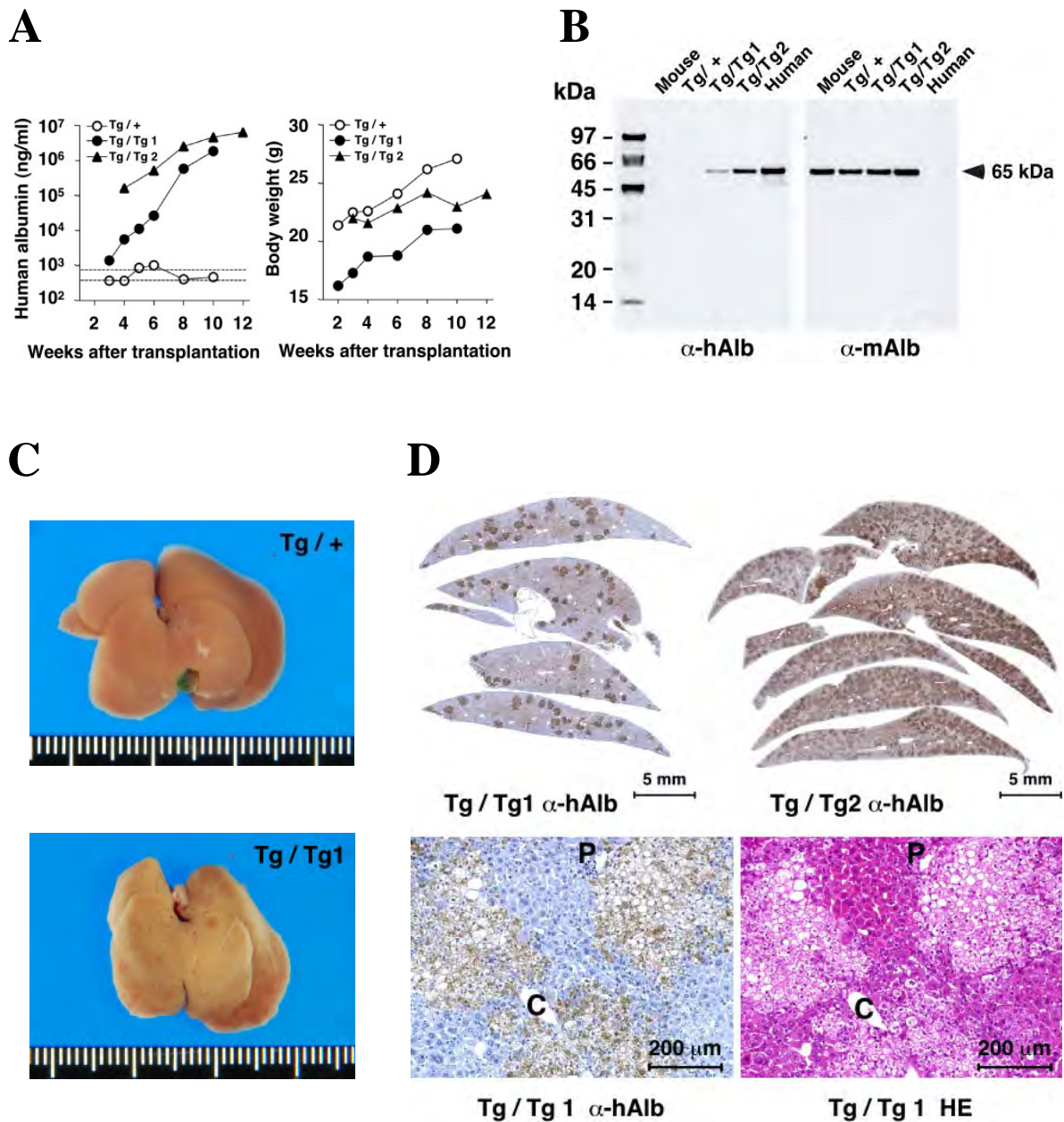


Figure 2. Engraftment and repopulation of human hepatocytes in uPA-NOG mice.

(A) Blood albumin concentrations in human cell recipients were assayed by ELISA. Dashed lines indicate the two standard deviation ranges for the values for the untransplanted uPA-NOG mice ($n = 6$). Body-weight changes after human hepatocyte transplantation are shown. (B) Immunoblot analysis shows human albumin (α -hAlb) and mouse albumin (α -mAlb) production in hemizygous (Tg/+) or homozygous (Tg/Tg) uPA-NOG transplant recipient mice. (C) Gross appearance of the uPA-NOG mouse liver 10 weeks after human hepatocyte transplantation. Tg/+, hemizygous; Tg/Tg, uPA-NOG homozygote. (D) Histology and immunohistochemistry of livers from uPA-NOG mice that were repopulated with human hepatocytes. Immunohistochemical staining for human albumin (top and lower left) and H&E staining (lower right). P, portal tract; C, central vein.

(Reprinted from *Biochem Biophys Res Commun* Vol. 377, H. Suemizu, M. Hasegawa, K. Kawai, K. Taniguchi, M. Monnai, M. Wakui, M. Suematsu, M. Ito, G. Peltz, and M. Nakamura. "Establishment of a humanized model of liver using NOD/Shi-scid IL2Rg(null) mice." , p251, Copyright(2008), with permission from Elsevier)

5-4. Other models

5-4-1. GVHD model

After intravenous transplantation of hPBMCs, NOG mice showed early onset of GVHD symptoms and a small number of hPBMCs (2.5×10^6) was sufficient to induce GVHD when compared with BALB/cA-RAG2^{null} IL2r^{null} and NOD/SCID mice. In addition, total body irradiation was not always necessary in the present model. CONCLUSIONS: These results indicate that our model using the NOG mouse is a useful tool to investigate GVHD, and to develop effective drugs for GVHD.

(Ito, R., I. Katano, K. Kawai, H. Hirata, T. Ogura, T. Kamisako, T. Eto, and M. Ito. 2009. Highly sensitive model for xenogenic GVHD using severe immunodeficient NOG mice. *Transplantation* 87:1654-1656, Wolters Kluwer Health)

Table 1. Comparison of transplantation routes for induction of GVHD in NOG mice

Route of transplantation	Cell numbers of PBMC transferred	Numbers of mice dying from GVHD	Mean days until death
I.P.	5×10^6	7/10	40.4±9.0
	10×10^6	4/4	23.3±9.7
I.V.	5×10^6	11/11	26.9±14.6
	10×10^6	8/8	14.5±1.4

I.P.: intraperitoneal, I.V.: intravenous inoculation

To investigate the appropriate route of hPBMC to induce xeno-GVHD, various numbers of hPBMCs were transferred into irradiated NOG mice by intravenous or intraperitoneal routes. On administration of 10×10^6 hPBMCs by the intraperitoneal route, all NOG mice died within 1 month, and 70 % (7 of 10) of NOG mice survived for longer than 2 months when 5×10^6 hPBMCs were transplanted. When 5 or 10×10^6 hPBMCs were transplanted by the intravenous route, all NOG mice died around 1 month or 2 weeks earlier than by the intraperitoneal route. (Ito, R., I. Katano, K. Kawai, H. Hirata, T. Ogura, T. Kamisako, T. Eto, and M. Ito. 2009. Highly sensitive model for xenogenic GVHD using severe immunodeficient NOG mice. *Transplantation* 87:1655, Wolters Kluwer Health)

Table 2. Minimum cell numbers for induction of GVHD in NOG mice

Cell numbers of PBMC transferred	Numbers of mice dying from GVHD	Mean days until death
5×10^6	3/3	34.7±6.7
2.5×10^6	3/3	46.3±14.3
1×10^6	0/3	-

Three different counts of hPBMCs (5×10^6 , 2.5×10^6 or 1×10^6) were intravenously administered to irradiated 3 NOG mice each for induction of GVHD. NOG mice transplanted with 5×10^6 and 2.5×10^6 hPBMCs died within 1 to 1.5 months after cell transfer. In contrast, all NOG mice transplanted with 1×10^6 cells survived for longer than 3 months. These results demonstrated that the intravenous route was more effective for GVHD induction than the intraperitoneal one, and at least 2.5×10^6 cells are necessary to induce GVHD in NOG mice.

(Ito, R., I. Katano, K. Kawai, H. Hirata, T. Ogura, T. Kamisako, T. Eto, and M. Ito. 2009. Highly sensitive model for xenogenic GVHD using severe immunodeficient NOG mice. *Transplantation* 87:1656, Wolters Kluwer Health)

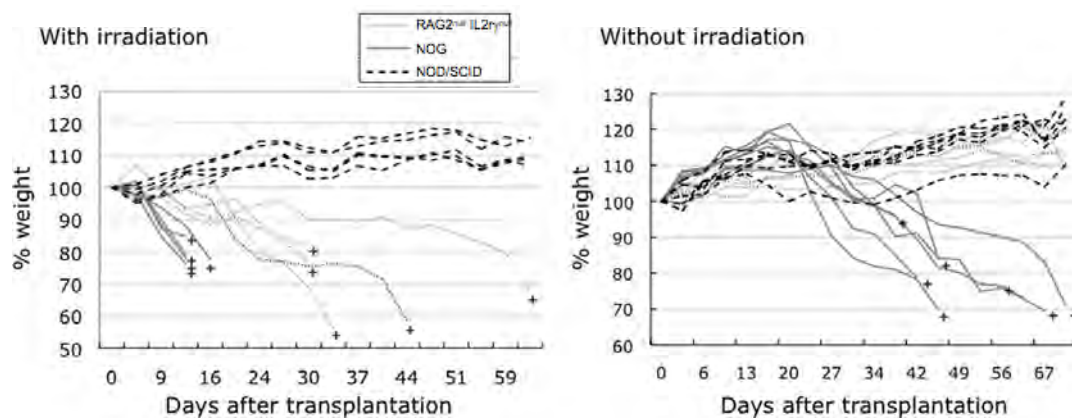


Figure 1. Induction of xeno-GVHD in NOG, RAG2^{null} IL2r^{null} and NOD/SCID mice

After irradiation (NOG: 2.5 Gy, RAG2^{null} IL2r^{null} and NOD/SCID: 3.5 Gy) and intravenous transplantation of 10×10^6 hPBMCs, all mice were weighed twice weekly. All NOG mice died from GVHD with (left panel; n=5) or without (right panel; n=7) irradiation earlier than other immunodeficient mice. All irradiated RAG2^{null} IL2r^{null} mice (n=5) died after 1 to 2 months, whereas all non-irradiated mice (n=7) survived for more than 2 months. NOD/SCID mice with or without irradiation (n=5 or n=7) did not die for more than 2 months. + indicates death of the mouse; % weight shows weight change percentage from the initial weight

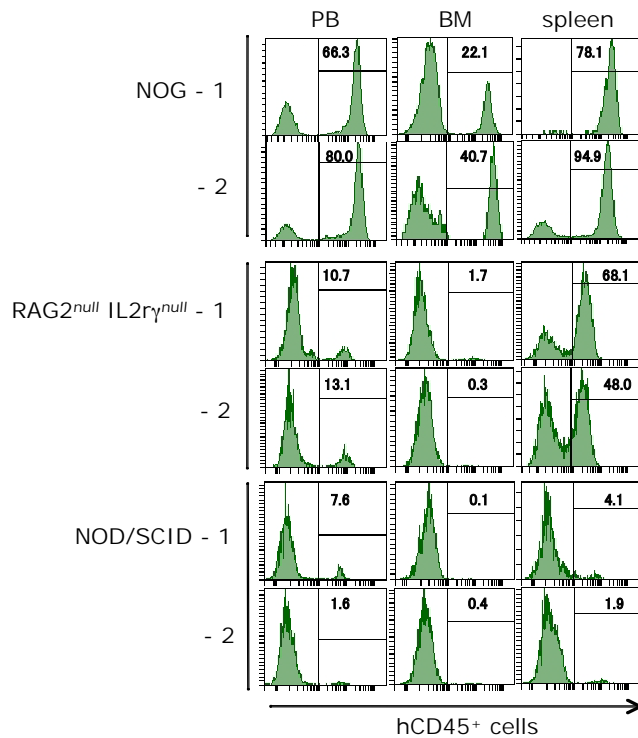


Figure 2. Engraftment of human cells in xeno-GVHD induced mice

Two weeks after intravenous transplantation of 5×10^6 hPBMCs, NOG, RAG2^{null} IL2r^γ^{null} and NOD/SCID mice were analyzed to determine the rates of human CD45⁺ cells in PB, BM and spleen by flow cytometry. The engraftment rates of human CD45⁺ cells increased more dramatically in PB, BM and spleens of NOG mice than in those of RAG2^{null} IL2r^γ^{null} and NOD/SCID mice. Low rates of engraftment of human CD45⁺ cells were observed in the spleen from RAG2^{null} IL2r^γ^{null} mice but not in NOD/SCID mice. Only a few human CD45⁺ cells were present in BM and PB of RAG2^{null} IL2r^γ^{null} and NOD/SCID mice.

(Ito, R., I. Katano, K. Kawai, H. Hirata, T. Ogura, T. Kamisako, T. Eto, and M. Ito. 2009. Highly sensitive model for xenogenic GVHD using severe immunodeficient NOG mice. *Transplantation* 87:1657, Wolters Kluwer Health)

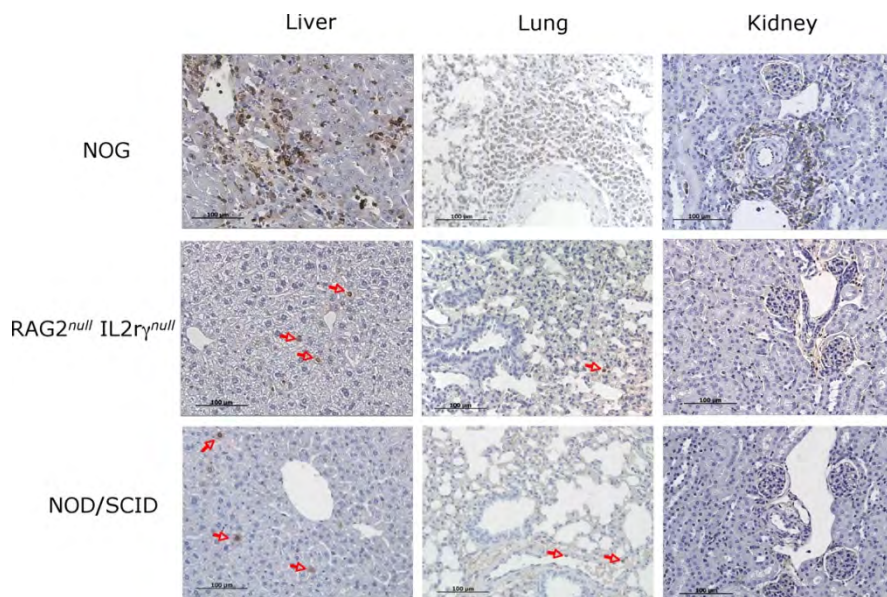


Figure 3. Immunohistochemistry in organs from xeno-GVHD induced mice To investigate the infiltration of human lymphocytes into non-lymphoid tissues in xeno-GVHD induced mice, we performed immunohistochemical analysis of the liver, lungs and kidneys from 3 strains of irradiated and 5×10^6 hPBMCs transplanted immunodeficient mice using an anti-human CD45 antibody. Remarkably abundant invasion of human CD45⁺ cells was observed around the veins in the liver, lungs and kidneys of NOG mice, whereas only a few human CD45 cells were observed in the liver and lungs and none in the kidneys of RAG2^{null} IL2r^γ^{null} and NOD/SCID mice.

(Ito, R., I. Katano, K. Kawai, H. Hirata, T. Ogura, T. Kamisako, T. Eto, and M. Ito. 2009. Highly sensitive model for xenogenic GVHD using severe immunodeficient NOG mice. *Transplantation* 87:1657, Wolters Kluwer Health)

5-4-2. Efficacy test model for thrombopoietic drugs

NIP-004 is a novel synthetic compound developed to display human thrombopoietin (TPO) receptor (c-Mpl) agonist activity. NIP-004 displays species specificity, stimulating proliferation or differentiation of human c-Mpl-expressing cells such as UT-7/TPO and human CD34⁺ cells but not murine c-Mpl-expressing cells or cynomolgus monkey cells. To test the mechanism of its action, we constructed mutant forms of c-Mpl; murine c-MplL490H displayed a response to NIP-004, where human c-MplH499L lost this response, indicating that histidine in the transmembrane domain of c-Mpl is essential for its activity. Because histidine is not present in the c-Mpl transmembrane domain of rats, hamsters, rhesus macaques, and cynomolgus monkeys, we examined the *in vivo* efficacy of NIP-004 using mice that received xenotransplants. In immunodeficient nonobese diabetic (NOD)/Shi-*scid*, IL-2R⁰ null (NOG) mice receiving transplants of umbilical cord blood-derived as CD34⁺ cells, NIP-004 increased human megakaryoblasts, mature megakaryocytes, and circulating human platelets 6-fold, the latter being morphologically and functionally indistinguishable from normal human platelets. These observations indicate that NIP-004 is a novel human c-Mpl activator and induces human thrombopoiesis. (Blood. 2006;107: 4300-4307)

(This research was originally published in Blood. Nakamura, T., Y. Miyakawa, A. Miyamura, A. Yamane, H. Suzuki, M. Ito, Y. Ohnishi, N. Ishiwata, Y. Ikeda, and N. Tsuruzoe. A novel nonpeptidyl human c-Mpl activator stimulates human megakaryopoiesis and thrombopoiesis. Blood. 2006;107:p4300. ©the American Society of Hematology.)

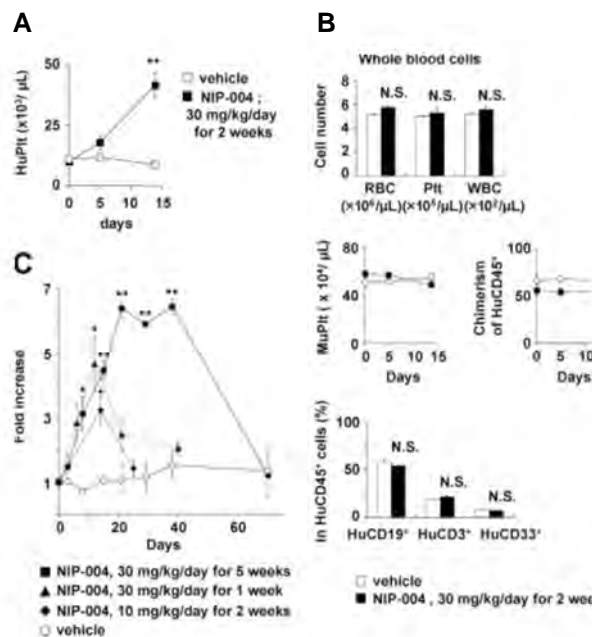


Figure 1. NIP-004-induced production of human platelets in NOG mice receiving xenotransplants.

(A) NIP-004 increased the number of circulating human platelets in NOG mice. (B) NIP-004 did not change the number of murine platelets or chimerism of HuCD45⁺ cells. NIP-004 had no effect on the percentage of human B (CD19⁺) cells, human T (CD3⁺) cells, and human myeloid (CD33⁺) cells in the peripheral HuCD45⁺ cells. Data from panels A-B are expressed as the mean (SEM (n & 3) or mean (SD (n & 2)). *P < .05, **P < .01 between NIP-004 and vehicle at individual time points. N.S. indicates no significant differences compared with vehicle.

(This research was originally published in Blood. Nakamura, T., Y. Miyakawa, A. Miyamura, A. Yamane, H. Suzuki, M. Ito, Y. Ohnishi, N. Ishiwata, Y. Ikeda, and N. Tsuruzoe. A novel nonpeptidyl human c-Mpl activator stimulates human megakaryopoiesis and thrombopoiesis. Blood. 2006;107:p4305. ©the American Society of Hematology.)

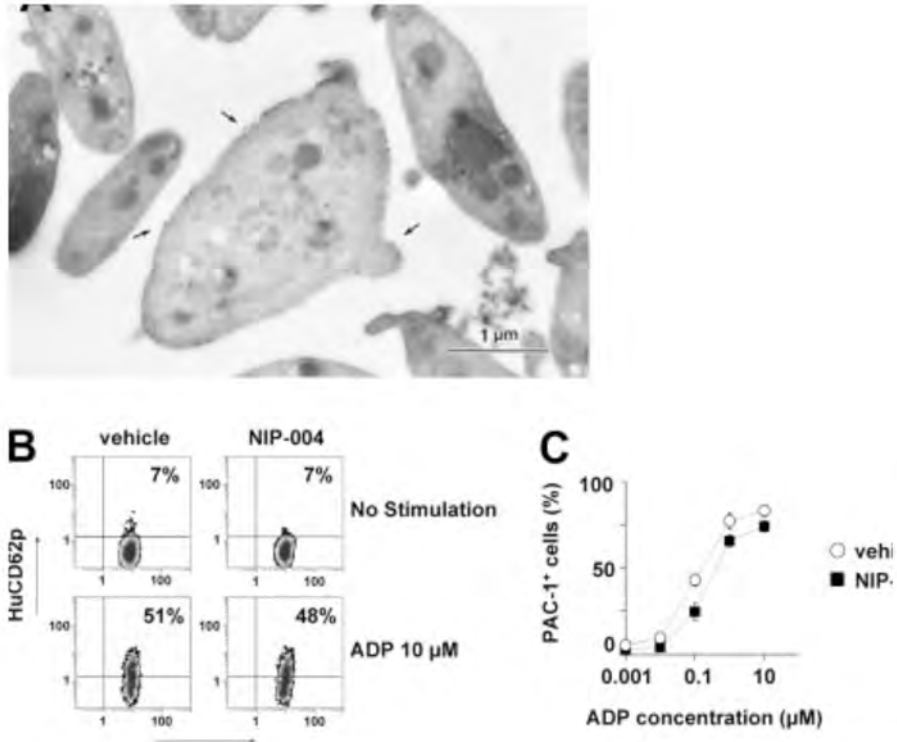


Figure 2. Morphologic and functional features of human platelets induced by NIP-004 in NOG mice.

(A) Immunoelectron microscopy using antibody against HuCD41a identified human platelets in PRP derived from NIP-004-treated mice. The surface of a platelet located in the center is labeled with gold particles (arrow), indicating that it is of human origin. Bar, 1 μ m. (B) P selectin (HuCD62p) expression upon ADP stimulation in human platelets was similarly increased in both vehicle- and NIP-004-treated mice. (C) After stimulation with various concentrations of ADP, there was a similar dose-dependent escalation in the percentage of PAC-1-positive human platelets from vehicle- and NIP-004-treated NOG mice receiving xenotransplants. PAC-1 antibody specifically recognizes the activated form of GPIIb/IIIa. Data are expressed as the mean \pm SEM (n & 4).

(This research was originally published in Blood. Nakamura, T., Y. Miyakawa, A. Miyamura, A. Yamane, H. Suzuki, M. Ito, Y. Ohnishi, N. Ishiwata, Y. Ikeda, and N. Tsuruzoe. A novel nonpeptidyl human c-Mpl activator stimulates human megakaryopoiesis and thrombopoiesis. Blood. 2006;107:p4306. ©the American Society of Hematology.)

5-4-3. Tumorigenicity test model for human cell transplantation

The purpose of tumorigenicity testing, as applied not only to cell substrates used for viral vaccine manufacture but also stem cells used for cell-based therapy, is to discriminate between cells that have the capacity to form tumors and cells that do not. Therefore, tumorigenicity testing is essential in assessing the safety of these biological materials. Recently developed NOD/Shi-*scid* IL2R γ ^{null} (NOG) mice have been shown to be superior to NOD/Shi-*scid* (SCID) mice for xenotransplantation of both normal and cancerous cells. To select a suitable mouse strain as a xenogenic host for tumorigenicity testing, we compared the susceptibility of NOG (T, B, and NK cell-defective), SCID (T and B cell-defective), and the traditionally used nude (T cell-defective) mice to tumor formation from xenotransplanted HeLa S3 cells. When 10⁴ HeLa S3 cells were subcutaneously inoculated into the flanks of these mice, the tumor incidence on day 22 was 10/10 (100%) in NOG, 2/10 (20%) in SCID, and 0/10 (0%) in nude mice. The subcutaneous tumors formed reproducibly and semiquantitatively in a dose-dependent manner. Unexpectedly, half of the NOG mice (5/10) that had been inoculated with a mere 10¹ HeLa S3 cells formed progressively growing subcutaneous tumors on day 78. We confirmed that the engrafted tumors originated from inoculated HeLa S3 cells by immunohistochemical staining with anti-HLA antibodies. These data suggest that NOG mice may be the best choice as a suitable strain for testing tumorigenicity.

(Reprinted from *J Toxicol Sci* Vol.34, K. Machida, H. Suemizu, K. Kawai, T. Ishikawa, R. Sawada, Y. Ohnishi, and T. Tsuchiya. "Higher susceptibility of NOG mice to xenotransplanted tumors." p123, (2009) with permission from Journal of Toxicological sciences)

Table 1. Comparative growth of HeLa S3 cells among BALB/cA *nu/nu*, NOD/Shi-*scid*, and NOG mice.

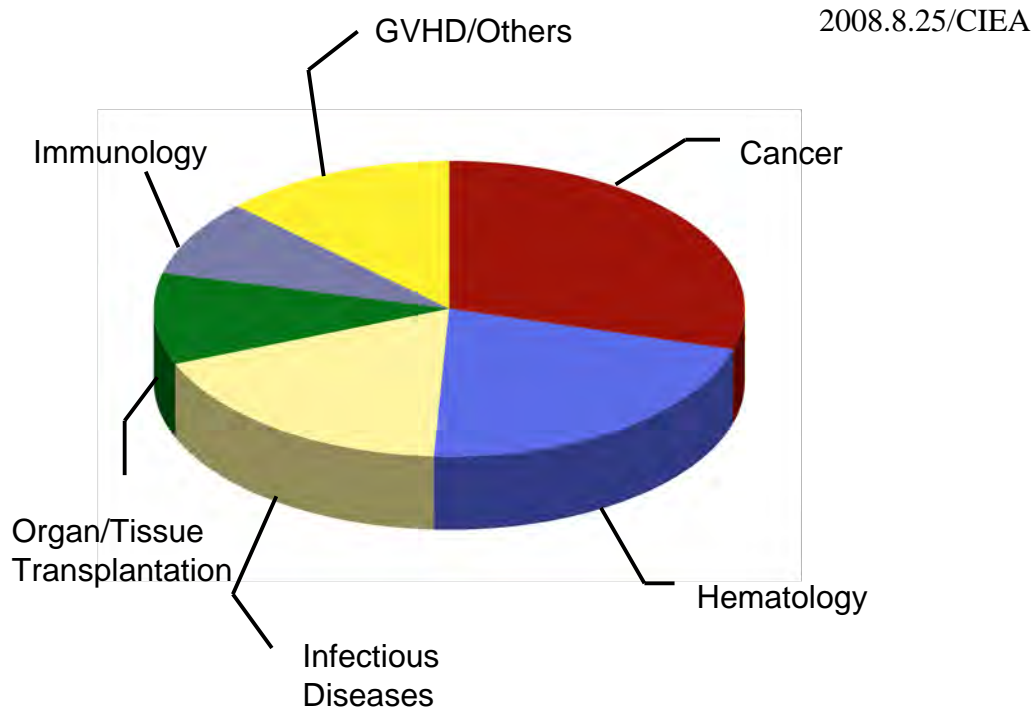
Cell dose (cells/head)	Sex	Number of mice with tumors (% engraftment) ^a		
		BALB/cA <i>nu/nu</i>	NOD/Shi- <i>scid</i>	NOG
1x10 ²	Male	NT	0/5 (0%)	3/5 (60%)
	Female	NT	0/5 (0%)	3/5 (60%)
	Total	NT	0/10 (0%)	6/10 (60%) [*]
1x10 ³	Male	0/5 (0%)	0/5 (0%)	3/5 (60%)
	Female	0/5 (0%)	0/5 (0%)	3/5 (60%)
	Total	0/10 (0%)	0/10 (0%)	6/10 (60%) [#]
1x10 ⁴	Male	0/5 (0%)	2/5 (40%)	5/5 (100%) ^{**}
	Female	0/5 (0%)	0/5 (0%)	5/5 (100%) ^{##}
	Total	0/10 (0%)	2/10 (20%)	10/10 (100%) ^{##}
1x10 ⁵	Male	5/5 (100%)	5/5 (100%)	NT
	Female	3/5 (60%)	4/5 (80%)	NT
	Total	8/10 (80%)	9/10 (90%)	NT

^a Engraftment was evaluated 22 days after inoculation by 1 x 10³, 10⁴, and 10⁵ cancer cells, and 43 days after inoculation by 1 x 10² cancer cells. Fisher's exact test was performed in statistical analysis. * *P* < 0.05 compared to the NOD/Shi-*scid* strain. ** *P* < 0.01 compared to the BALB/cA *nu/nu* strain. # *P* < 0.05 compared to the BALB/cA *nu/nu* and NOD/Shi-*scid* strain. ## *P* < 0.01 compared to the BALB/cA *nu/nu* and NOD/Shi-*scid* strain. NT: not tested.

(Reprinted from *J Toxicol Sci* Vol.34, K. Machida, H. Suemizu, K. Kawai, T. Ishikawa, R. Sawada, Y. Ohnishi, and T. Tsuchiya. "Higher susceptibility of NOG mice to xenotransplanted tumors." p125, (2009) with permission from Journal of Toxicological sciences)

6. Collaborative studies at CIEA

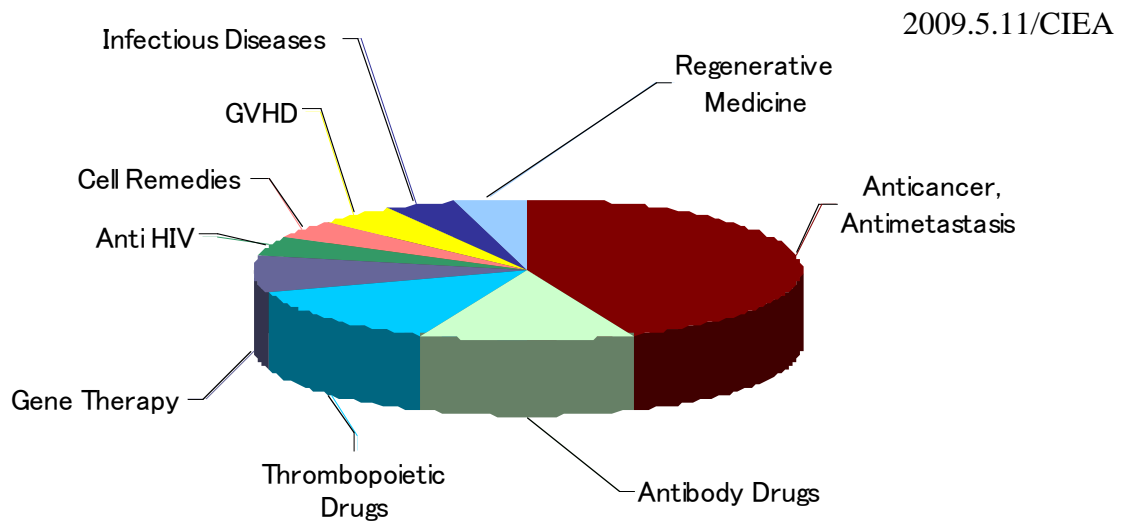
6-1. Collaborative studies with Japanese Academic Societies



Application

1. Infectious disease models
 - HIV-1 infection
 - ATL infection
 - EBV infection model
 - Hodgkin's disease model
2. Cancer models
 - Liver metastasis
 - Multiple myeloma
 - Acute myeloid leukemia
3. Human tissue or organ models
 - Model with human ovary
 - Model with human liver
 - Model with human endometrium
4. Other models
 - GVHD model
 - Efficacy test model for thrombopoietic drugs
 - Safety test for human cell (ES, iPS, gene-manipulated cells) transplantation

6-2. Collaborative Studies/Contract Studies with/from Pharmaceutical Companies



Application

1. Cancer models, Antibody drugs
 - Liver metastasis
 - Multiple myeloma
 - Breast cancer
 - Acute myeloid leukemia
2. Efficacy models for thrombopoietic drugs
3. Efficacy/safety testing for gene therapy
 - Gene induced cells
 - Antibody drug anti-gene induced cells transplanted in NOG
4. Safety testing for cell remedies
 - GVHD study
5. Safety testing for regenerative medicine
 - Skeletal myoblasts
6. Model for infectious diseases
 - HIV-1
 - Others
7. Others
 - GVHD model of hematopoietic cells

Reference List

1. Inoue, M., S. Senju, S. Hirata, A. Irie, H. Baba, and Y. Nishimura. 2009. An in vivo model of priming of antigen-specific human CTL by Mo-DC in NOD/Shi-scid IL2rgamma(null) (NOG) mice. *Immunol Lett* 126:67-72.
2. Nie, C., K. Sato, N. Misawa, H. Kitayama, H. Fujino, H. Hiramatsu, T. Heike, T. Nakahata, Y. Tanaka, M. Ito, and Y. Koyanagi. 2009. Selective infection of CD4+ effector memory T lymphocytes leads to preferential depletion of memory T lymphocytes in R5 HIV-1-infected humanized NOD/SCID/IL-2Rgammanull mice. *Virology* 394:64-72.
3. Yajima, M., K. Imadome, A. Nakagawa, S. Watanabe, K. Terashima, H. Nakamura, M. Ito, N. Shimizu, N. Yamamoto, and S. Fujiwara. 2009. T cell-mediated control of Epstein-Barr virus infection in humanized mice. *J Infect Dis* 200:1611-1615.
4. Tanaka, Y., T. Ikeda, Y. Kishi, S. Masuda, H. Shibata, K. Takeuchi, M. Komura, T. Iwanaka, S. Muramatsu, Y. Kondo, K. Takahashi, S. Yamanaka, and Y. Hanazono. 2009. ERas is expressed in primate embryonic stem cells but not related to tumorigenesis. *Cell Transplant* 18:381-389.
5. Ito, A., T. Ishida, A. Utsunomiya, F. Sato, F. Mori, H. Yano, A. Inagaki, S. Suzuki, H. Takino, M. Ri, S. Kusumoto, H. Komatsu, S. Iida, H. Inagaki, and R. Ueda. 2009. Defucosylated anti-CCR4 monoclonal antibody exerts potent ADCC against primary ATLL cells mediated by autologous human immune cells in NOD/Shi-scid, IL-2R gamma(null) mice in vivo. *J Immunol* 183:4782-4791.
6. Kato, C., E. Fujii, Y. J. Chen, B. B. Endaya, K. Matsubara, M. Suzuki, Y. Ohnishi, and N. Tamaoki. 2009. Spontaneous thymic lymphomas in the non-obese diabetic/Shi-scid, IL-2R gamma (null) mouse. *Lab Anim* 43:402-404.
7. Ito, R., I. Katano, K. Kawai, H. Hirata, T. Ogura, T. Kamisako, T. Eto, and M. Ito. 2009. Highly sensitive model for xenogenic GVHD using severe immunodeficient NOG mice. *Transplantation* 87:1654-1658.
8. Watanabe, Y., T. Takahashi, A. Okajima, M. Shiokawa, N. Ishii, I. Katano, R. Ito, M. Ito, M. Minegishi, N. Minegishi, S. Tsuchiya, and K. Sugamura. 2009. The analysis of the functions of human B and T cells in humanized NOD/shi-scid/gammac(null) (NOG) mice (hu-HSC NOG mice). *Int Immunol* 21:843-858.
9. Watanabe, T., H. Hayashi, K. Kita, Y. Kubota, and T. Ogawa. 2009. Ectopic porcine spermatogenesis in murine subcutis: tissue grafting versus cell-injection methods. *Asian J Androl*.

10. Shima, H., K. Takubo, H. Iwasaki, H. Yoshihara, Y. Gomei, K. Hosokawa, F. Arai, T. Takahashi, and T. Suda. 2009. Reconstitution activity of hypoxic cultured human cord blood CD34-positive cells in NOG mice. *Biochem Biophys Res Commun* 378:467-472.
11. Ogawa, D., Y. Okada, M. Nakamura, Y. Kanemura, H. J. Okano, Y. Matsuzaki, T. Shimazaki, M. Ito, E. Ikeda, T. Tamiya, S. Nagao, and H. Okano. 2009. Evaluation of human fetal neural stem/progenitor cells as a source for cell replacement therapy for neurological disorders: properties and tumorigenicity after long-term in vitro maintenance. *J Neurosci Res* 87:307-317.
12. Machida, K., H. Suemizu, K. Kawai, T. Ishikawa, R. Sawada, Y. Ohnishi, and T. Tsuchiya. 2009. Higher susceptibility of NOG mice to xenotransplanted tumors. *J Toxicol Sci* 34:123-127.
13. Kawaguchi, A. T., Y. Kametani, S. Kato, H. Furuya, K. Tamaoki, and S. Habu. 2009. Effects of liposome-encapsulated hemoglobin on human immune system: evaluation in immunodeficient mice reconstituted with human cord blood stem cells. *Artif Organs* 33:169-176.
14. Kai, M., T. Hagiwara, C. Emuta, Y. Chisaka, K. Tsuruhata, C. Endo, Y. Inagaki, H. Miyazaki, and S. Kataoka. 2009. In vivo efficacy of anti-MPL agonist antibody in promoting primary human hematopoietic cells. *Blood* 113:2213-2216.
15. Dewan, M. Z., M. Tomita, H. Katano, N. Yamamoto, S. Ahmed, M. Yamamoto, T. Sata, and N. Mori. 2009. An HIV protease inhibitor, ritonavir targets the nuclear factor-kappaB and inhibits the tumor growth and infiltration of EBV-positive lymphoblastoid B cells. *Int J Cancer* 124:622-629.
16. Chijiwa, T., Y. Abe, N. Ikoma, H. Yamazaki, H. Tsukamoto, H. Suemizu, K. Kawai, M. Wakui, C. Nishime, H. Matsumoto, M. Matsuyama, M. Mukai, Y. Ueyama, and M. Nakamura. 2009. Thrombospondin 2 inhibits metastasis of human malignant melanoma through microenvironment-modification in NOD/SCID/gammaCnull (NOG) mice. *Int J Oncol* 34:5-13.
17. Yamane, A., T. Nakamura, H. Suzuki, M. Ito, Y. Ohnishi, Y. Ikeda, and Y. Miyakawa. 2008. Interferon-alpha 2b-induced thrombocytopenia is caused by inhibition of platelet production but not proliferation and endomitosis in human megakaryocytes. *Blood* 112:542-550.
18. Yajima, M., K. Imadome, A. Nakagawa, S. Watanabe, K. Terashima, H. Nakamura, M. Ito, N. Shimizu, M. Honda, N. Yamamoto, and S. Fujiwara. 2008. A new humanized mouse model of Epstein-Barr virus infection that reproduces persistent infection,

- lymphoproliferative disorder, and cell-mediated and humoral immune responses. *J Infect Dis* 198:673-682.
19. Yahata, T., Y. Muguruma, S. Yumino, Y. Sheng, T. Uno, H. Matsuzawa, M. Ito, S. Kato, T. Hotta, and K. Ando. 2008. Quiescent human hematopoietic stem cells in the bone marrow niches organize the hierarchical structure of hematopoiesis. *Stem Cells* 26:3228-3236.
 20. Ueda, H., Y. Miyazaki, T. Matsusaka, Y. Utsunomiya, T. Kawamura, T. Hosoya, and I. Ichikawa. 2008. Bmp in podocytes is essential for normal glomerular capillary formation. *J Am Soc Nephrol* 19:685-694.
 21. Terunuma, H., X. Deng, Z. Dewan, S. Fujimoto, and N. Yamamoto. 2008. Potential role of NK cells in the induction of immune responses: implications for NK cell-based immunotherapy for cancers and viral infections. *Int Rev Immunol* 27:93-110.
 22. Terada, Y., Y. Terunuma-Sato, T. Kakoi-Yoshimoto, H. Hasegawa, T. Ugajin, Y. Koyanagi, M. Ito, T. Murakami, H. Sasano, N. Yaegashi, and K. Okamura. 2008. Development of human Graafian follicles following transplantation of human ovarian tissue into NOD/SCID/gammacnull mice. *Am J Reprod Immunol* 60:534-540.
 23. Suemizu, H., C. Yagihashi, T. Mizushima, T. Ogura, T. Etoh, K. Kawai, and M. Ito. 2008. Establishing EGFP congenic mice in a NOD/Shi-scid IL2Rg(null) (NOG) genetic background using a marker-assisted selection protocol (MASP). *Exp Anim* 57:471-477.
 24. Suemizu, H., M. Hasegawa, K. Kawai, K. Taniguchi, M. Monnai, M. Wakui, M. Suematsu, M. Ito, G. Peltz, and M. Nakamura. 2008. Establishment of a humanized model of liver using NOD/Shi-scid IL2Rgnull mice. *Biochem Biophys Res Commun* 377:248-252.
 25. Saitoh, Y., N. Yamamoto, M. Z. Dewan, H. Sugimoto, V. J. Martinez Bruyn, Y. Iwasaki, K. Matsubara, X. Qi, T. Saitoh, I. Imoto, J. Inazawa, A. Utsunomiya, T. Watanabe, T. Masuda, and S. Yamaoka. 2008. Overexpressed NF-kappaB-inducing kinase contributes to the tumorigenesis of adult T-cell leukemia and Hodgkin Reed-Sternberg cells. *Blood* 111:5118-5129.
 26. Okuma, K., R. Tanaka, T. Ogura, M. Ito, S. Kumakura, M. Yanaka, M. Nishizawa, W. Sugiura, N. Yamamoto, and Y. Tanaka. 2008. Interleukin-4-Transgenic hu-PBL-SCID Mice: A Model for the Screening of Antiviral Drugs and Immunotherapeutic Agents against X4 HIV-1 Viruses. *J Infect Dis* 197:134-141.
 27. Nomura, T., N. Tamaoki, A. Takakura, and H. Suemizu. 2008. Basic concept of development and practical application of animal models for human diseases. *Curr Top Microbiol Immunol* 324:1-24.

28. Nogami, W., H. Yoshida, K. Koizumi, H. Yamada, K. Abe, A. Arimura, N. Yamane, K. Takahashi, A. Yamane, A. Oda, Y. Tanaka, H. Takemoto, Y. Ohnishi, Y. Ikeda, and Y. Miyakawa. 2008. The effect of a novel, small non-peptidyl molecule butyramide on human thrombopoietin receptor and megakaryopoiesis. *Haematologica* 93:1495-1504.
29. Nakamura, M., and H. Suemizu. 2008. Novel metastasis models of human cancer in NOG mice. *Curr Top Microbiol Immunol* 324:167-177.
30. Miyake, A., M. Z. Dewan, T. Ishida, M. Watanabe, M. Honda, T. Sata, N. Yamamoto, K. Umezawa, T. Watanabe, and R. Horie. 2008. Induction of apoptosis in Epstein-Barr virus-infected B-lymphocytes by the NF-kappaB inhibitor DHMEQ. *Microbes Infect* 10:748-756.
31. Mine, N., R. M. Anderson, and J. Klingensmith. 2008. BMP antagonism is required in both the node and lateral plate mesoderm for mammalian left-right axis establishment. *Development* 135:2425-2434.
32. Koyanagi, Y., Y. Tanaka, M. Ito, and N. Yamamoto. 2008. Humanized mice for human retrovirus infection. *Curr Top Microbiol Immunol* 324:133-148.
33. Kishi, Y., Y. Tanaka, H. Shibata, S. Nakamura, K. Takeuchi, S. Masuda, T. Ikeda, S. Muramatsu, and Y. Hanazono. 2008. Variation in the incidence of teratomas after the transplantation of nonhuman primate ES cells into immunodeficient mice. *Cell Transplant* 17:1095-1102.
34. Ito, R., M. Shiina, Y. Saito, Y. Tokuda, Y. Kametani, and S. Habu. 2008. Antigen-specific antibody production of human B cells in NOG mice reconstituted with the human immune system. *Curr Top Microbiol Immunol* 324:95-107.
35. Ito, R., S. Maekawa, K. Kawai, H. Suemizu, S. Suzuki, H. Ishii, Y. Tanioka, M. Satake, H. Yagita, S. Habu, and M. Ito. 2008. Novel monoclonal antibodies recognizing different subsets of lymphocytes from the common marmoset (*Callithrix jacchus*). *Immunol Lett* 121:116-122.
36. Ito, M., K. Kobayashi, and T. Nakahata. 2008. NOD/Shi-scid IL2rgamma(null) (NOG) mice more appropriate for humanized mouse models. *Curr Top Microbiol Immunol* 324:53-76.
37. Ito, A., T. Ishida, H. Yano, A. Inagaki, S. Suzuki, F. Sato, H. Takino, F. Mori, M. Ri, S. Kusumoto, H. Komatsu, S. Iida, H. Inagaki, and R. Ueda. 2008. Defucosylated anti-CCR4 monoclonal antibody exercises potent ADCC-mediated antitumor effect in the novel tumor-bearing humanized NOD/Shi-scid, IL-2Rgamma(null) mouse model. *Cancer Immunol Immunother.*

38. Hamada, K., M. Monnai, K. Kawai, C. Nishime, C. Kito, N. Miyazaki, Y. Ohnishi, M. Nakamura, and H. Suemizu. 2008. Liver metastasis models of colon cancer for evaluation of drug efficacy using NOD/Shi-scid IL2Rgamma null (NOG) mice. *Int J Oncol* 32:153-159.
39. Dewan, M. Z., N. Takamatsu, T. Hidaka, K. Hatakeyama, S. Nakahata, J. Fujisawa, H. Katano, N. Yamamoto, and K. Morishita. 2008. Critical role for TSLC1 expression in the growth and organ infiltration of adult T-cell leukemia cells in vivo. *J Virol* 82:11958-11963.
40. Amet, T., M. Nonaka, M. Z. Dewan, Y. Saitoh, X. Qi, S. Ichinose, N. Yamamoto, and S. Yamaoka. 2008. Statin-induced inhibition of HIV-1 release from latently infected U1 cells reveals a critical role for protein prenylation in HIV-1 replication. *Microbes Infect* 10:471-480.
41. Watanabe, S., K. Terashima, S. Ohta, S. Horibata, M. Yajima, Y. Shiozawa, M. Z. Dewan, Z. Yu, M. Ito, T. Morio, N. Shimizu, M. Honda, and N. Yamamoto. 2007. Hematopoietic stem cell-engrafted NOD/SCID/IL2Rgamma null mice develop human lymphoid systems and induce long-lasting HIV-1 infection with specific humoral immune responses. *Blood* 109:212-218.
42. Watanabe, S., S. Ohta, M. Yajima, K. Terashima, M. Ito, H. Mugishima, S. Fujiwara, K. Shimizu, M. Honda, N. Shimizu, and N. Yamamoto. 2007. Humanized NOD/SCID/IL2Rgamma(null) mice transplanted with hematopoietic stem cells under nonmyeloablative conditions show prolonged life spans and allow detailed analysis of human immunodeficiency virus type 1 pathogenesis. *J Virol* 81:13259-13264.
43. Watanabe, S., S. Ohta, M. Yajima, K. Terashima, M. Ito, H. Mugishima, S. Fujiwara, K. Shimizu, M. Honda, N. Shimizu, and N. Yamamoto. 2007. Humanized NOD/SCID/IL2R{gamma}null Mice Transplanted with Hematopoietic Stem Cells under non-Myeloablative Condition Show Prolonged Lifespans and Allow Detailed Analysis of HIV-1 Pathogenesis. *J Virol*.
44. Watanabe, M., M. Z. Dewan, M. Taira, M. Shoda, M. Honda, T. Sata, M. Higashihara, M. E. Kadin, T. Watanabe, N. Yamamoto, K. Umezawa, and R. Horie. 2007. IkappaBalpha independent induction of NF-kappaB and its inhibition by DHMEQ in Hodgkin/Reed-Sternberg cells. *Lab Invest* 87:372-382.
45. Suemizu, H., M. Monnai, Y. Ohnishi, M. Ito, N. Tamaoki, and M. Nakamura. 2007. Identification of a key molecular regulator of liver metastasis in human pancreatic

- carcinoma using a novel quantitative model of metastasis in NOD/SCID/gammacnull (NOG) mice. *Int J Oncol* 31:741-751.
46. Ono, M., T. Maruyama, H. Masuda, T. Kajitani, T. Nagashima, T. Arase, M. Ito, K. Ohta, H. Uchida, H. Asada, Y. Yoshimura, H. Okano, and Y. Matsuzaki. 2007. Side population in human uterine myometrium displays phenotypic and functional characteristics of myometrial stem cells. *Proc Natl Acad Sci U S A*.
 47. Ninomiya, M., A. Abe, A. Katsumi, J. Xu, M. Ito, F. Arai, T. Suda, M. Ito, H. Kiyoi, T. Kinoshita, and T. Naoe. 2007. Homing, proliferation and survival sites of human leukemia cells in vivo in immunodeficient mice. *Leukemia* 21:136-142.
 48. Masuda, H., T. Maruyama, E. Hiratsu, J. Yamane, A. Iwanami, T. Nagashima, M. Ono, H. Miyoshi, H. J. Okano, M. Ito, N. Tamaoki, T. Nomura, H. Okano, Y. Matsuzaki, and Y. Yoshimura. 2007. Noninvasive and real-time assessment of reconstructed functional human endometrium in NOD/SCID/{gamma}Formula immunodeficient mice. *Proc Natl Acad Sci U S A* 104:1925-1930.
 49. Fujino, H., H. Hiramatsu, A. Tsuchiya, A. Niwa, H. Noma, M. Shiota, K. Umeda, M. Yoshimoto, M. Ito, T. Heike, and T. Nakahata. 2007. Human cord blood CD34+ cells develop into hepatocytes in the livers of NOD/SCID/gamma(c)null mice through cell fusion. *Faseb J* 21:3499-3510.
 50. Dewan, M. Z., H. Terunuma, M. Takada, Y. Tanaka, H. Abe, T. Sata, M. Toi, and N. Yamamoto. 2007. Role of natural killer cells in hormone-independent rapid tumor formation and spontaneous metastasis of breast cancer cells in vivo. *Breast Cancer Res Treat* 104:267-275.
 51. Yahata, T., S. Yumino, Y. Seng, H. Miyatake, T. Uno, Y. Muguruma, M. Ito, H. Miyoshi, S. Kato, T. Hotta, and K. Ando. 2006. Clonal analysis of thymus-repopulating cells presents direct evidence for self-renewal division of human hematopoietic stem cells. *Blood* 108:2446-2454.
 52. Ninomiya, M., A. Abe, T. Yokozawa, K. Ozeki, K. Yamamoto, M. Ito, H. Kiyoi, N. Emi, and T. Naoe. 2006. Establishment of a myeloid leukemia cell line, TRL-01, with MLL-ENL fusion gene. *Cancer Genet Cytogenet* 169:1-11.
 53. Nakamura, T., Y. Miyakawa, A. Miyamura, A. Yamane, H. Suzuki, M. Ito, Y. Ohnishi, N. Ishiwata, Y. Ikeda, and N. Tsuruzoe. 2006. A novel nonpeptidyl human c-Mpl activator stimulates human megakaryopoiesis and thrombopoiesis. *Blood* 107:4300-4307.
 54. Muguruma, Y., T. Yahata, H. Miyatake, T. Sato, T. Uno, J. Itoh, S. Kato, M. Ito, T. Hotta, and K. Ando. 2006. Reconstitution of the functional human hematopoietic

- microenvironment derived from human mesenchymal stem cells in the murine bone marrow compartment. *Blood* 107:1878-1887.
55. Kametani, Y., M. Shiina, I. Katano, R. Ito, K. Ando, K. Toyama, H. Tsukamoto, T. Matsumura, Y. Saito, D. Ishikawa, T. Taki, M. Ito, K. Imai, Y. Tokuda, S. Kato, N. Tamaoki, and S. Habu. 2006. Development of human-human hybridoma from anti-Her-2 peptide-producing B cells in immunized NOG mouse. *Exp Hematol* 34:1239-1247.
56. Horiuchi, S., N. Yamamoto, M. Z. Dewan, Y. Takahashi, A. Yamashita, T. Yoshida, M. A. Nowell, P. J. Richards, and S. A. Jones. 2006. Human T-cell leukemia virus type-I Tax induces expression of interleukin-6 receptor (IL-6R): Shedding of soluble IL-6R and activation of STAT3 signaling. *Int J Cancer* 119:823-830.
57. Dewan, M. Z., J. N. Uchihara, K. Terashima, M. Honda, T. Sata, M. Ito, N. Fujii, K. Uozumi, K. Tsukasaki, M. Tomonaga, Y. Kubuki, A. Okayama, M. Toi, N. Mori, and N. Yamamoto. 2006. Efficient intervention of growth and infiltration of primary adult T-cell leukemia cells by an HIV protease inhibitor, ritonavir. *Blood* 107:716-724.
58. Dewan, M. Z., H. Terunuma, M. Toi, Y. Tanaka, H. Katano, X. Deng, H. Abe, T. Nakasone, N. Mori, T. Sata, and N. Yamamoto. 2006. Potential role of natural killer cells in controlling growth and infiltration of AIDS-associated primary effusion lymphoma cells. *Cancer Sci* 97:1381-1387.
59. Dewan, M. Z., S. Ahmed, Y. Iwasaki, K. Ohba, M. Toi, and N. Yamamoto. 2006. Stromal cell-derived factor-1 and CXCR4 receptor interaction in tumor growth and metastasis of breast cancer. *Biomed Pharmacother* 60:273-276.
60. Nakata, H., K. Maeda, T. Miyakawa, S. Shibayama, M. Matsuo, Y. Takaoka, M. Ito, Y. Koyanagi, and H. Mitsuya. 2005. Potent anti-R5 human immunodeficiency virus type 1 effects of a CCR5 antagonist, AK602/ONO4128/GW873140, in a novel human peripheral blood mononuclear cell nonobese diabetic-SCID, interleukin-2 receptor gamma-chain-knocked-out AIDS mouse model. *J Virol* 79:2087-2096.
61. Matsuura-Sawada, R., T. Murakami, Y. Ozawa, H. Nabeshima, J. Akahira, Y. Sato, Y. Koyanagi, M. Ito, Y. Terada, and K. Okamura. 2005. Reproduction of menstrual changes in transplanted human endometrial tissue in immunodeficient mice. *Hum Reprod* 20:1477-1484.
62. Dewan, M. Z., M. Watanabe, S. Ahmed, K. Terashima, S. Horiuchi, T. Sata, M. Honda, M. Ito, T. Watanabe, R. Horie, and N. Yamamoto. 2005. Hodgkin's lymphoma cells are efficiently engrafted and tumor marker CD30 is expressed with constitutive nuclear

- factor-kappaB activity in unconditioned NOD/SCID/gammac(null) mice. *Cancer Sci* 96:466-473.
63. Dewan, M. Z., H. Terunuma, S. Ahmed, K. Ohba, M. Takada, Y. Tanaka, M. Toi, and N. Yamamoto. 2005. Natural killer cells in breast cancer cell growth and metastasis in SCID mice. *Biomed Pharmacother* 59 Suppl 2:S375-379.
64. Dewan, M. Z., K. Terashima, S. Ahmed, K. Ohba, M. Taruishi, and N. Yamamoto. 2005. Mouse serum factor(s) down-modulate the CD4 and CXCR4 molecules on human T cells conferring resistance to HIV infection in NOG mice. *Med Microbiol Immunol* 194:175-180.
65. Yahata, T., K. Ando, H. Miyatake, T. Uno, T. Sato, M. Ito, S. Kato, and T. Hotta. 2004. Competitive repopulation assay of two gene-marked cord blood units in NOD/SCID/gammac(null) mice. *Mol Ther* 10:882-891.
66. Ninomiya, M., H. Kiyoi, M. Ito, Y. Hirose, and T. Naoe. 2004. Retinoic acid syndrome in NOD/scid mice induced by injecting an acute promyelocytic leukemia cell line. *Leukemia* 29:29.
67. Miyakawa, Y., Y. Ohnishi, M. Tomisawa, M. Monnai, K. Kohmura, Y. Ueyama, M. Ito, Y. Ikeda, M. Kizaki, and M. Nakamura. 2004. Establishment of a new model of human multiple myeloma using NOD/SCID/gammac(null) (NOG) mice. *Biochem Biophys Res Commun* 313:258-262.
68. Kambe, N., H. Hiramatsu, M. Shimonaka, H. Fujino, R. Nishikomori, T. Heike, M. Ito, K. Kobayashi, Y. Ueyama, N. Matsuyoshi, Y. Miyachi, and T. Nakahata. 2004. Development of both human connective tissue-type and mucosal-type mast cells in mice from hematopoietic stem cells with identical distribution pattern to human body. *Blood* 103:860-867.
69. Ito, M. 2004. Development of multiple immunodeficient NOD/SCID/gc null (NOG) mice and their application on in vivo experimental medicine. *J. Germfree Life Gnotobiol.* 34:18-21.
70. Dewan, M. Z., M. Watanabe, K. Terashima, M. Aoki, T. Sata, M. Honda, M. Ito, S. Yamaoka, T. Watanabe, R. Horie, and N. Yamamoto. 2004. Prompt tumor formation and maintenance of constitutive NF-kappaB activity of multiple myeloma cells in NOD/SCID/gamma c(null) mice. *Cancer Sci* 95:564-568.
71. Matsumura, T., Y. Kametani, K. Ando, Y. Hirano, I. Katano, R. Ito, M. Shiina, H. Tsukamoto, Y. Saito, Y. Tokuda, S. Kato, M. Ito, K. Motoyoshi, and S. Habu. 2003. Functional CD5+ B cells develop predominantly in the spleen of NOD/SCID/gammac(null)

- (NOG) mice transplanted either with human umbilical cord blood, bone marrow, or mobilized peripheral blood CD34+ cells. *Exp Hematol* 31:789-797.
72. Ito, M., Y. Koyanagi, K. Terashima, N. Yamamoto, T. Nakahata, Y. Ueyama, N. Tamaoki, and T. Nomura. 2003. NOG(NOD/Shi-scid, gcnnull)mouse-HIV-1 and HTLV-1 infection model using NOG mice allowing an efficient transplantation of human cells. *Proc. Japanese Society of Animal Models for Human Diseases* 19:23-30.
73. Hiramatsu, H., R. Nishikomori, T. Heike, M. Ito, K. Kobayashi, K. Katamura, and T. Nakahata. 2003. Complete reconstitution of human lymphocytes from cord blood CD34+ cells using the NOD/SCID/gammanull mice model. *Blood* 102:873-880.
74. Dewan, M. Z., K. Terashima, M. Taruishi, H. Hasegawa, M. Ito, Y. Tanaka, N. Mori, T. Sata, Y. Koyanagi, M. Maeda, Y. Kubuki, A. Okayama, M. Fujii, and N. Yamamoto. 2003. Rapid Tumor Formation of Human T-Cell Leukemia Virus Type 1-Infected Cell Lines in Novel NOD-SCID/gammanull Mice: Suppression by an Inhibitor against NF-kappaB. *J Virol* 77:5286-5294.
75. Yahata, T., K. Ando, Y. Nakamura, Y. Ueyama, K. Shimamura, N. Tamaoki, S. Kato, and T. Hotta. 2002. Functional human T lymphocyte development from cord blood CD34+ cells in nonobese diabetic/Shi-scid, IL-2 receptor gamma null mice. *J Immunol* 169:204-209.
76. Saito, Y., Y. Kametani, K. Hozumi, N. Mochida, K. Ando, M. Ito, T. Nomura, Y. Tokuda, H. Makuuchi, T. Tajima, and S. Habu. 2002. The in vivo development of human T cells from CD34(+) cells in the murine thymic environment. *Int Immunol* 14:1113-1124.
77. Ito, M., H. Hiramatsu, K. Kobayashi, K. Suzue, M. Kawahata, K. Hioki, Y. Ueyama, Y. Koyanagi, K. Sugamura, K. Tsuji, T. Heike, and T. Nakahata. 2002. NOD/SCID/gamma(c)(null) mouse: an excellent recipient mouse model for engraftment of human cells. *Blood* 100:3175-3182.